NASA CONTRACTOR REPORT

NASA CR-7

NASA CR-709

FEASIBILITY STUDY OF AN EXPLOSIVE GUN

by John K. Crosby and Stephen P. Gill

Prepared by
STANFORD RESEARCH INSTITUTE
Menlo Park, Calif.
for Ames Research Center

NATIONAL AERONAUTICS AND SPACE ADMINISTRATION • WASHINGTON, D. C. • APRIL 1967

FEASIBILITY STUDY OF AN EXPLOSIVE GUN

By John K. Crosby and Stephen P. Gill

Prepared under Contract No. NAS 2-1361 by
STANFORD RESEARCH INSTITUTE
Menlo Park, Calif.

for Ames Research Center

NATIONAL AERONAUTICS AND SPACE ADMINISTRATION

For sale by the Clearinghouse for Federal Scientific and Technical Information
Springfield, Virginia 22151 – Price $3.00

CONTENTS

ILLUSTRATIONS

TABLES

SECTION 1

INTRODUCTION

1.1 BACKGROUND

Laboratory attainment of relative velocities of macroscopic particles comparable to those encountered in space flight has proved to be extremely difficult. During the past decade numerous laboratories have tried a variety of schemes, as evidenced by the substantial literature reported in *Proceedings of the Hypervelocity Impact Symposia*. At the present time the most useful devices are the light gas guns, capable of accelerating models of controlled shape to velocities of approximately 10 km/sec, and explosive shaped-charge arrangements which produce higher velocities, up to 21 km/sec, but at the expense of lack of good control of particle shape and mass.

It is widely conceded that major improvements in the performance of breech-loaded devices such as the standard light gas gun are not to be expected because of the fundamental limitation that the gas must expend some of its own internal energy to accelerate itself in order to maintain pressure at the base of the projectile. This limitation can only be overcome by increasing the temperature of the gas while maintaining unchanged pressure. As yet, no simple means exists for substantially increasing temperature. There is also evidence that there are optimum gas temperatures beyond which the final velocity actually decreases, presumably owing to erosion of the barrel and projectile and to radiative losses.[1]

It is clear that important increases in projectile velocity can be achieved only by continuing to supply energy to the gas as the projectile accelerates. That this procedure is effective is shown by the substantial increase in performance produced by the modification developed at NASA-Ames in the "accelerated reservoir light gas gun."[2]

One possibility for combining the advantages of light gas guns with those of explosive arrangements is to use the explosive to drive a piston which acts essentially as the pump piston of a "constant-velocity reservoir" light gas gun. In this case, projectile velocity is increased by the

amount of piston velocity and may be substantially enhanced by the gas heating that results from very strong shock compression.

Viewed another way, if a piston of substantial mass can be made to move at high velocity by explosive acceleration, and if through a controlled collision part of its energy and momentum can be transferred to a projectile of controlled shape while maintaining projectile acceleration within acceptable bounds, then a very high-performance launcher results. The projectile velocity is a factor of 1 to 2 or more greater than the piston velocity, depending on energy losses in the system and the relative mass of gas confined between piston and projectile. In such a system, the gas serves primarily as a buffer to reduce projectile acceleration; energy is continually fed into it by the advancing piston and is extracted from it by the projectile.

This report describes the results of the second year's work (November 1964 - April 1966) on a study of the feasibility of an explosive system as a high-performance launcher.

1.2 STATUS AT YEAR'S BEGINNING

At the completion of the first year's work, the system depicted in Fig. 1.1 had been shown to be feasible in the sense that explosively collapsed glass tubes had been proved to be capable of driving strong shocks into pressurized helium. The shock velocities (8 to 10 mm/μsec) and the distance of travel beyond the portion of the tube surrounded by explosive suggested that a piston of significant mass was formed during tube collapse. In addition, computer runs had been made with a simple

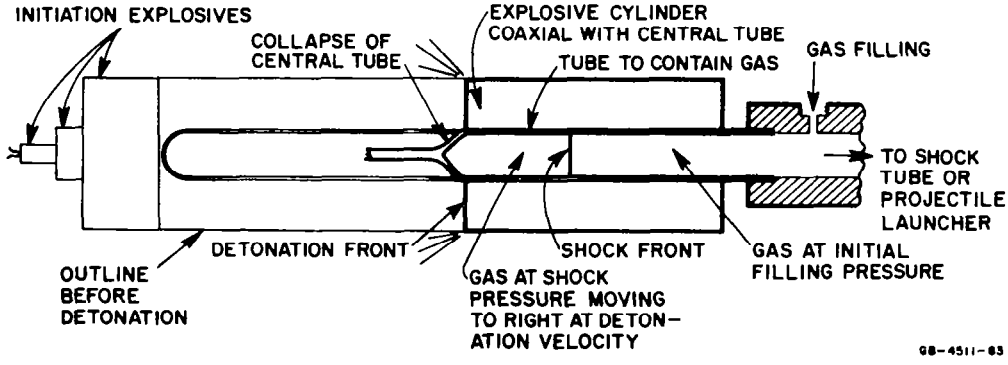

FIG. 1.1 SCHEMATIC OF EXPLOSIVE ACCELERATOR

one-dimensional, artificial viscosity code which gave considerable insight into the relationships between piston mass, gas mass, projectile mass, and pressure and velocity histories.

1.3 GENERAL OUTLINE OF CURRENT YEAR'S WORK

When experiments were made to investigate the behavior of a collapsing glass tube, it was quickly learned that any jet formed by this collapse is of minor importance in the operation of a high-pressure gun and that it is the collapse itself, moving with a velocity equal to the detonation velocity, that is the effective piston. This discovery made the theoretical analysis of the gun design much simpler, and as the theory of operation was studied more thoroughly, the components required for a gun with near-optimum performance began to be made clear:

1. Low detonation velocity in the first stages to allow the use of a short, high-pressure helium reservoir.
2. A transition section around the original projectile position to allow containment of high pressures during the low-velocity stages of projectile acceleration.
3. Detonation velocities increasing gradually to very high values as the acceleration proceeds.

The experimental work performed on these three problems is discussed in Section 2. Also described there is work done on a constant velocity-constant wall-thickness gun using thin-walled, high-strength steel tubing which offered promise of eliminating the transition section requirement. Finally, investigations of the feasibility of using a shaped charge jet as a massive, high-velocity piston are described.

The artificial viscosity computer code developed during the project made possible nonexperimental investigation of many different modes of gun operation which could be used to increase efficiency. These studies are described in Section 3, along with a theoretical design of an explosive system which will provide a piston with constant acceleration.

Section 4 describes the theoretical work done on the gas dynamics of the gun, including studies of ionization, radiative cooling, and boundary layer effects. A short theoretical study of the collapse process which yielded an estimate of the jet mass is also included. Finally, the development and operation of the computer code are described, and the extension of this code to allow calculations of the behavior of the Ames accelerating reservoir light gas gun is covered.

SECTION 2

EXPERIMENTAL STUDIES

2.1 TUBE COLLAPSE AND SHOCK DEVELOPMENT IN A GLASS TUBE DESIGN

The shock velocities observed in shots fired during the first year's work were higher than those that would be expected from a piston moving at detonation velocity. This suggested that some sort of jet was being formed during the collapse of the tube and that this jet moved out ahead of the detonation front. If any but a very simple theory of operation were to be devised, it was essential to know as much as possible about this piston. Because attempts to observe the piston after it had left the explosive were largely unsuccessful last year, it was decided to attempt observation during the process of formation, in the hope that there might be early stages during which it is more visible than later, when it has had opportunity to disperse. In addition, pictures of the collapse process would yield information on the wall velocity, which could be used to predict the jet mass theoretically.

Another facet of the operation of a glass-lined design which had not been studied during the first year's work was the reaction of the glass tube and the surrounding explosive to sudden application of kilobar pressures upon arrival of the helium shock. It was expected that the tube would fracture and begin to expand, but the extent of this expansion and its effect on the detonation front when it arrived were unknown.

The instruments used to study these effects were the flash X-ray unit, which gave accurate measurements of the tube expansion and collapse velocity, and the framing camera, which showed the effects of tube breakup and expansion on detonation and also gave an accurate measure of the growth of the shocked gas slug as detonation progressed along the tube.

2.1.1 X-Ray Observations

Taking flash X-ray photographs of explosive events is always difficult since, for good detail, the film cassette should be as close as

possible to the shot and is therefore vulnerable. The problem is most acute when events in the explosive itself are to be observed, as in this case, since only light shielding (up to a maximum of ½ inch of aluminum) can then be used between explosive and film.

After several attempts, a technique was devised which usually allowed recovery of the film after the shot. This technique reduced the hazard to the film by limiting the area observed by apertures defined by steel plates placed so as to successively attenuate the shock and blast on their way to the cassette holder. A ½-inch aluminum plate on the face of the holder stopped the fragments and usually bent enough to absorb the blast without damaging the cassette.

Because of the thickness of explosive penetrated by the X rays, and the need to use ½ inch of aluminum, the pictures obtained by this method are not very clear. Figure 2.1 is one of the best records obtained from early shots in which nitromethane was used. In the original, a second shock can be seen radiating from the collapsed stem of glass. This particular shot had a 0.003-inch copper foil wrapped around the Pyrex glass tube to make it more visible. No jet or other material is visible in the tube ahead of the detonation front.

The mass ratio of explosive charge to glass tube used in these early nitromethane shots ranged from 20:1 to 40:1, depending on the characteristics of the glass tube. Since charge-to-mass ratios over 10:1 had been shown in other studies to yield very little additional mass velocity, the next series of shots investigating the glass driver used a charge reduced to this level. This made the problems of X-ray penetration and film protection much less severe

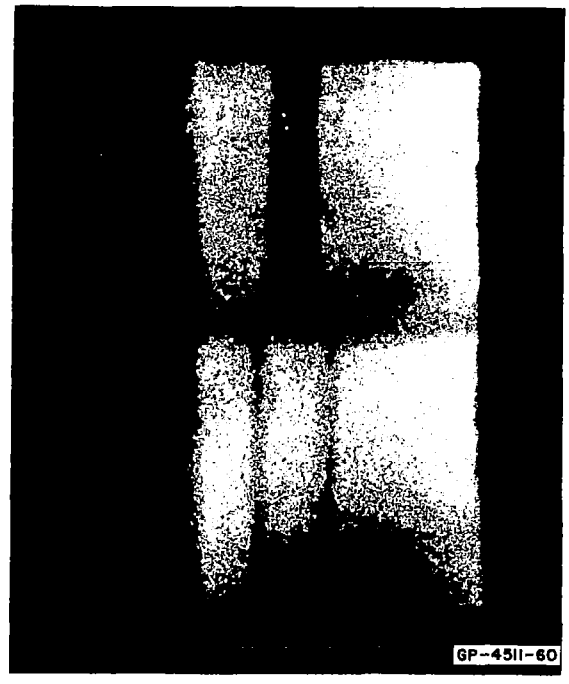

FIG. 2.1 COPPER-WRAPPED GLASS TUBE BEING IMPLODED BY NITROMETHANE, SHOT 10,929

and allowed the recording of much clearer pictures of a larger area of the shot.

Figure 2.2 shows some of the X rays obtained from this series. The width of the strip observed through the blast shields could be as great as an inch before pressure printing on the film became serious. In the beginning (*e.g.*, Shot No. 11,191) this strip was centered on the liner tube so that the expansion of both sides could be observed. Some of the later shots (*e.g.*, Shot No. 11,288) covered only one side of the liner tube and an outside surface of the explosive in order to see how much this surface was affected by the liner expansion.

2.1.2 Framing Camera Observations

Three shots using nitromethane in an all-glass system were fired in front of the framing camera. The part of the shot observed by the camera was about 6 inches long and was chosen farther along the tube for each successive shot. Figure 2.3 shows sample frames from each of the experiments. Back lighting and a system of crossed grid lines made it possible to observe the shock in helium, the shock induced in the nitromethane, and the breakup of the inner and outer glass tubes.

2.1.3 Summary of Collapse and Shock Formation

Table 2.1 summarizes all the shots fired during this study; the measurements are given as read from the film without any of the corrections to be discussed below. The following conclusions are drawn from these shots:

1. The expansion of the outside of the explosive, even in these shots with little or no confinement, is low enough that it should not interfere with the progress of detonation.
2. The angle of the collapse cone is high enough that phase velocities substantially higher than the normal detonation velocities can be used before closure of the tube will cover an inordinate length.
3. The glass jet, if present, has a mass too low to be detected by X ray or framing cameras.

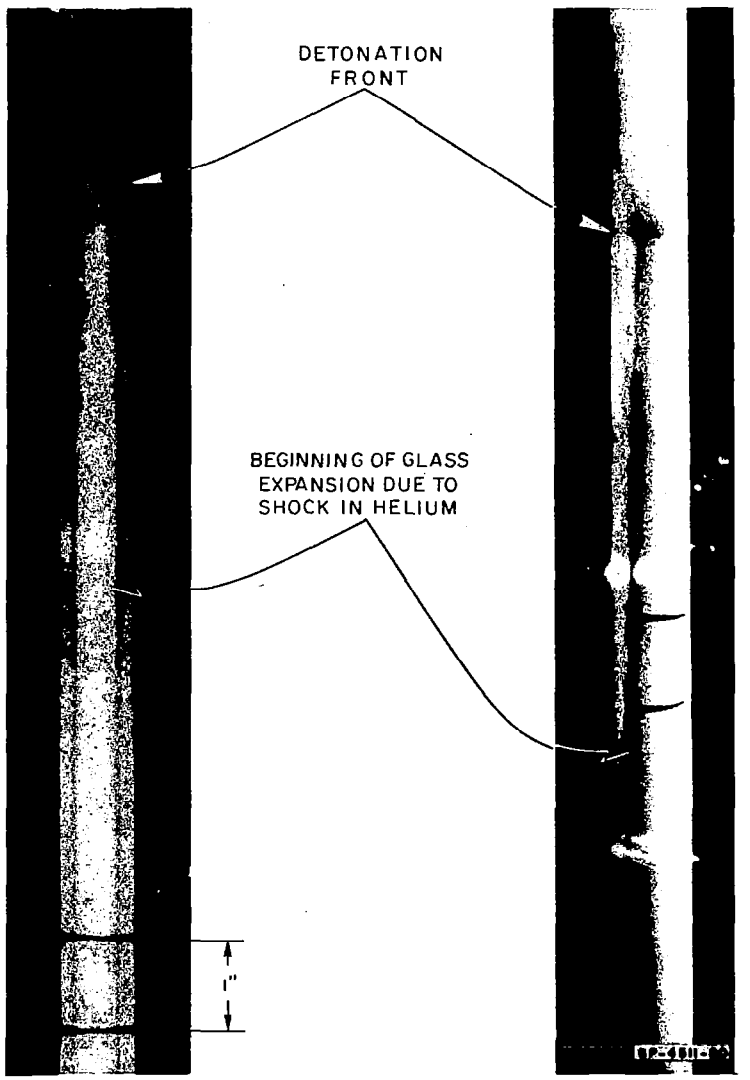

FIG. 2.2 X RAYS OF SHOCK AND TUBE INTERACTIONS

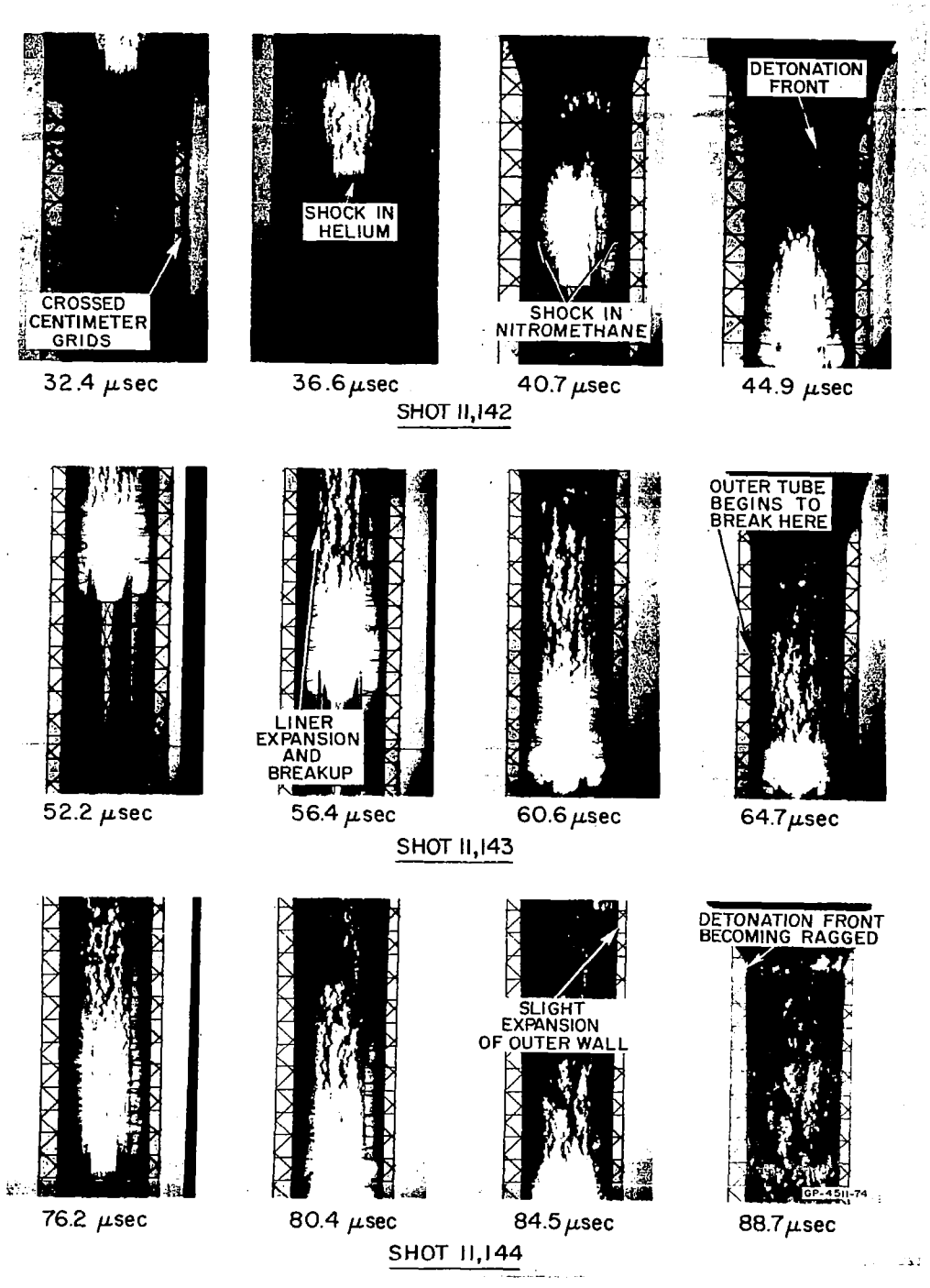

FIG. 2.3 GROWTH OF SHOCKED HELIUM SLUG SHOWING INTERACTION OF HELIUM SHOCK WITH LINER TUBE AND EXPLOSIVE
(Times shown are after initiation.)

Table 2.1

SUMMARY OF SHOTS TO OBSERVE COAXIAL DRIVER OPERATION

SHOT NO.	DETONATION FRONT POSITION (cm from initiation point)	APPARENT SHOCK POSITION (cm from detonation front)	RATIO OF TUBE DIAM. AT DETONATION FRONT TO NORMAL DIAM.	POSITION AT WHICH OUTSIDE OF EXPLOSIVE BEGINS TO EXPAND (cm from detonation front)	MAXIMUM OBSERVED EXPLOSIVE EXPANSION RATIO	REMARKS
10,988	15.6	5.2	1.2	--	--	0.003" copper sheath on liner tube; X ray; Nitromethane
11,142	16.7 19.3	5.7 ± 0.2 7.3 ± 0.2	1.13 ± 0.01 1.16 ± 0.01	-- --	-- --	Framing camera Nitromethane
11,143	29.8 33.8	12.9 ± 0.2	1.19 ± 0.01	3.2 5.4	1.01 1.04	Framing camera Nitromethane
11,144	40.4 45.5	16.7 ± 0.2		8.5 10.5	1.08 1.10	Framing camera Nitromethane
11,191	47.2	10.8 ± 1.0	1.35 ± 0.02	--	--	X ray C-3
11,192	59.4	15.0 ± 3.0	1.6 ± 0.1	8.0 ± 1.0	1.08	X ray C-3
11,257	11.5	2.8 ± 1.0	1.10 ± 0.02	--	--	X ray Comp B
11,258	21.6	9.1 ± 1.0	1.10 ± 0.05	--	--	X ray Comp B
11,274	47.2	8.5 ± 1.0	1.15 ± 0.05	--	--	X ray Comp B
11,275	72.6	--	1.45 ± 0.05	--	--	X ray Comp B
11,288	79.6	14.5 ± 2.5	1.55 ± 0.1	8.5	1.12	X ray Comp B

4. When the separation of the apparent shock front from the detonation front is plotted as a function of the length of run of the detonation, a very confused plot results. Although the framing camera records of the nitromethane shots and the two shortest Comp B X-ray shots plot up as a nice curve following the ideal gas line fairly closely, all the X-ray shots in which the detonation has gone more than 45 cm give unreasonably low values for the shock separation. To explain this discrepancy, it is suggested that the turning point noted on these shots is not at the helium shock front itself, but at the place where the rarefaction produced by the reflection of the explosive shock (induced by the helium shock) at the explosive free surface first reaches the liner.

The geometry of this situation for one of the Comp B shots is shown in Fig. 2.4. The helium shock position shown is calculated assuming a perfect gas and a detonation velocity in Comp B of 7.9 mm/μsec. The shock velocity in Comp B is assumed to be the sonic velocity, since it is quite a weak shock. Using these velocities and the Comp B thickness shown, the calculated position of the second turning of the glass liner is 12 cm behind the real shock front.

Figure 2.5 shows the plot of shocked gas thickness versus detonation front travel. When the four low points beyond 45 cm are arbitrarily raised by 12 cm, the figure begins to look much more reasonable. For the two C-3 points, 12 cm may not be the correct figure. However, the detonation velocity is somewhat lower, which would tend to lower the figure, and the sonic velocity (although unmeasured) is also probably lower, which would tend to raise the figure. Thus, 12 cm is probably a good first approximation for these shots.

When corrected in this way the curves in Fig. 2.5 suggest that, at least initially, the shocked helium region thickens faster than would be predicted from perfect gas theory. This is probably due to a glass jet of low mass. Although the experimental uncertainties of the later shots are too large to draw any definite conclusions, it appears that this jet effect is leveling out after adding about 3 to 4 cm to the apparent shocked helium thickness, and that the late behavior is thus essentially that of a gun with a piston moving at detonation velocity.

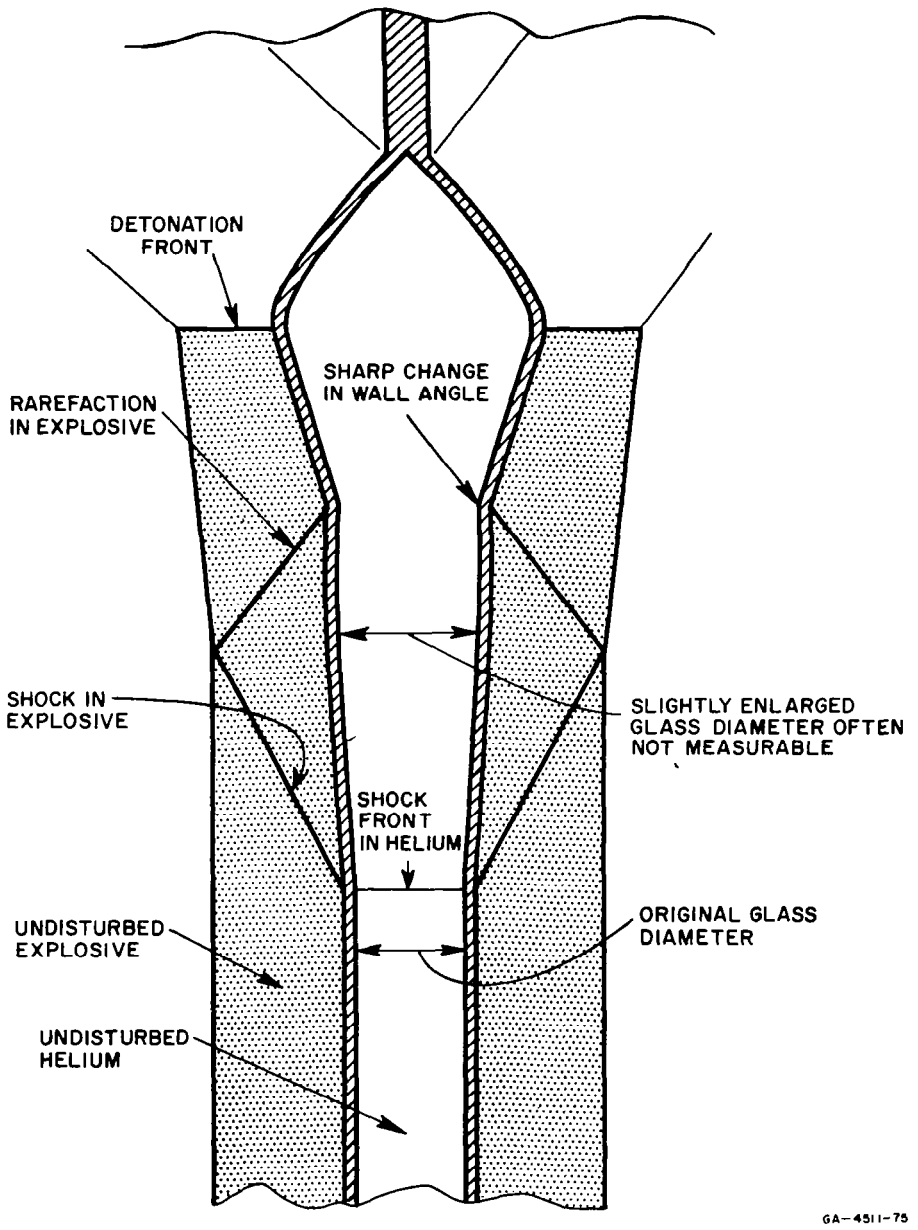

FIG. 2.4 ORIGIN OF SHARP WALL ANGLE CHANGE IN LONG X-RAY SHOTS

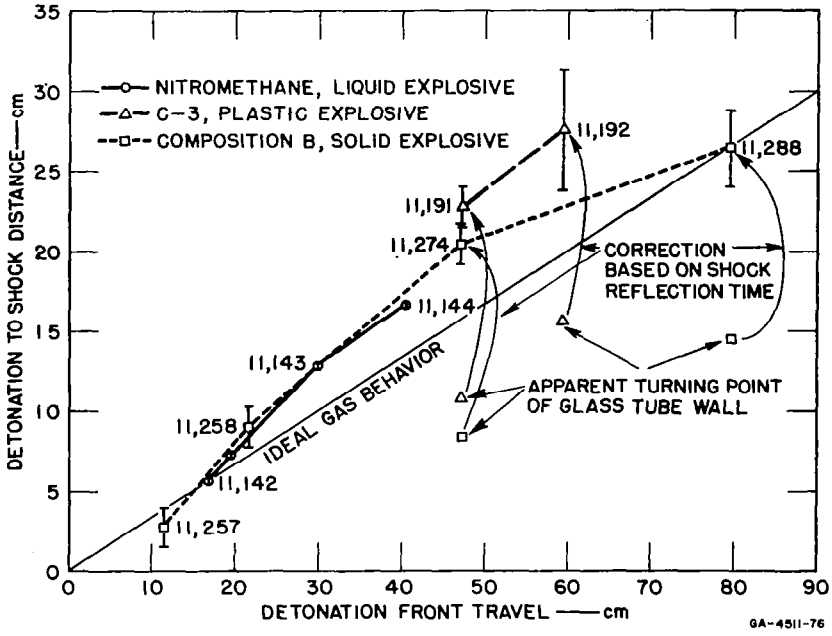

FIG. 2.5 GROWTH OF SHOCKED HELIUM SLUG vs. DETONATION FRONT TRAVEL

5. The diameter of the liner increases rapidly, by 10 to 20%, after the shock passes and then remains essentially constant until about the time that the rarefaction wave comes in from the outside. This is shown in Fig. 2.6. Although the expansion is approaching serious levels in some of the longer shots, the addition of steel confinement on the outside of the explosive will reduce this significantly and allow much longer charges to be fired if necessary.

2.2 PROJECTILE LAUNCH SERIES WITH STOPPING PISTON

2.2.1 Criteria for a Continuous Piston Design

During the first year's work on this project, flow calculations were performed to investigate the behavior of designs with a variety of characteristics. The parameters varied included piston and projectile mass, piston velocity, initial gas pressure, and initial gas reservoir length. The calculated cases closest to feasible designs were those in which a heavy piston was assumed so that the piston velocity was approximately constant, as it is in a continuously driven system. It was shown that

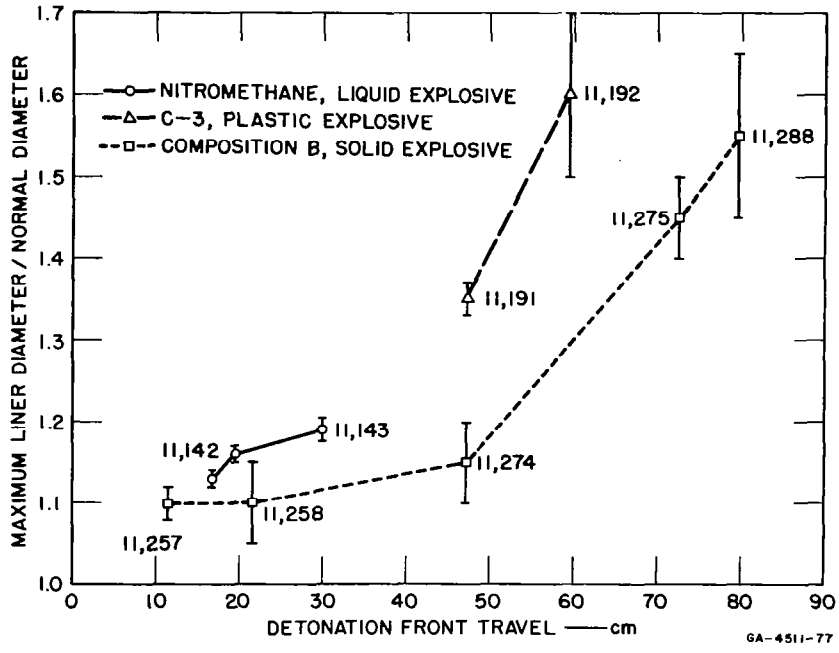

FIG. 2.6 INNER TUBE EXPANSION vs. DETONATION FRONT TRAVEL

such a piston will accelerate a projectile by driving into the gas a shock which will reflect off the projectile to produce a pressure spike, and that this shock will be reflected again off the piston and then off the projectile, producing another pressure spike before the projectile reaches or exceeds the piston velocity.

When performance is limited by the strength of the projectile, the optimum design will be one in which these two spikes have equal peak pressures. By varying the gas pressure and gas reservoir length, it was discovered empirically that the condition for this optimum is that the mass of gas be about equal to the mass of the projectile. The magnitude of the peak pressure is determined by the piston velocity and the initial gas pressure, so that the first-order design of a gun becomes straightforward once the projectile mass and strength have been assumed:

1. Determine projectile strength and mass per unit area.
2. Choose a driving explosive and determine its detonation velocity.

3. Read, from Fig. 2.7, the maximum initial gas pressure allowable to give a peak reflected pressure below the projectile strength, using the line for the detonation velocity of the explosive to be used.

4. For the initial pressure determined in 3, determine the gas reservoir length required to give a gas mass equal to the projectile mass. Values for a projectile mass of 0.5 gm/cm^2 are given in Fig. 2.7.

We wished to fire a Lexan projectile with a mass of 0.5 gm/cm^2 and an expected strength of about 5 kbar. Nitromethane (detonation velocity 6.35 mm/μsec) was chosen as the explosive; this led to a design with 10 atm initial pressure and 306 cm reservoir length. While such a design could be fired, the excessive explosive length posed some problems and it was decided to try a different system—a "stopping piston" design—for the first series of shots.

2.2.2 Stopping Piston Launch Shots

If the explosive used to collapse the tube forming the helium reservoir does not cover the entire length of the reservoir, the piston formed by the collapse can be made to stop some distance from the projectile. In this case, a rarefaction wave will be created at the stopped piston and will propagate into the shocked gas, reducing the pressure and particle velocity. If the piston is stopped soon enough, this rarefaction will reach and attenuate the shock front itself, so that the peak pressure upon reflection from the projectile will also be reduced. In this way, a high initial gas pressure can be used in a short reservoir, so that enough gas is present to act as a buffer without having excessive pressure on the projectile.

The shot design for the first series of experiments to launch a projectile is shown in Fig. 2.8. The part of the helium reservoir surrounded by explosive was 50 cm long and consisted of a 9-mm-ID glass tube surrounded by the nitromethane. The remainder of the reservoir consisted of a 98-cm-long, 9-mm-ID, steel shock tube section. The entire reservoir was initially pressurized with helium to 21.6 bars. Surrounding the glass liner was a steel cylinder which acted as a container for the nitromethane.

The nitromethane was initiated at one end, and the detonation collapsed the glass liner to form a piston moving at the detonation

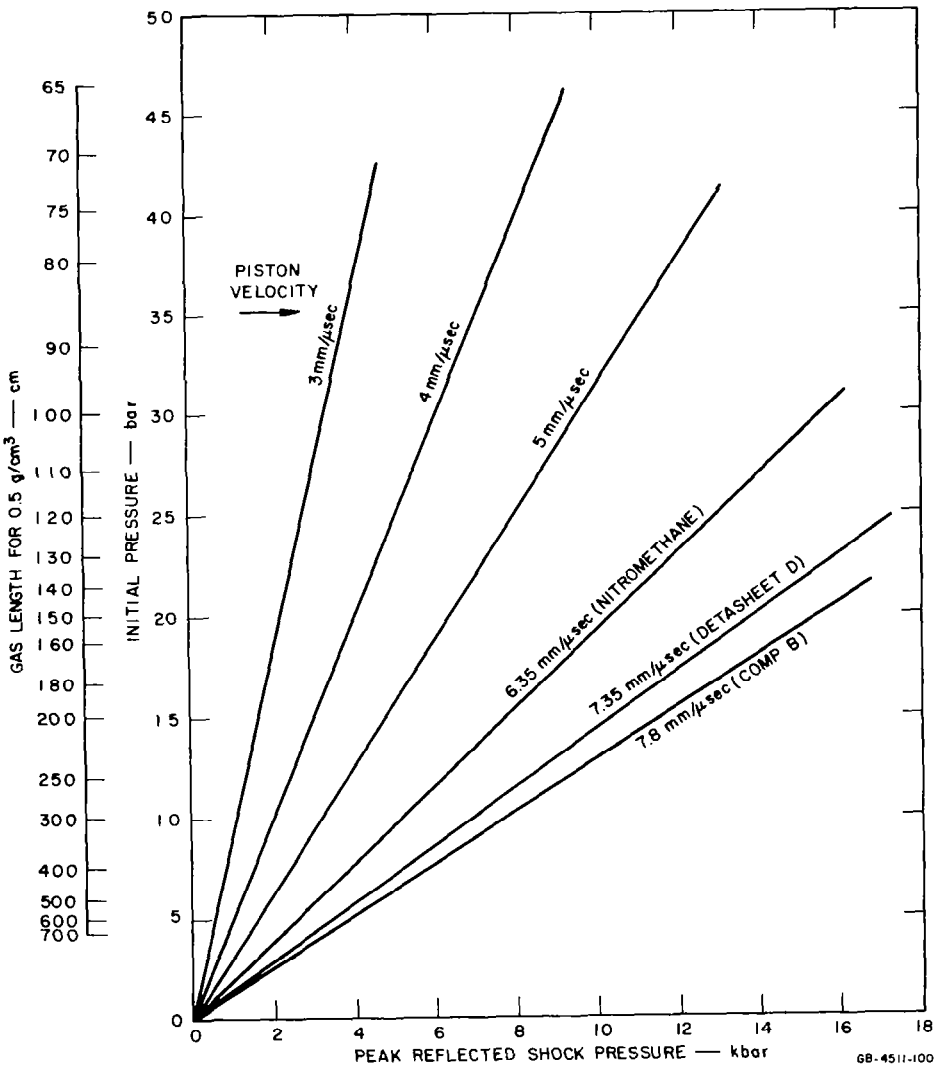

FIG. 2.7 DESIGN CHART RELATING INITIAL PRESSURE, PISTON VELOCITY, AND PEAK REFLECTED PRESSURE

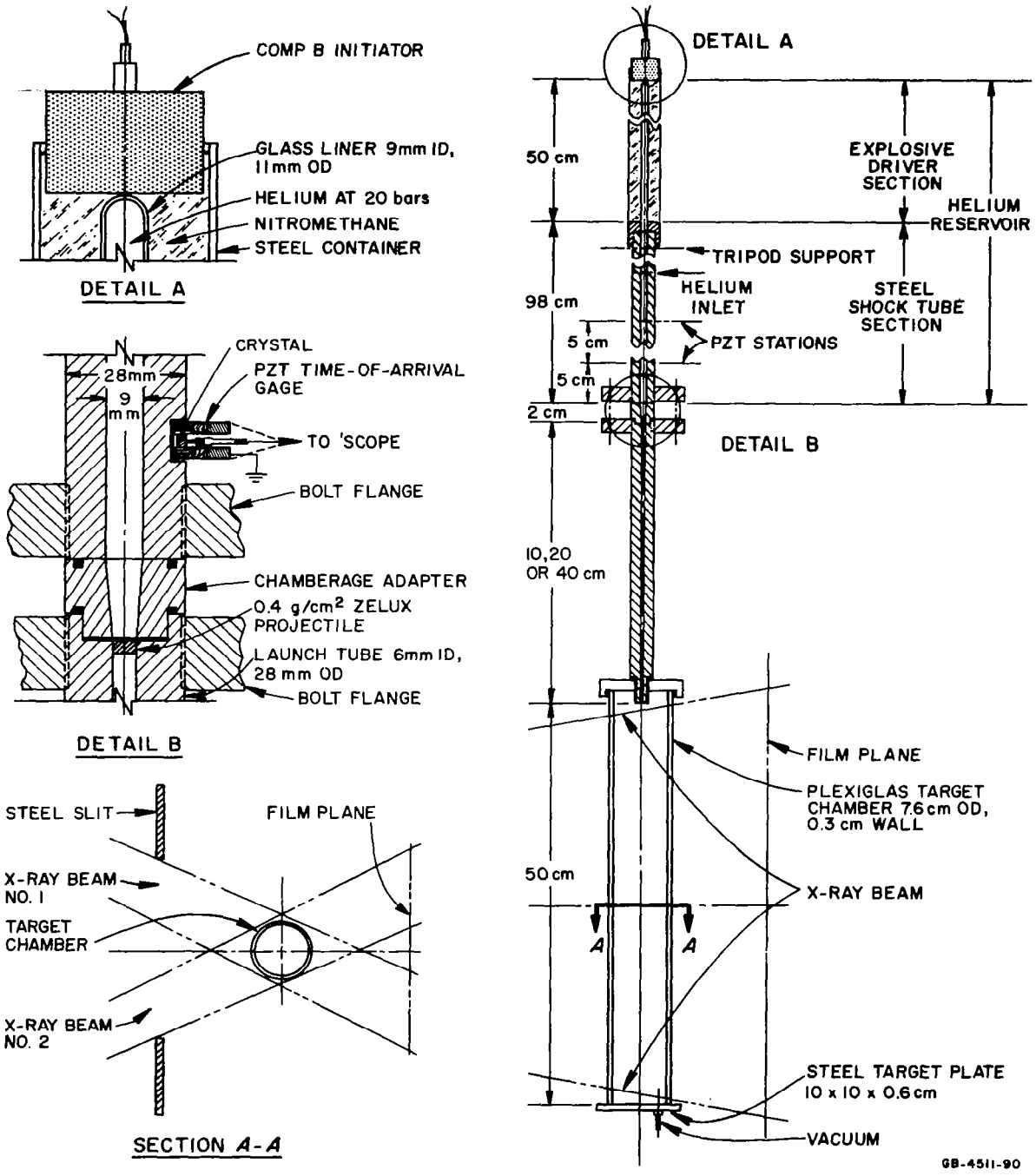

FIG. 2.8 SHOT DESIGN FOR STOPPING PISTON LAUNCH SHOTS

velocity—6.3 mm/μsec—driving a shock into the helium ahead of it. At the end of the explosive section the collapsing liner stopped while the helium shock continued to propagate through the shock tube section toward the projectile. As mentioned earlier, it is possible that a cloud of glass particles stayed slightly ahead of the actual liner collapse point. This glass cloud might have continued to follow the driver gas into the shock tube section and act like a piston.

The driver section was mated to the launch tube by a convergent steel section, 2 cm long, which matched the 9-mm inside diameter of the shock tube section to the 6-mm inside diameter of the launch tube and sealed against the projectile. The projectile was a machined Zelux cylinder, 6 mm in diameter, 3.33 mm long, with a 22.9-mm-diameter by 0.13-mm-thick flange at the reservoir end which sealed the high-pressure reservoir section from the evacuated launch tube. The launch tubes were precision-bored and -honed 6.0-mm-ID tubes of lengths ranging from 10 to 60 cm. Attached to the end of the launch tube was a thin-walled, 3-inch-diameter, Plexiglas tube through which flash X-ray exposures or framing camera pictures could be made. The end of the Plexiglas target chamber was sealed by a steel target plate for evaluation of impact cratering.

In addition to the X-ray or framing camera instrumentation, small PZT gages and electrical break screens proved valuable in shot analysis and as backup velocity measurement devices. Two PZT gage assemblies were attached to the shock tube section at stations 5 cm and 10 cm from the projectile. These gages measured the time of arrival of the helium shock by sensing the pulse in the steel tube wall induced by the shock, and their output was displayed and photographed on oscilloscopes.

The break screens were thin paper disks with a conductive grid of lines silk-screened on them. Each shot used two screens positioned near the beginning and end of the target chamber. The pulses from these screens were used to trigger the double-flash X-ray unit and the time between them was displayed on a 1-Mc counter and an oscilloscope.

Table 2.2 summarizes the eight shots fired in this series. The primary variable parameter for the series was launch tube length. The lengths were chosen to obtain information about the strength and timing of the various possible pressure pulses. These choices were based on the results of the calculations of Cases 2-1 and 2-2 performed last year.[3] As shown

Table 2.2

PROJECTILE LAUNCHING SHOTS

SHOT NO.	HELIUM RESERVOIR LENGTH (cm)	DRIVER SECTION LENGTH (cm)	LAUNCH TUBE LENGTH (cm)	PROJECTILE VELOCITY (mm/μsec)	INSTRUMENTATION	REMARKS
11,398	150	50	10	--	X-ray and break screen	Timing wrong
11,399	150	50	10	3.0 ± 0.1	X-ray	
11,438	150	50	20	3.8 ± 0.1	X-ray	
11,444	150	50	40	4.0 ± 0.1	X-ray	
11,445	300	50	10	1.6 ± 0.1	X-ray and break screen	
11,489	150	50	20	3.73 ± 0.02	Time-of-arrival PZT and X-ray	Gas shock velocity 6.2 ± 0.2 mm/μsec, 1.8 meter target chamber
11,684	150	50	60	4.6 ± 0.2	Framing camera	Last 20 cm of launcher was glass tube
11,685	150	50	60	4.6 ± 0.1	Framing camera and PZT	Gas shock velocity 6.9 ± 0.2 mm/μsec. Last 20 cm of launcher was glass tube

in Fig. 2.9, a length of 10 cm allows time for only the first shock-projectile interaction before the projectile leaves the launch tube. Increasing the length to 20 cm allows time for this first reflection and for the interaction with the shock reflected from the piston, provided the piston mass is of the order of 4 g/cm^2. The 40-cm-long launch tube allows time for the first and second projectile-gas shock interactions, even if the piston mass is only 0.4 g/cm^2. An estimation of the strength of the second reflected gas shock, and hence the massiveness of the glass piston, is possible by comparing the experimental launch velocities with those predicted by calculation.

Two launchings were performed with 10-cm launch tubes. Because of a timing error, the first attempt (Shot No. 11,398) resulted in only one picture of the projectile. The record allowed the timing to be corrected, so that Shot No. 11,399 obtained two pictures showing a projectile velocity of 3.0 mm/μsec.

The two shots with 20-cm launch tubes gave projectile velocities of about 3.8 mm/μsec. The second of these two shots was fired into a target chamber 1.8 meters long with X-ray exposure positions near the muzzle and near the target plate. The purpose of the shot was to determine if the projectile had broken, by allowing it enough flight time to come apart. The radiographs of this shot, shown in Fig. 2.10(a), indicate that the projectile had rotated between flashes but had not come apart.

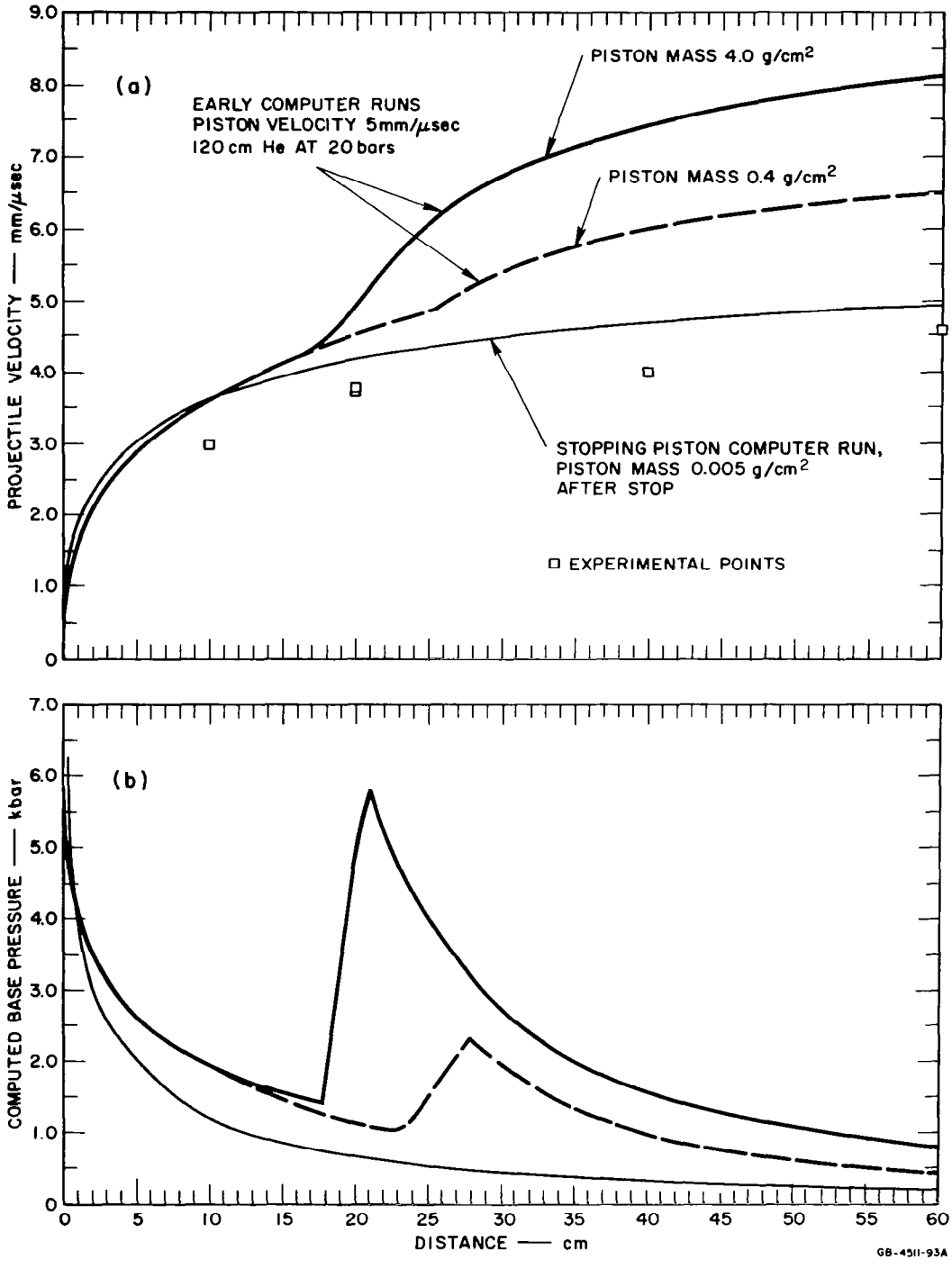

FIG. 2.9 CALCULATED PRESSURES AND VELOCITIES AND COMPARISON WITH EXPERIMENTAL VELOCITIES

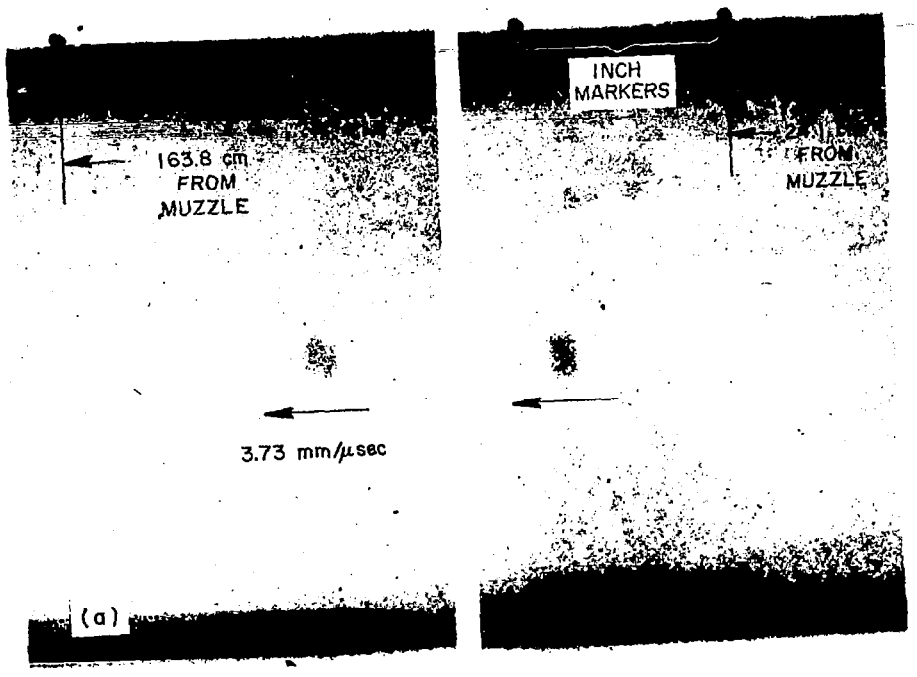

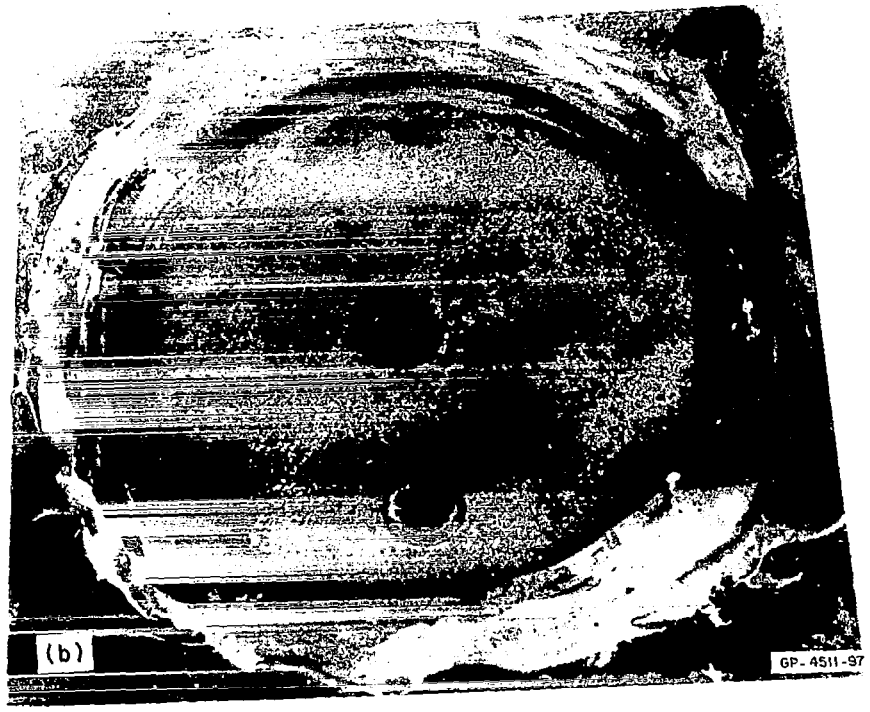

FIG. 2.10 X RAYS AND IMPACT CRATER FROM SHOT WITH 1.8-METER FLIGHT CHAMBER, SHOT 11,489

Confirmation that the projectile was intact appears in Fig. 2.10(b), a photograph of the single impact crater on the target after the 1.83-meter projectile flight. The projectile velocity for the shot was 3.73 ± 0.02 mm/μsec—in very good agreement with Shot No. 11,438. The installation of PZT gages on the shot permitted measurement of the helium driver shock velocity immediately before its first reflection from the projectile. The incident shock velocity was 6.2 ± 0.2 mm/μsec, corresponding to a peak pressure on the projectile of 5.5 kbar.

To determine the limits of performance to be expected of such a design, three shots with longer launch tubes were fired. In the first of these with a 40-cm launch tube, the projectile velocity was 4.0 ± 0.1 mm/μsec. The two other long launcher shots used precision-bore glass tubing for the last 20 cm of their 60-cm launchers and gave projectile velocities of 4.6 mm/μsec. These two shots are discussed in more detail in the next section.

Shot No. 11,445 was performed to determine the effect of increased driver gas mass on projectile launch velocity. The helium reservoir length was 300 cm, including the 50-cm coaxial explosive section and the 2-cm adapter section. The projectile velocity for the shot was found to be 1.0 ± 0.1 mm/μsec, indicating that the rarefaction from the stopped piston had definitely caught up with and attenuated the shock front.

The projectile velocities of the experiments are plotted in Fig. 2.9(b) as a function of launch tube length. Included in the graph are the velocity versus launch-distance curves predicted by Cases 2-1 and 2-2 of the early computer run mentioned above. In addition, a curve has been included based on a recent calculation duplicating the experimental conditions as closely as possible. This run included the diameter change just in front of the projectile and approximated the real behavior of the stopping piston. The piston was driven at a constant velocity for 50 cm; its mass was then reduced to 0.005 gm and it was allowed to react to the gas pressure by slowing down, stopping, and moving backwards in a way similar to the behavior of gas in an open-ended tube. In the calculation, the piston coasted only about 1.5 cm beyond the point where its mass was reduced and then began moving backwards. The rarefaction wave produced by this reversal caught up with the shock front about 25 cm from the projectile and began to attenuate the shock. Upon arrival at the projectile, the shock particle velocity had been reduced from 6.35 mm/μsec to about

5.5 mm/μsec, corresponding to a shock velocity reduction from 8.4 mm/μsec to 7.3 mm/μsec.

The experimental projectile velocities are all lower than the calculated values, especially for the shorter launch tube lengths. Also, the shock velocity measured in Shot No. 11,489 was 6.25 mm/μsec, which is lower than the calculated value of 7.3 mm/μsec; this probably accounts for most of the reduction of projectile velocity. The reason for the reduction in shock velocity is not known, but the timing of the interaction of the shock and the rarefaction is quite critical, and the real gas in the tube (helium with air impurities and ablation products from the tube walls) may behave in a way quite different from pure helium.

2.2.3 High Pressure Coaxial Drivers

In an effort to subject the projectile to higher pressures and thus to determine its strength limitations, four shots (summarized in Table 2.3) were fired in which the explosive extended over substantially the entire length of the helium reservoir. Two of these shots used a plastic explosive, C-3, and the other two a cast explosive, Comp B.

Table 2.3

HIGH PRESSURE PROJECTILE LAUNCH ATTEMPTS

SHOT NO.	HELIUM RESERVOIR LENGTH (cm)	DRIVER SECTION LENGTH (cm)	EXPLOSIVE	HELIUM PRESSURE (bars)	LAUNCH TUBE LENGTH (cm)	PROJECTILE HISTORY	INSTRUMENTATION	REMARKS
11,504	135	120	C-3	21.6	20	Shallow crater	Time-of-arrival PZT and X ray	Detonation failed halfway down
11,505	135	120	C-3	21.6	20	Shallow crater	Time-of-arrival PZT and X ray	Detonation failed halfway down
11,572	65	50	Comp B	21.6	10	Broke up	Time-of-arrival PZT and X ray	Gas shock velocity 10.2 ± 0.4 mm/μsec
11,609	65	50	Comp B	11.4	10	Broke up	Time-of-arrival PZT and X ray	Gas shock velocity 10.4 ± 0.9 mm/μsec

The two C-3 shots used a coaxial driver system consisting of a 120-cm long glass tube, 9 mm ID and 11 mm OD, surrounded by explosive (with a C/M of 10) confined by a steel tube with 1/8-inch-thick walls. The explosive driver was followed by a 13.0-cm-long steel shock tube section, used primarily for plumbing connections and for PZT gage mounting, and a 2.0-cm-long chamberage section. The lack of any evidence of

the projectile in flash X-ray exposures indicates that although the target plate showed an impact mark, the launching was later and slower than expected. The gages gave only anomalous early signals. Examination of the shot after the firing indicated that detonation in the C-3 did not propagate more than about 60 cm down the driver. Since the design is probably quite close to the explosive's failure diameter even when undisturbed, it is possible that the disturbance caused by the precompression of the C-3 explosive by the helium shock was enough to cause detonation failure.

The two Comp B shots, Nos. 11,572 and 11,609, were the same as the C-3 shots except that the driver length was reduced to 50 cm.

The first shot, No. 11,572, had a 21.6-bar helium initial pressure in the reservoir; ignoring attenuation in the shock tube section, the gas shock should have produced a peak reflected pressure of about 16.8 kbar. The second shot, No. 11,609, had a 11.4-bar helium initial pressure and should have produced about 8.9-kbar peak reflected pressure. The amount of helium in these shots was not sufficient to satisfy the condition that the mass of gas equals projectile mass. This disparity would normally result in a destructively large pressure when the shock arrives at the projectile the second time, after reflection from the piston. However, the launcher was so short in these shots that the projectile was expected to be out before the second arrival.

Both shots apparently destroyed the projectile during launch. The high-pressure shot had a measured gas shock velocity of 10.2 mm/μsec, which would produce a reflected pressure of 15.9 kbar, and this may have been high enough to destroy the projectile. However, the low-pressure shot may have destroyed its projectile because the acceleration was low enough that the projectile stayed too long in the launch tube and was overtaken by the large second shock.

2.2.4 Glass Launcher Extension Shots

The two shots with glass extensions on the launch tube were fired as the first step in developing a design in which the driving piston can be made to continue on past the original projectile position and follow it down the launch tube. Such a design will enable programming the later piston velocity by the use of explosives of increasing detonation velocities, to collapse the glass launch tube after the projectile has passed. In

this way, the pressure on the projectile will be kept high until it reaches velocities well above the highest available detonation velocity.

The basic driver and steel launch tube system was identical to that used in Shot No. 11,444; it consisted of a 50-cm glass-driven section, followed by a 100-cm steel barrel to allow the shock pressure to decay to a reasonable level before arriving at the projectile. The projectile was accelerated through a 40-cm steel launch tube into a 20-cm extension made of precision-bore glass tubing. The steel and glass tubes were glued together in a jig after they were made concentric by use of an alignment telescope. The progress of the projectile down the glass and out its end was observed with the framing camera. Both shots were very successful. Observation of the projectile in the glass was difficult because of a small cloud of opaque gases traveling with it, but it was possible to make an estimate of the projectile velocity in the glass from the record of the first shot, and clear pictures of the projectile during launch were obtained from the second shot (see Fig. 2.11). The projectile did not appear to be damaged, and it was moving at a velocity of 4.6 mm/μsec which is significantly higher than the 4.0-mm/μsec velocity measured when the 40-cm steel launcher was used alone. Glass breakup did not occur until well after the projectile had passed; therefore, it appears that the glass could subsequently be collapsed by explosive to form a second-stage piston.

2.3 FEASIBILITY OF A ONE-PIECE STEEL DRIVER-LAUNCHER

Although the launch tube shots just described are quite encouraging, the major drawback to such a design is the difficulty of fabricating a smooth joint between the steel and glass launcher sections. If a driver can be made of steel tubing that is strong enough to serve as a launch tube also, a simple, one-piece design can be made. A steel tube collapsed by a large concentric explosive charge will ordinarily form a thin, highly penetrating jet which, in this application, would destroy the projectile before it could be accelerated. However, if the explosive loading is reduced, a point is reached at which the tube is just barely collapsed and there is not sufficient additional energy to form a jet. In addition, when high gas pressures are present in the region of collapse, the formation of a jet may be inhibited even at fairly substantial explosive loadings. The feasibility of a gun designed on this basis was investigated during the last few months of the project.

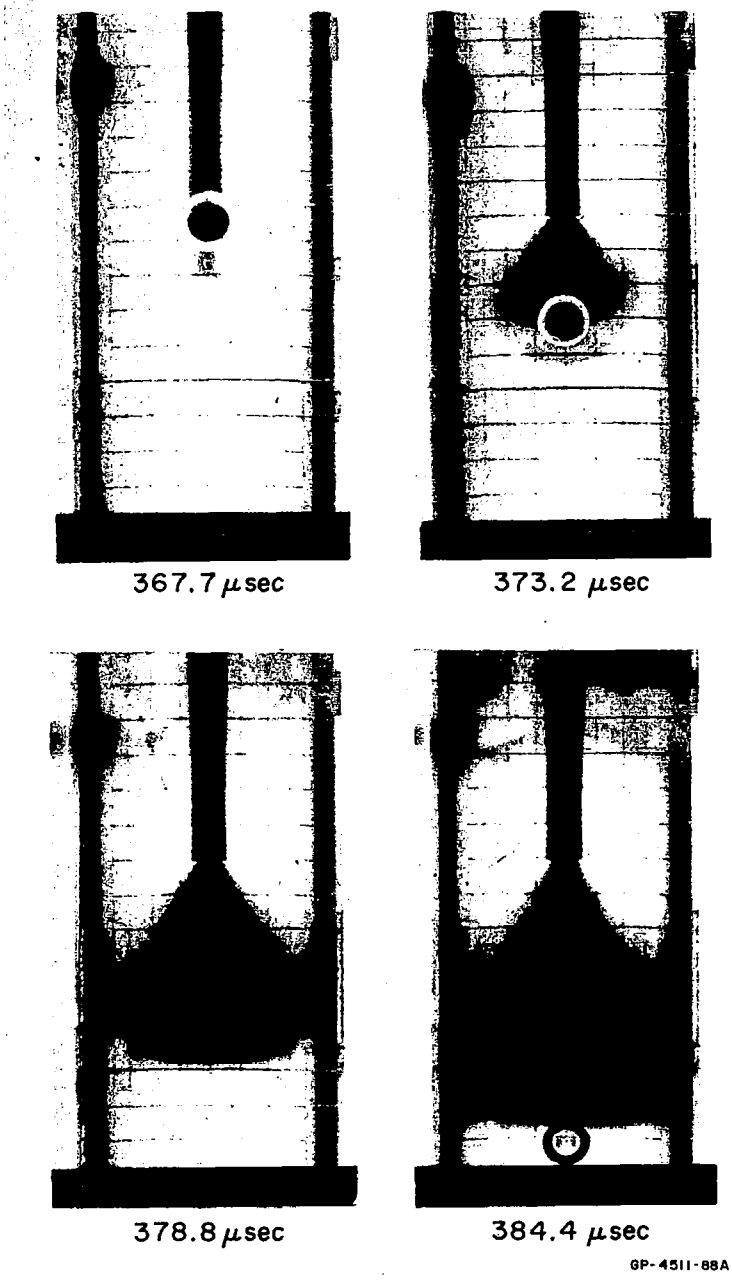

FIG. 2.11 RECORD OF PROJECTILE LAUNCH FROM A GLASS LAUNCH TUBE, SHOT 11,685
(Times shown are after initiation.)

2.3.1 Collapse of Pressurized Steel Tubes

The tubing chosen for the study is 4130 steel seamless aircraft tubing of a nominal 3/8-inch outside diameter, with 0.050-inch walls. The first experiment was made to determine the approximate amount of explosive required to just collapse the tube. For economy, a simple open length of tubing was used, wrapped in Du Pont sheet explosive with a stepwise increase in thickness every two inches. This test showed that 0.075 inch of explosive was just sufficient to close down the tube, while 0.100 inch caused complete breakup of the tube after collapse.

After this preliminary test, five shots were fired in which the tubes were filled with helium at 11.4 or 21.6 bars. Flash X rays were taken when the detonation was near the end of the tube where a thin-walled aluminum extension was attached to allow detection of any jet, and the collapsed tubes were collected for terminal observation. Table 2.4 summarizes the results of these shots and Fig. 2.12 shows some of the records obtained.

Table 2.4

PRESSURIZED STEEL TUBE CLOSING EXPERIMENTS

SHOT NO.	HE THICKNESS (inches)	INITIAL HE PRESSURE (bar)	RESULTS
11,964	0.080	21.6	Did not quite close; no pitting on witness plate.
11,965	0.100	21.6	Record lost; no pitting.
11,966	0.120	21.6	Closed and bounced open; a few small pits.
11,981	0.080	11.4	Closed solidly with no bounce; a few very small pits.
11,982	0.120	11.4	Closed and bounced; several pits $\sim$ 0.5 mm diameter.

These experiments demonstrate that shots with 11.4-bar helium are significantly different from those with 21.6 bars in that the low pressure shots require 0.020 to 0.030 inch less explosive thickness to collapse the tube completely. However, in both cases the difference between the explosive loading just sufficient to collapse the tube and that required to form a jet seems to be in excess of 0.040 inch.

The gas pressure acting on the insides of the collapsing tubes in the series of experiments described above was 1.3 and 2.5 kbar. When tubes are collapsed in a gun, the pressure at the collapse point will

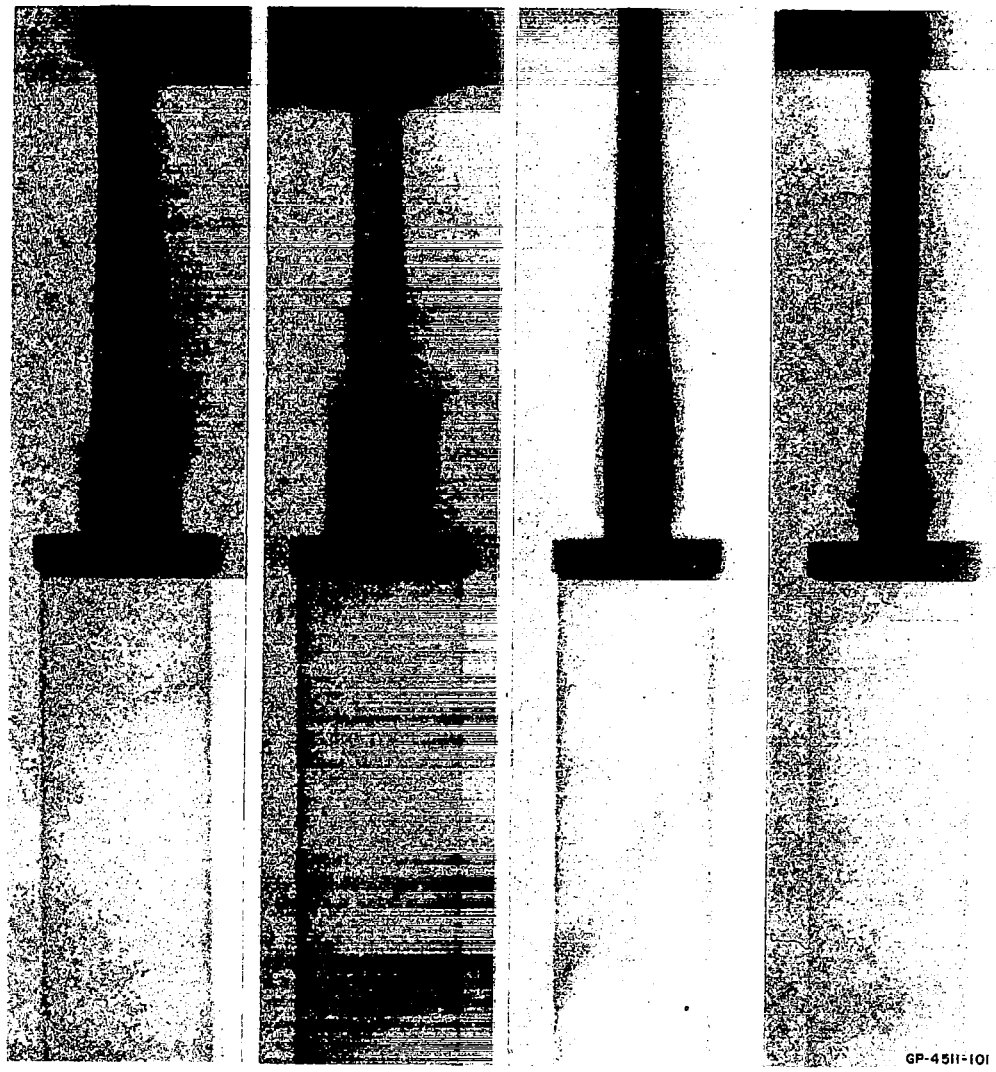

SHOT	11,964	11,966	11,981	11,982	
EXPLOSIVE	0.080	0.120	0.080	0.120	in.
PRESSURE	21.6	21.6	11.4	11.4	bar

FIG. 2.12 PRESSURIZED STEEL TUBE CLOSING EXPERIMENTS

rise at times to much higher values, comparable to the 5 to 10 kbar acting on the projectile. Thus the collapse behavior under higher pressure conditions needed to be investigated before a gun could be designed.

Four shots were fired in which the gas shock was allowed to reflect from the sealed end of the tube and interact with the advancing detonation front and the collapsing tube. This interaction should have occurred first about 12 cm from the sealed end; two X-ray pictures were taken, timed to catch the collapse before and just after the interaction. The initial gas pressure in these tubes was 16.2 bars.

Table 2.5 summarizes these shots, and Fig. 2.13 shows the pictures from the two most informative shots. These records indicate that there may be a small effect due to the reflected pressure pulse, but that tailored explosive loading will not be necessary, since increasing the explosive load over the entire length can eliminate any problems without overloading the lower pressure portion. It was therefore decided that a loading of 0.140 to 0.150 inch, made by three wraps of nominal 0.050-inch sheet explosive, would be used on the actual guns.

Table 2.5

STEEL TUBE CLOSING EXPERIMENTS VS. REFLECTED SHOCK PRESSURES

SHOT NO.	HE THICKNESS (inches)	DISTANCE FROM SEALED END TO POINT BEING CLOSED (cm)		RESULTS
		Picture 1	Picture 2	
12,046	0.100	37.1	15.9	Not closed in 1 or 2
12,047	0.120	26.3	13.2	Closed in 1 possible small opening in 2
12,048	0.120	20.1	9.3	Closed in 1 possible small opening in 2
12,049	0.140	21.5	9.5	Closed in both 1 and 2

2.3.2 All-Steel Gun Firings

Two guns using a continuous steel tube for the driver tube and the launch tube were constructed and fired. Honed 4130 tubing supplied by NASA-Ames was used with the same nominal 3/8-inch OD and 0.050-inch wall studied earlier.

2.3.2.1 FIRST GUN

The tubing supplied by NASA was 9 feet long, and the first shot was designed to fit within this total length. A Lexan projectile 0.160 inch long was chosen to insure stability in the 0.275-inch bore of the tubing; this gave a projectile mass of about 0.49 gm/cm^2. Two-thirds of the tube length was used as the helium reservoir and driver and one-third as the launch tube. To provide a gas mass of 0.49 gm/cm^2, an initial pressure of 16.4 bars was required, and assuming a piston velocity of 7.0 mm/μsec, this resulted in a peak pressure on the projectile of 10 to 11 kbar.

Figure 2.14 shows the calculated performance of this gun. According to the calculation, the projectile should reach 12.0 mm/μsec at the end of the launcher and the base pressure at that time should be about 1 kbar. Both the peak pressures and the muzzle pressure are probably near the upper limit for projectiles of this type, but since the design of the second gun could be modified if this one failed, it was decided to proceed.

A 4-inch aluminum H-beam, 12 feet long, was used to support and align the gun tube. Two pairs of adjustable screws were provided at seven stations down the beam, so that vertical and horizontal adjustments could be made during the final alignment. The ends of these screws were turned down to 3/32 inch so that they could penetrate the explosive easily and bear directly on the steel without seriously affecting the detonation of the explosive.

The projectile was made slightly oversize and forced into the tube so that it would act as a seal between the pressurized helium section and the evacuated launch section. At the muzzle of the launch tube an evacuated Plexiglas viewing chamber about 60 cm long was provided for observation of the projectile. At the far end, two timing screens were mounted and a steel witness plate sealed the chamber.

Final alignment was done with the viewing chamber removed but resting on top of the H-beam so that the weight distribution would be close to the final state. A close-fitting brass slider with a concentric hole was placed in the launch tube and observed with an alignment telescope. When the telescope had established the position of the tube at the projectile and at the muzzle, the intermediate positions were brought onto the line joining these two. The telescope used for this reads to

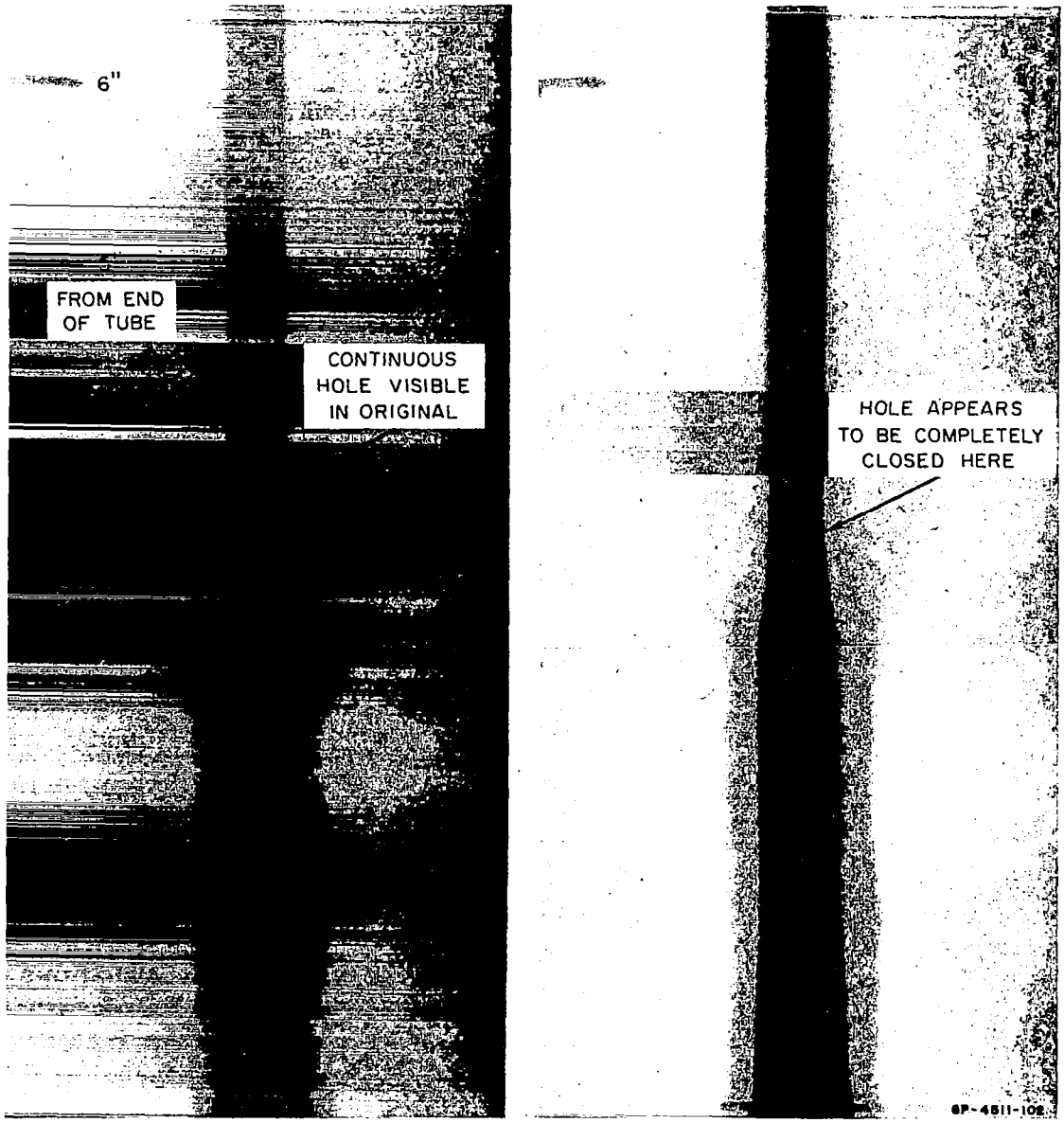

SHOT	12,048	12,049	
EXPLOSIVE	0.120	0.140	in.
PRESSURE	16.2	16.2	bar

FIG. 2.13 STEEL TUBES CLOSING AGAINST REFLECTED SHOCK PRESSURES

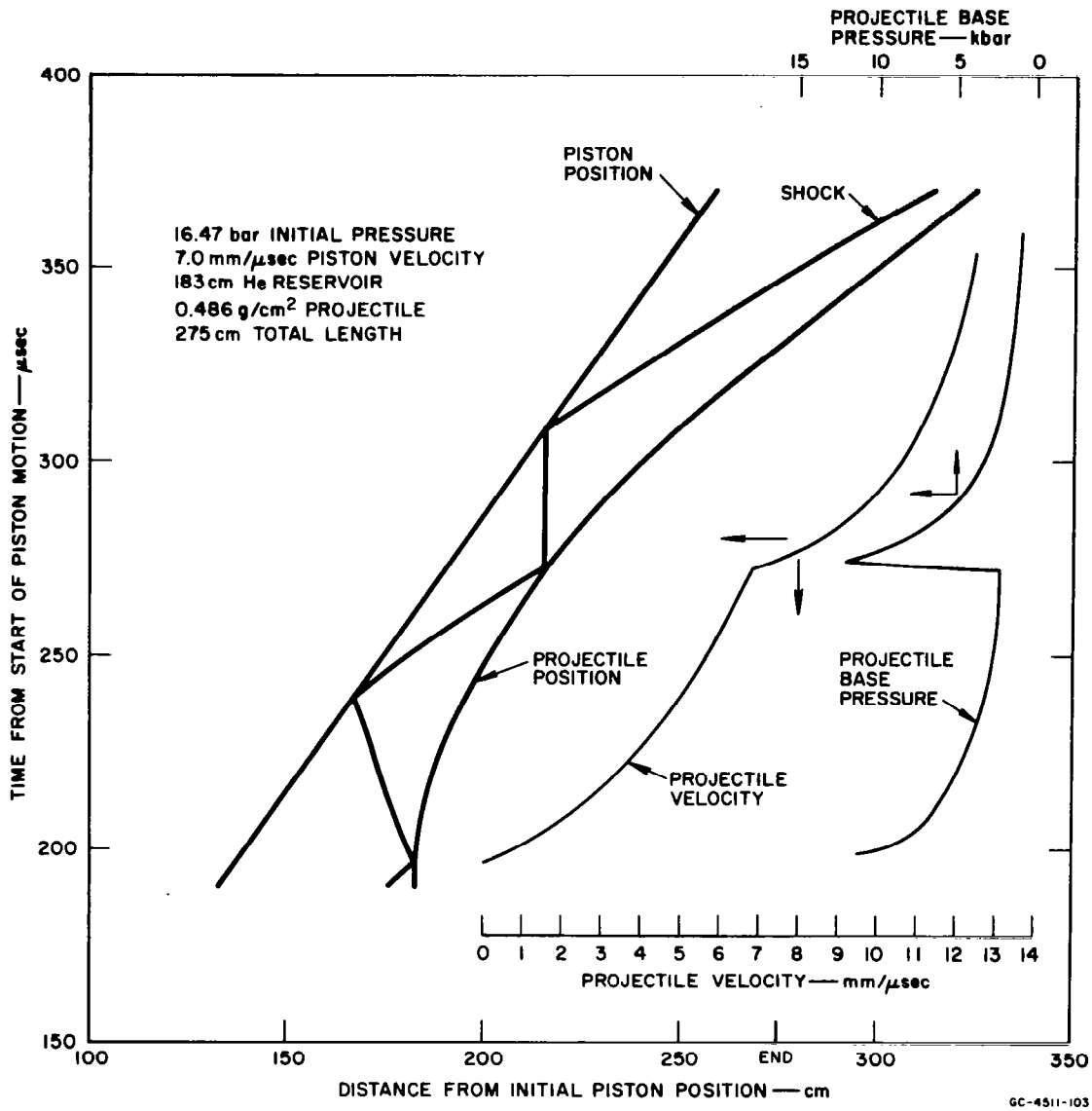

FIG. 2.14 CALCULATED BEHAVIOR OF FIRST STEEL GUN SHOT

0.0002 inch, but setting errors probably limited the alignment accuracy to about ± 0.001 inch. After alignment, the viewing chamber was put in place and sealed to the muzzle of the gun with Duxseal to provide a vacuum seal without transmitting appreciable stress from the chamber to the launch tube.

This first shot was unsuccessful, due to an error by the project leader just before firing. The valve from the reservoir to the vacuum pump was opened instead of the one to the helium tank, so that little or no gas was in the reservoir when the shot was fired. This would result in a destructively large second shock arrival pressure or in overtaking and destruction of the projectile by the detonation front.

2.3.2.2 SECOND GUN

For the second gun, it was decided to extend the tube length so that a larger reservoir with a lower gas pressure could be used. Six feet of tubing were added to the reservoir end, so that a 10-foot reservoir and a 5-foot launcher could be used. Figure 2.15 shows the calculated behavior of such a design. Note that the peak pressures have been reduced to about 7 kbar and the pressure at the muzzle to 0.85 kbar, while the muzzle velocity is still 12.0 mm/μsec.

This gun was mounted and aligned in the same way as the first one, except that the extra length of reservoir was supported only by an ordinary chair stand, since its alignment was not critical. Figure 2.16 shows the shot after alignment and assembly.

No clear pictures of the projectile were obtained from this shot, and no record was obtained from the timing screens. A single crater was formed on the witness plate, which was somewhat deeper than those observed in the earlier launch shots.

The camera pictures are uninformative because there is enough opaque smoke to obscure any projectile that might have been present. As in some earlier shots, however, the arrival of the projectile at the muzzle does appear to be signaled by a sudden change in the flow of gases at that point. In addition, the approximate time of arrival of the detonation front at the muzzle can be inferred from the arrival of smoke outside of the viewing chamber.

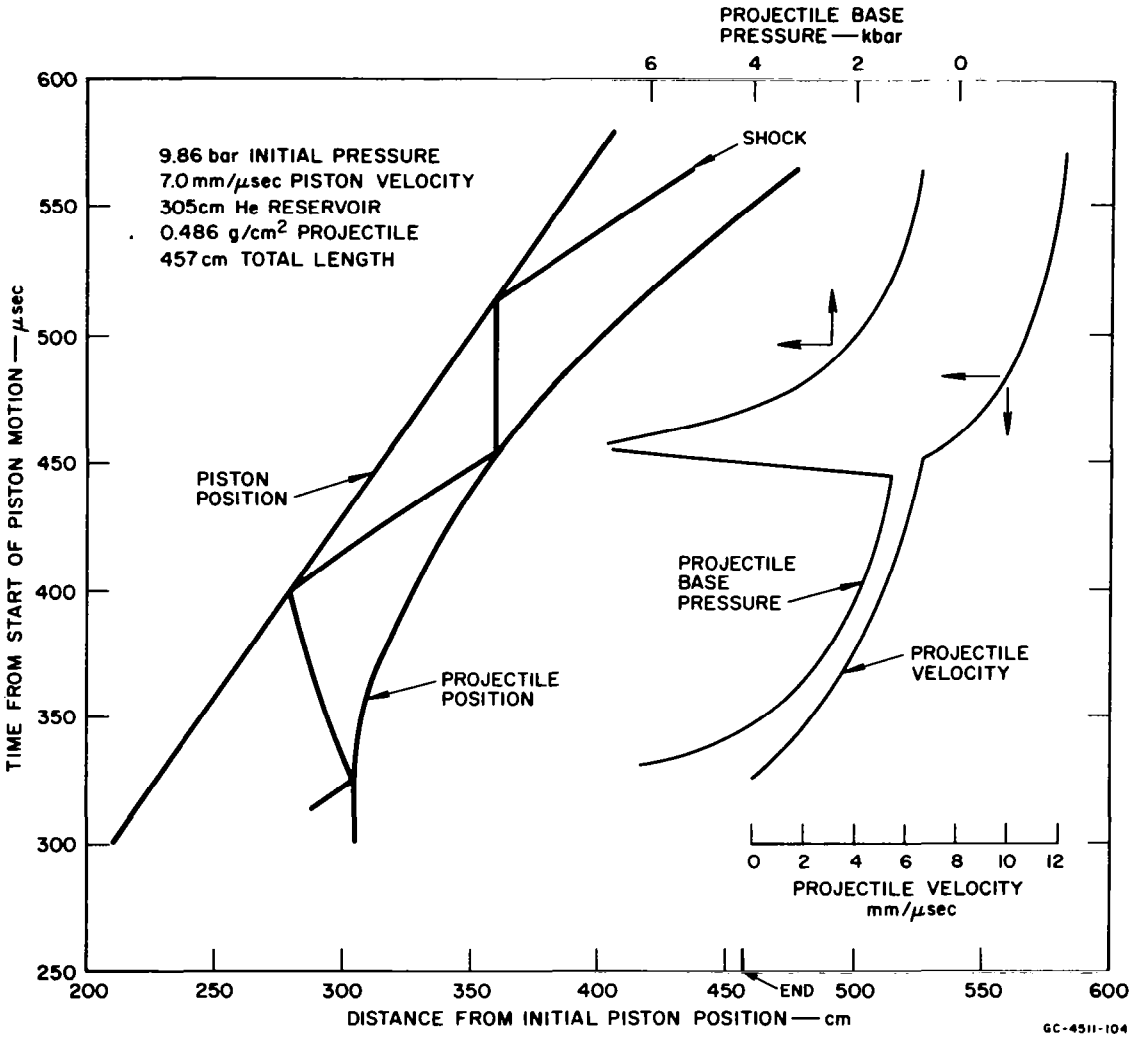

FIG. 2.15 CALCULATED BEHAVIOR OF SECOND STEEL GUN SHOT

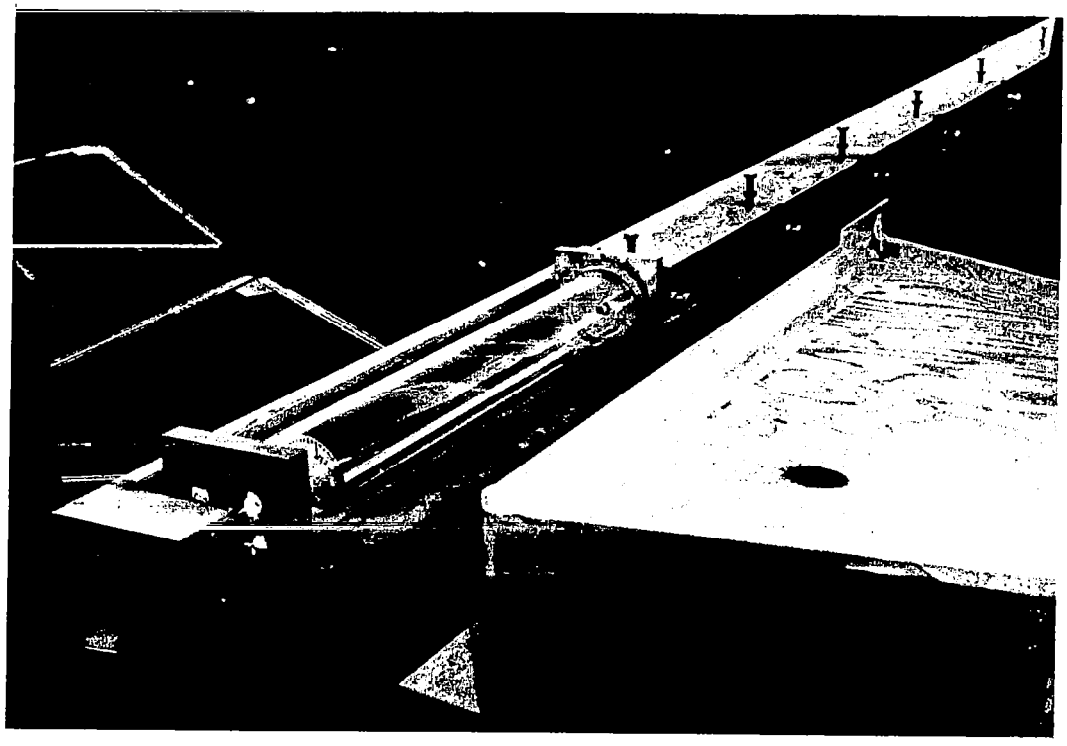

FIG. 2.16 SECOND STEEL GUN READY TO FIRE

Figure 2.17 shows a portion of the x-t diagram calculated for this design. This has been modified slightly to reflect the detonation velocity of 7.1 mm/μsec, which is what was measured for this explosive in a timing shot just before the second gun shot. Three possible projectile paths are sketched in this figure to illustrate the possible experimental behavior of the shot.

Path (1) assumes instantaneous acceleration to the final velocity and gives a velocity of 5.3 mm/μsec. This is physically unrealistic, but gives a lower limit to the projectile velocity.

Path (2) assumes that the calculated acceleration took place up to a certain point and that the projectile coasted at constant velocity from there. This gives a velocity of 6.2 mm/μsec.

Path (3) is the constant acceleration path and gives a final velocity of 10.7 mm/μsec. It is unrealistic because its distance from

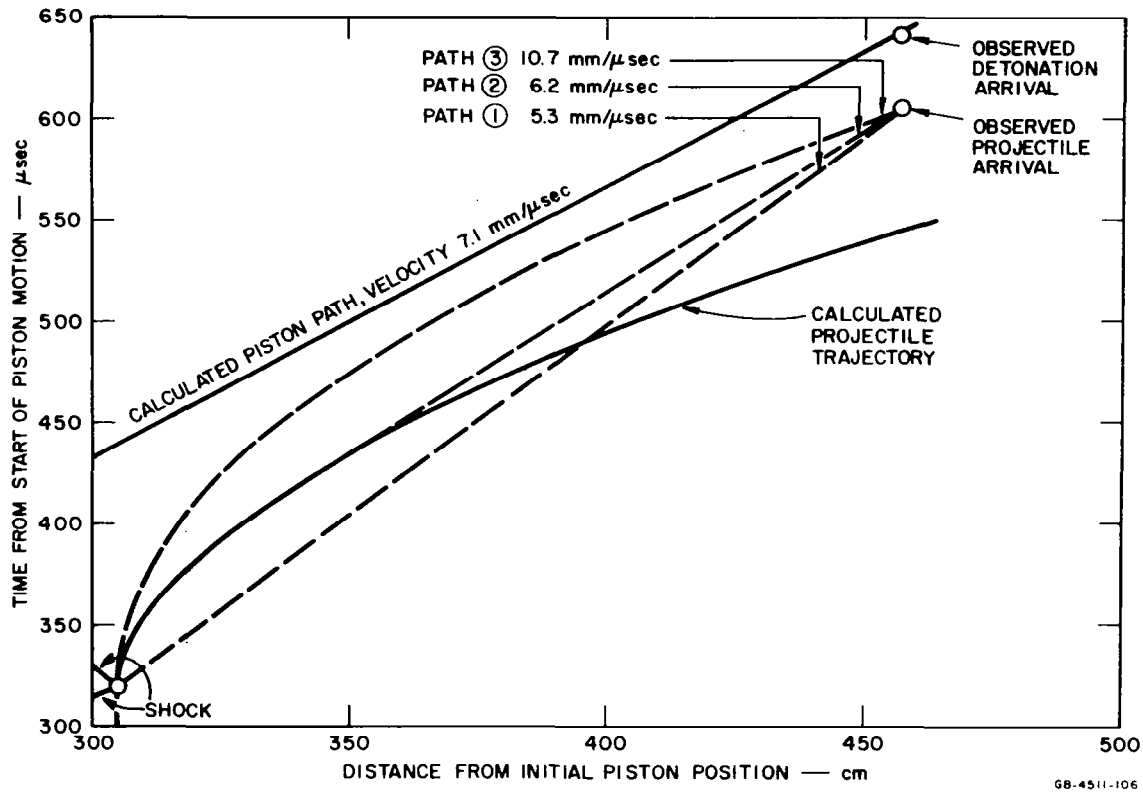

FIG. 2.17 POSSIBLE PROJECTILE TRAJECTORIES FOR SECOND STEEL GUN SHOT

the piston varies by a large factor, so that the acceleration would be expected to vary also. It probably gives a good upper limit on the actual velocity, however.

The crater formed by this projectile was only 3.1 mm deep, which suggests a velocity below even the 5.3 mm/μsec minimum. A velocity lower than 5.3 mm/μsec can only be explained by assuming that the acceleration started earlier than shown in Fig. 2.17, which seems extremely unlikely. The most probable curve is somewhere between Paths 2 and 3. The initial acceleration was probably lower than the calculated values (Path 2) because of gas leakage around the projectile during the initial high pressure pulse, but it is unlikely that it was as low as that for the constant acceleration case (Path 3). We can therefore estimate the final velocity at 7 ± 1 mm/μsec.

2.4 LOW VELOCITY EXPLOSIVE DEVELOPMENT

In Section 2.2 the parameters affecting a gun design were discussed and it was shown that a very important one is the detonation velocity of the explosive used for the initial driver. If a low detonation rate explosive can be used, the driver length and hence the total amount of explosive required can be reduced considerably. For the all-steel gun described in Section 2.3, Du Pont Detasheet is used because it will detonate reliably in the thin sections required to avoid jetting due to overloading the tube. If a suitable explosive with a detonation velocity of 4 mm/μsec can be found to replace the 7.35 mm/μsec Detasheet, the initial driver length can be reduced to about 30% of the length required by the Detasheet; if we could go as low as 3 mm/μsec, only 16% of the Detasheet length would be required.

Other project work precluded an extensive effort to develop a reliable low velocity explosive, but work was done to determine the failure thickness of nitromethane, Baratol, and a PETN-plaster mix which had been investigated earlier at these Laboratories.

2.4.1 NITROMETHANE

To determine the failure thickness of nitromethane in the coaxial geometry required for a gun, three shots were fired in which a piece of the tubing being used for the all-steel gun design was collapsed by a coaxial layer of nitromethane contained in a glass tube. Thickness was reduced from shot to shot until the detonation failed. Failure was detected both by observation with the streak camera and by terminal observation of the recovered tube and end plate. In addition, the condition of the recovered tube allowed an estimate of the likelihood that a given loading would result in a jet, based on the experience gained from the shots with Detasheet.

Table 2.6 summarizes these shots. It appears that the failure thickness and the maximum thickness allowable without jetting are quite close together, but even so it should be possible to use nitromethane in this design. If so, this can reduce initial launcher lengths to 75% of those required for Detasheet.

Table 2.6

FAILURE THICKNESS TESTS WITH NITROMETHANE

SHOT NO.	TUBING ID (mm)	NITROMETHANE THICKNESS (mm)	GAS PRESSURE (bar)	RESULTS
11,993	21.8	6.2	21.6	Detonated; collapsed completely; one split in collapsed tube.
11,994	19.0	4.8	21.6	Detonated; may be incomplete collapse.
12,044	17.5	4.0	11.4	Failed after ~ 18 cm of travel.

2.4.2 Baratol

Baratol, a commercially available castable explosive, consists of a mixture of TNT and barium nitrate. In large sections, it has a detonation velocity which can vary from 5.0 to about 5.5 mm/μsec. To test its applicability to an explosive gun design, one shot simulating a glass-lined driver was fired. This shot consisted of a cylinder of Baratol of 2-inch outside diameter with a central hole 29/64 inch in diameter. Its total length was 8 inch (built up from 2-inch segments). The shot was initiated by a P-40 plane wave lens at one end and was observed by the streak camera. The detonation velocity near the P-40 lens was 5.4 mm/μsec and fell steadily as the detonation progressed along the charge; a velocity of 4.6/μsec was reached at the far end. This decay below Baratol's usual detonation velocity shows that long shots using this explosive will almost surely fail unless much larger diameters are used. Steel confinement usually serves to reduce the failure diameter of explosives, but the experience with long, well confined Comp B and Comp C-3 shots described in Section 2.2.3 suggests that this may not be the case when explosive is preshocked by the helium shock ahead of the detonation. It thus appears that Baratol is not suitable for any but very large guns.

2.4.3 PETN-Plaster

Mixtures of PETN and Duroc (a dental plaster) were studied at Poulter Laboratories ten years ago. It was found that detonation velocities as low as 3.0 mm/μsec could be reached before the proportion of plaster became so large that failures began to occur[4]. Since most of this work had been done with cylinders cast in tubing of 1½-inch ID, a few shots were fired to see how slowly an explosive could be made to detonate in diameters comparable to dimensions appropriate to an explosive gun. Table 2.7 summarizes these shots.

Table 2.7
FAILURE DIAMETER TESTS WITH PETN-DUROC

SHOT NO.	PETN (%)	TUBE ID (mm)	RESULTS
11,988	50	19	Detonated at 5.03 mm/μsec.
11,989	50	13.5	Failed.
12,039	50	13.5	Failed; may have been damp.
12,040	50	13.5	Failed; may have been damp.
12,041	60	13.5	Thoroughly dry. Detonated at 4.3 mm/μsec.
12,042	60	13.5	Failed; may have been damp.
12,043	60	9.8	Failed; may have been damp.

These shots generally confirm the earlier work on these mixtures but suggest that the water content of the final explosive has a large effect on both the failure diameter and the detonation rate. Additional tests with closer control of the amount of water used in the mix and of the dryness after hardening will be required before reliable results can be assured.

2.5 HIGH SPEED DRIVER DEVELOPMENT

Although a projectile in a simple explosive gun should, in theory, reach velocities as high as twice the piston velocity, the total gun length required will be quite large due to the low pressures present in the later stages of acceleration. To reduce this length, the piston must be accelerated as the projectile accelerates, so that the pressure on the projectile remains essentially constant. Since the upper limit on detonation velocity is about 9 mm/μsec, projectile velocities significantly higher than this will require some way of artificially accelerating the detonation for a period near the muzzle of the gun. One method of doing this is to initiate the main explosive by striking it with a coaxial metal cone accelerated inward by a secondary layer of explosive. By suitable variation of the cone angle and thickness and the secondary explosive thickness, the phase velocity of the point of impact between the cone and the primary explosive can be made almost any value desired.

2.5.1 Plane Geometry Shots

Three shots were fired to determine the minimum velocity required for a 1/8-inch-thick flying aluminum plate to reliably initiate Comp B when striking it. The flat aluminum flyer plate used for these tests was accelerated by Du Pont Detasheet. The plate was driven onto one face of a flat slab of Comp B and the detonation arrival at the opposite face was recorded by the streak camera. The amount of Detasheet and the angle between the flyer plate and the Comp B were varied as shown in Table 2.8.

A Detasheet thickness of 0.445 cm was required to accelerate the aluminum to a velocity high enough—about 1 mm/μsec—to initiate the Comp B reliably.

Table 2.8

TWO-DIMENSIONAL HIGH PHASE VELOCITY SHOTS

SHOT NO.	FLYER EXPLOSIVE THICKNESS (cm)	FLYER ANGLE (deg)	FLYER VELOCITY (mm/μsec)	PHASE VELOCITY IN COMP B (mm/μsec)	REMARKS
11,573	0.246	3.50	0.69	21.1	Very poor breakout; ragged detonation.
11,574	0.358	4.64	0.90	21.7	Initial breakout weak; strong detonation at late end only.
11,575	0.445	5.25	0.99	22.7	Excellent, strong, uniform detonation.

2.5.2 Conical Geometry Shots

With the information derived from the plane geometry shots a conical assembly was designed to collapse on a central core of Comp B and glass in such a way that the point of impact moved along the Comp B surface at about 15 mm/μsec. This impact then initiated a conical detonation front in the Comp B with a phase velocity along the glass of 15 mm/μsec. Two shots were fired to test this design.

The coaxial, conical, high speed explosive driver is illustrated in Fig. 2.18. The interior of the driver system cannot be directly observed optically so the plastic viewing barrel shown in the figure was attached

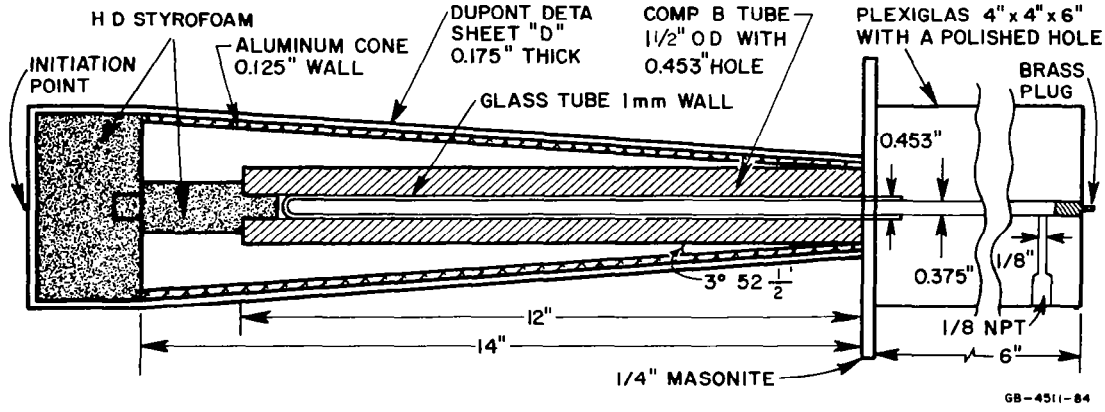

FIG. 2.18 COAXIAL CONICAL HIGH-SPEED DRIVER

to allow measurement of velocity of the resultant shock in 21.6-bar helium. The design phase velocity for these shots was 14.3 mm/μsec, which would result in a perfect gas shock velocity of 19 mm/μsec. Because of ionization, the helium became significantly different from a perfect gas under the high speed driver conditions, and the expected shock velocity was therefore lowered to 18.2 mm/μsec. The actual gas shock velocities of the two shots (one record is shown in Fig. 2.19)were 18.3 and 18.5 mm/μsec, in good agreement with the calculated value. The small discrepancy is easily accounted for by possible errors in the explosive driver design. The method appears to work very well, and there seems to be no reason why it could not be extended to velocities at least as high as the 22.7 mm/μsec recorded in Shot No. 11,575 if required.

2.6 SHAPED CHARGE DRIVERS

Although the coaxial glass- or steel-lined charges discussed above show great promise as drivers, it still seems possible that other explosive systems may be better for some applications. One alternate system investigated during the project used a shaped charge jet as the piston driving the helium down the barrel. It was felt that such a design might have at least two advantages over the glass-lined system—greater piston mass and higher piston velocity. At the same time, there was the possibility that the tip of the jet might not be large enough to fill the barrel, so that gas leakage would be serious.

2.6.1 Previous Work at BRL

A shaped charge design which seemed well suited to this application was described by Kronmav and Merendino of BRL[5]. This design, which is shown in Fig. 2.20, has the apex of the conical liner removed and replaced by what is called a "spitback tube." Although the details of operation of this system are not known, the effect of the modification is to produce a jet which has a blunt tip of an unusually large diameter. Typically, for the size charge shown in Fig. 2.20, this tip is 10 to 15 mm in diameter and 20 to 30 mm long. For aluminum liners and the cone angle shown, the tip velocity is about 9.9 mm/μsec. Other velocities have been produced by varying the cone angle, but the mass in the tip and its diameter begin to decline if the velocity is raised too far.

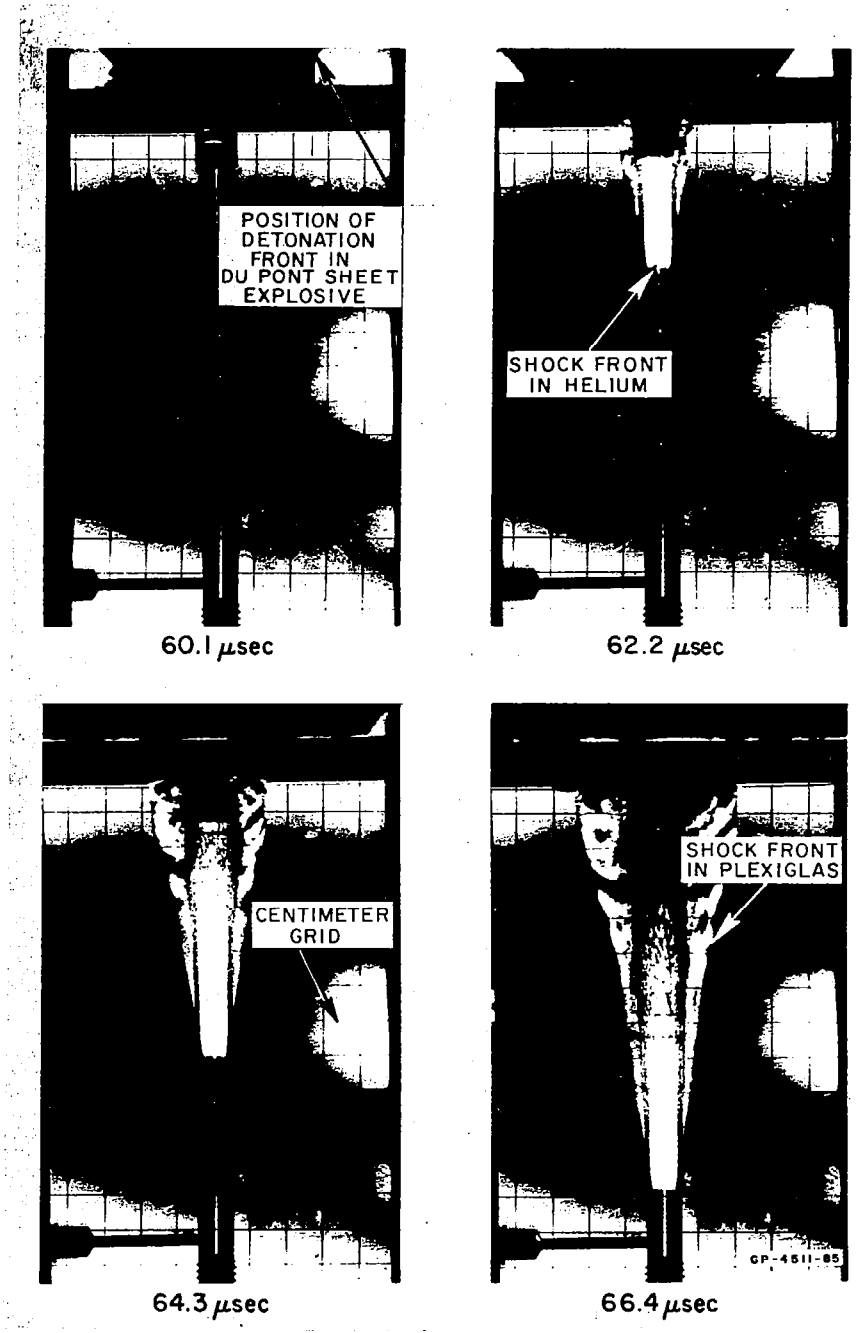

FIG. 2.19 SHOCK IN 21.6-bar HELIUM DRIVEN BY 15 mm/μsec DRIVER, SHOT 11,626 (Times shown are after initiation.)

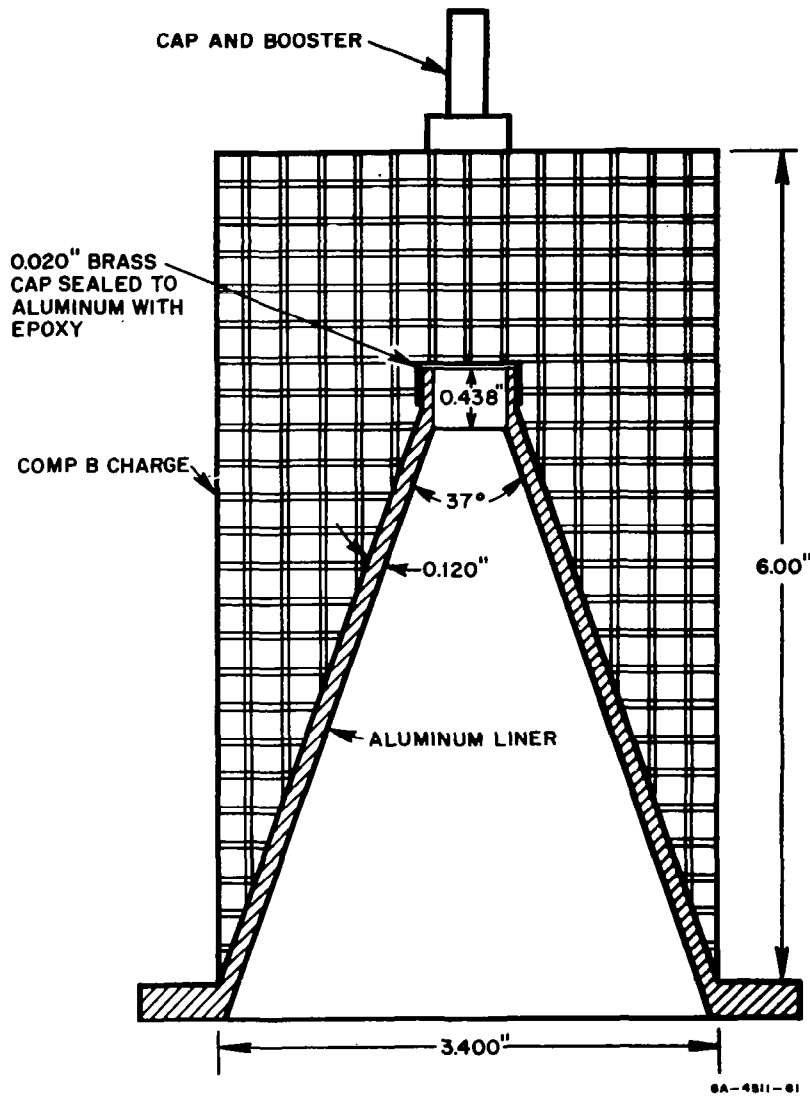

FIG. 2.20 DESIGN OF SHAPED CHARGE FOR PISTON FORMATION

2.6.2 Work Performed at SRI

Twelve shots were fired at SRI to determine the behavior of this shaped charge jet as a piston. These shots are summarized in Table 2.9 and will be briefly discussed here.

The first shot was fired to confirm that the behavior of SRI jets in free air was the same as that reported by BRL. Following this, four shots were fired in which the interaction of the jet with steel tubes was studied. These showed that a tube of 6-mm ID was too small to allow a significant amount of the jet to pass through, while a 12-mm tube was much more satisfactory.

The final seven shots were fired to study the efficiency of the jet as a piston driving helium in a long (120 to 240 cm) tube. The three types of experiments performed are illustrated in Fig. 2.21. Figure 2.21(b) was the configuration used to measure the shock velocity. The large pressurized chamber in Fig. 2.21(c) was used to observe the separation of the shock front and the jet, and in Fig. 2.21(d) the projectile launch design is shown.

It appears from these experiments that, although one successful launch was made, the shaped charge jet driver has several severe drawbacks. The worst of these is the leakage of gas around the jet which slows the buildup of the compressed gas slug and thus requires very long barrels. This defect is made more serious by the apparent attrition of the jet itself as it travels down the barrel. If we assume a nonleaking piston, the decay in velocity between 120 and 240 cm can only be explained by a decrease of piston mass and/or velocity. Leakage alone would result in a decrease of shock velocity only down to a steady state value equal to the jet velocity, 9.8 mm/μsec, so that this is obviously not the major cause of the decrease observed.

In spite of these drawbacks, the shaped charge jet driver may still be a useful design for some applications. These might include use as a transition stage between two sections of coaxial glass-lined driver in order to cover a region where a massive tube is required because of very high gas pressures or because of the guidance requirements of a projectile during the early subsonic stages of its acceleration.

Table 2.9

SHAPED CHARGE DRIVER SHOTS

SHOT NO.	BARREL DIAMETER (mm)	BARREL LENGTH (cm)	END CONFIGURATION (Fig. 2.21)	RESULTS
10,893	--	--	Shaped charge only.	Jet tip 12 mm dia. x 20 mm long; Velocity 9.9 mm/μsec.
10,900	6	15	(a) but barrel starts at base of cone.	Very faint cloud of Al got through.
10,901	6	30	(a) but barrel starts at base of cone.	Essentially nothing got through.
10,925	6	15	(a) with 5 cm standoff.	Diffuse cloud got through, better than 10,900. Made 5-mm-deep crater in 25-mm steel witness plate.
10,927	12	15	(a)	Definite jet got through. Penetrated 25-mm steel plate. Tip velocity 9.5 mm/μsec.
11,087	12	120	(b)	Shock velocity 8.7 mm/μsec in Plexiglas; average velocity 9.7 mm/μsec to first view.
11,088	12	120	(c)	Very small separation between jet and shock; jet still quite massive.
11,089	12	120	(d)	No view of projectile; thick clouds of opaque material obscured view.
11,094	12	240	(b)	Shock velocity 6.0 mm/μsec in Plexiglas; 8.6 mm/μsec average to first sight; gas appears to be clear at least 22 μsec after shock passage.
11,194	12	240	(c)	Shock going 4-5 mm/μsec barely visible ahead of early cloud; if this is shock slowed by expansion, it would be 8 cm ahead of solid part of cloud seen later. Early cloud probably ablation from muzzle edge.
11,217	12	240	(d)	Projectile velocity 2.9 mm/μsec implies 2.4 kbar average; shock velocity of 6 mm/μsec would result in 5 kbar peak pressure.
11,506	12	160	(d) with 6 mm launcher	No sign of projectile on X rays.

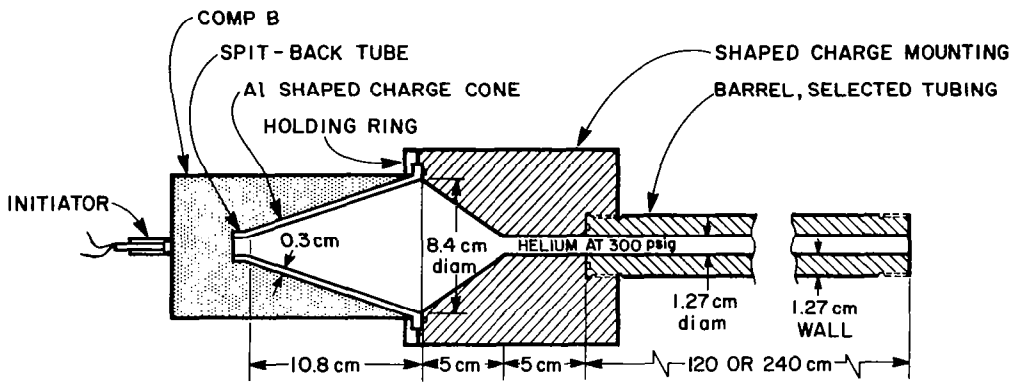

(a) SHAPED CHARGE DRIVER AND BARREL ASSEMBLY

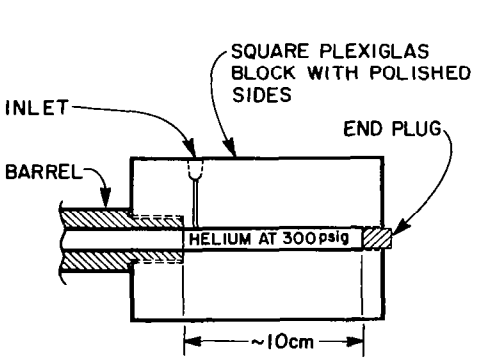

(b) VIEWING BARREL FOR GAS SHOCK VELOCITY MEASUREMENT

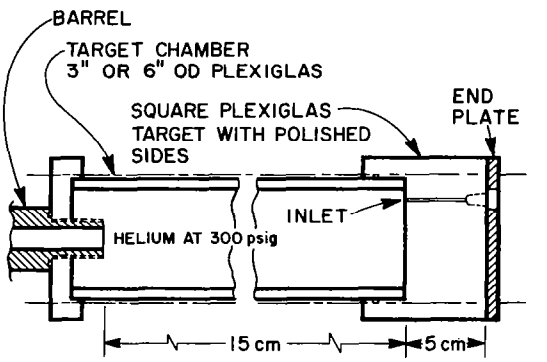

(c) PRESSURIZED TARGET CHAMBER FOR JET OBSERVATION

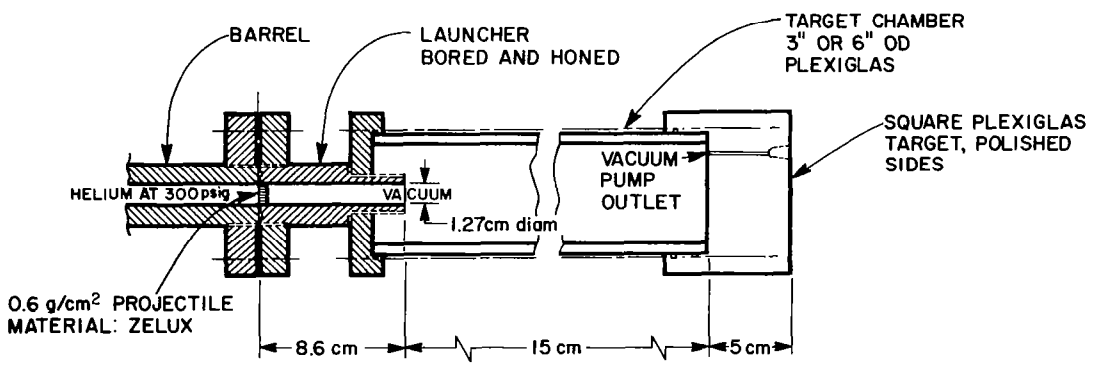

(d) EVACUATED LAUNCHER AND TARGET CHAMBER FOR PROJECTILE ACCELERATION AND VELOCITY MEASUREMENT

GC-4511-71

FIG. 2.21 HARDWARE FOR SHAPED CHARGE EXPERIMENTS

SECTION 3

NUMERICAL GUN DESIGN STUDIES

In addition to the experimental work discussed in Section 2 and the basic theoretical work discussed in Section 4, several studies were made of an intermediate nature. Four of these used the artificial viscosity computer code developed during this project to investigate the behavior of some special gun designs. The final study was a preliminary design of a system to provide a piston with constant acceleration up to twice detonation velocity.

3.1 DOUBLE SHOCK CALCULATIONS

Most of the gun designs discussed in this report produce a pressure history on the base of the projectile which consists of a series of peaks caused by the arrival and reflection of shock waves. Between the peaks the pressure falls rapidly, resulting in a longer acceleration distance than would be the case if the pressure were more nearly constant.

One way to reduce the drop between peaks is to generate a second shock wave (or more) which will arrive at the projectile between the arrivals of the primary shock and thus provide a more nearly constant base pressure. A few computer runs were made during the project to see how practical such a system might be. Figure 3.1 shows the time-distance plot for one of the more successful runs. An initial barrel length of 170 cm filled with helium at 20 bars had a piston driven down it at 6 mm/μsec. After this piston had gone 120 cm and the shock was at 160 cm, the piston velocity was changed to 12 mm/μsec, generating a second shock. The figure follows the action as these two shocks reflect back and forth between the piston and a 0.5 g/cm^2 projectile.

The first shock applied 8.5 kbar to the projectile; this decayed slowly to about 4.6 kbar by the time the second shock arrived. Although the timing of this second shock was good, its magnitude was too great, since the pressure after its reflection was 54 kbar. These peak pressures

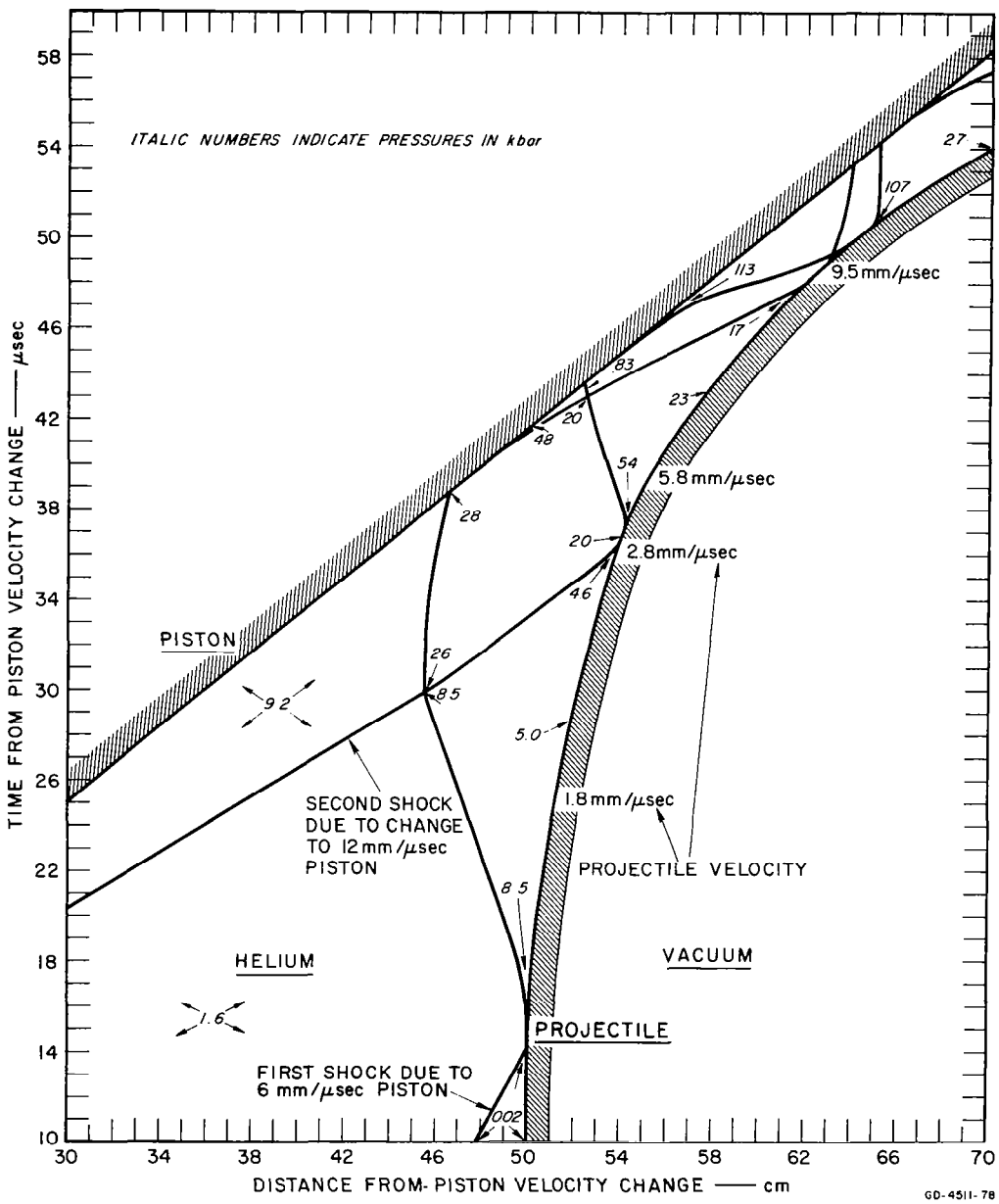

FIG. 3.1 CALCULATED BEHAVIOR OF DOUBLE SHOCK SYSTEM

continued to rise as the piston and projectile got closer and closer together. At the closest approach, the pressure reached 107 kbar and the original 170 cm of gas had been compressed into about 4 cm.

Although the pressures reached in this experiment are much higher than desired, it is encouraging to see that a system of multiple reflecting shocks can be set up and maintained for a reasonable length of time without coalescing. In this way, many closely spaced pulses can be applied to a projectile. Additional calculations will be required before a workable design can be chosen, but this concept looks very promising as a means of reducing launcher length.

3.2 CONTROL OF SECOND SHOCK ARRIVAL

In a single shock gun of constant piston velocity, the first shocks and the reflected shock will produce identical peak pressures on the projectile only if the gas mass is about equal to the projectile mass. As we have shown earlier, this may often lead to an excessively long gun, and it was decided to see if this condition could be circumvented.

The technique discovered for controlling the second shock arrival pressure is to change the velocity of the piston just at the time when the shock reflects off it. In the extreme case of a very massive projectile, for example, after the shock reflects from the projectile all the gas between the projectile and the reflected shock is stationary. Thus, if the piston is brought to a halt just as the reflected shock reaches it, the whole system will be at rest and all the gas will be at the reflected shock pressure. Extensive calculations of cases with finite-mass projectiles have not been made, but it appears that if, at the time the shock reflects from the piston, the piston velocity is set equal to the projectile velocity, the pressure produced on the projectile when this reflected shock reaches it will not be more than the pressure produced at first arrival.

3.3 ACCELERATING PISTON CALCULATION

It was determined that the first and second shock pulses can be controlled by the techniques described above; it then remained to be established what the remainder of the piston velocity history should be. One computer run was made in which the piston velocity was programmed to follow the projectile at a constant distance as it accelerated. The time-distance plot of this run is shown in Fig. 3.2.

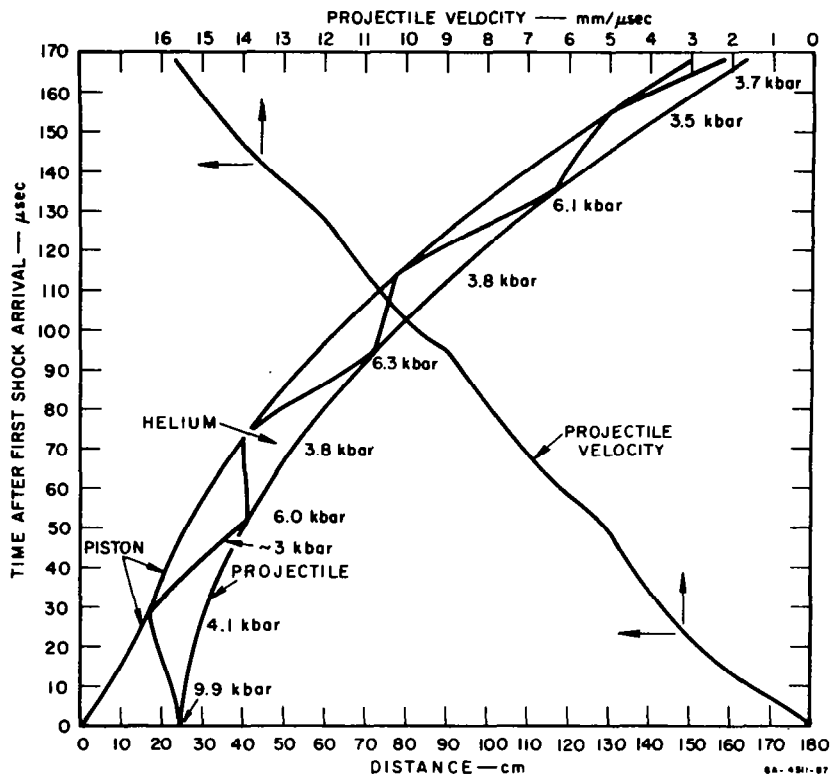

FIG. 3.2 CALCULATED ACCELERATION OF A PROJECTILE BY AN ACCELERATING PISTON

The piston velocity was initially 6.3 mm/μsec, the helium pressure was 20 bars, and the coaxial explosive driver tube length was 100 cm. The helium was treated as a perfect gas, and a projectile of 0.5 g/cm^2 was to be accelerated. As shown in the figure, the helium driver shock arrived at the projectile at t = 0, at which time the piston was 25 cm behind the projectile. Under these conditions, the incident helium shock velocity was 9.4 mm/μsec, which raised the gas pressure to 1.6 kbar. Upon reflection from the projectile base, the pressure rose to 9.9 kbar and a shock propagated back toward the piston, arriving there after about 30 μsec. The program was then directed to set the piston velocity equal to the projectile velocity and to reset it to the new velocity at every step thereafter. Thus the piston was made to follow the projectile at a constant distance.

At the first resetting, the projectile velocity was about 4 mm/μsec; therefore the piston velocity was decreased to that value. The reduction weakened the reflected shock sufficiently that, when it reached the piston, it raised the pressure to only 6 kbar. Since the gas mass did not equal the projectile mass, the second pressure peak ordinarily would have been higher than the first one. After about 30 μsec more, the velocities had risen again to 6.3 mm/μsec, and the end of the run, 140 μsec after the first resetting, the velocities were 15.8 mm/μsec. During the entire acceleration process a single shock was reflecting back and forth between the projectile and the piston, making almost four round trips in all. Each time the shock arrived at the projectile, the base pressure rose to slightly over 6 kbar and then fell to approximately 3 to 4 kbar before the next shock arrival. The comparatively uniform pressure resulted in efficient acceleration. The average acceleration was 0.094 mm/μsec^2, (approximately 10^7 g), and the projectile reached 15.8 mm/μsec after traveling only 140 cm.

3.4 ACCELERATING PISTON DESIGN

The gun operation calculated in Section 3.3 appears very promising; it is therefore interesting to see if such a programmed piston velocity history can actually be produced. The conical high velocity shots described in Section 2.5.2 showed that the maximum velocity called for here is feasible; the only question then, involves the size of a device which will give the correct intermediate history.

Figure 3.3 illustrates the geometry of the situation. For this calculation it is assumed that a shell of aluminum is driven across an air gap at a constant velocity, V, and that this velocity vector is perpendicular to the axis of symmetry at all points. We also will assume that the component of the detonation velocity parallel to the axis is constant and equal to the detonation velocity, D. These approximations are reasonable, provided the slope of the shell is not large.

We define $t = 0$ as the time the detonation starts at the point of origin. Then the shell will impact at x at a time, t, given by:

$$t = \frac{x}{D} + \frac{r}{V}$$

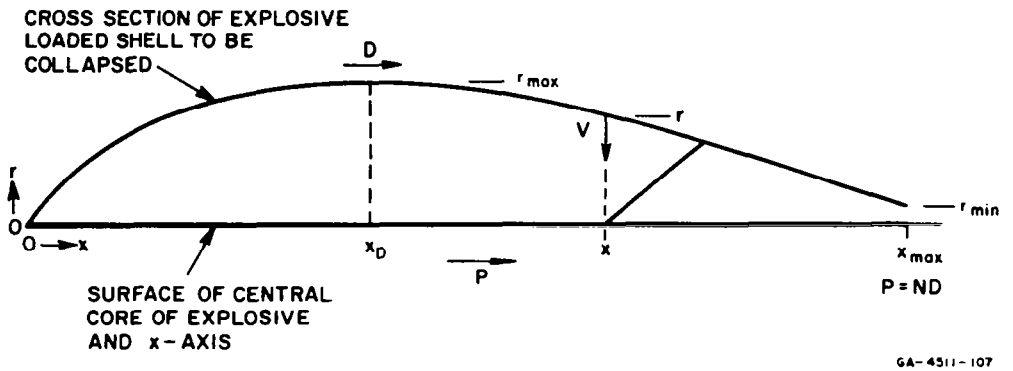

FIG. 3.3 GEOMETRY OF SHELL DESIGN FOR A CONSTANTLY ACCELERATING PISTON

We wish to have the phase velocity, P, of the point of impact increase with constant acceleration, a, so:

$$x = \frac{1}{2} a t^2 \quad \text{and} \quad t = \sqrt{\frac{2x}{a}}$$

Substituting this for t in Eq. (3.1), we solve for r:

$$r = V\left[\sqrt{\frac{2x}{a}} - \frac{x}{D}\right] \tag{3.2}$$

to get the equation of the curve.

The value of x at the point where the phase velocity is equal to the detonation velocity is x_D, given by

$$x_D = \frac{D^2}{2a}$$

If the final phase velocity is given by ND, then the total length will be:

$$x_{max} = \frac{N^2 D^2}{2a}$$

Since a real design would probably start at the point where $P = D$, the length required will be

$$x_{max} - x_D = \frac{D^2}{2a}(N^2 - 1) \tag{3.3}$$

The maximum r occurs at x_D and is given by

$$r_{max} = \frac{VD}{2a}$$

The minimum r of interest in a real design occurs at x_{max} and is given by

$$r_{min} = \frac{VND}{a}\left(1 - \frac{N}{2}\right)$$

and the difference between these two radii is

$$r_{max} - r_{min} = \frac{VD(N-1)^2}{2a} \qquad (3.4)$$

To get a rough idea of the dimensions of such a device, consider the case for $D = 10^6$, $a = 10^{10}$, and $V = 10^5$; these cgs values are of the right order of magnitude for a real case.

When $N = 2$:

$$x_{max} - x_D = 150 \text{ cm}$$

and

$$r_{max} - r_{min} = 5 \text{ cm}$$

When $N = 3$:

$$x_{max} - x_D = 400 \text{ cm}$$

and

$$r_{max} - r_{min} = 20 \text{ cm}$$

These values show that a design to provide a piston moving at twice detonation velocity should be quite straightforward. The diameter of a shell giving three times detonation velocity is rather large, but could be cut down by dividing the shell into sections. Each section would have the proper slopes but the radii would be reduced so that the smallest end of each section would just touch the central explosive. Separate initiation systems would be provided for each section to allow proper sequencing.

3.5 STOP-START GUN DESIGN

It has become clear during this project that a truly high performance gun must allow the piston to continue past the original projectile position and follow the projectile down the launch tube. The all-steel gun was studied as one of the simplest of such designs. Since its performance was not very close to the predicted values, the simple continuous-tube design may have to be modified to provide increased tube confinement where the early stages of acceleration take place. This increased confinement will probably make it impossible to collapse this part of the tube satisfactorily, so the piston will have to stop at the projectile and then be reformed later at some point a short distance away.

Figure 3.4 shows a time-distance plot of a design which has been studied using the computer code. Nitromethane was assumed as the explosive and a 0.5 gm/cm^2 projectile was to be accelerated. The initial pressure was 12.4 bars which resulted in peak pressures between 5 and 10 kbar. On the basis of our experience with the glass launch tubes described in Section 2.2.4, we assumed that a heavy launch tube would be required only until the projectile velocity had reached 4 $mm/\mu sec$.

With the first computer run we studied what happened when the piston was stopped at the projectile position and not restarted. From this run the early projectile acceleration was determined, so that the point at which velocity exceeded 4 $mm/\mu sec$ could be found. In addition, the trajectories of the gas cells near the piston could be followed to aid in determining the best time to restart the projectile. (These are the trajectories shown in the figure.)

The time chosen for restarting the piston was on the extrapolated time-distance line of the original piston. This time is experimentally convenient, since the detonation can be led around the heavy walled section without any complicated delays or auxiliary initiation systems.

Three runs were made with the piston restarted. In one, the restarted piston continued at 6.35 $mm/\mu sec$. The second had it restart at 7.1 $mm/\mu sec$ and then shift to 7.9 and 8.5 $mm/\mu sec$ as the projectile accelerated. This second run showed that all the velocity shifting took place in a time short compared to the shock transit time from piston

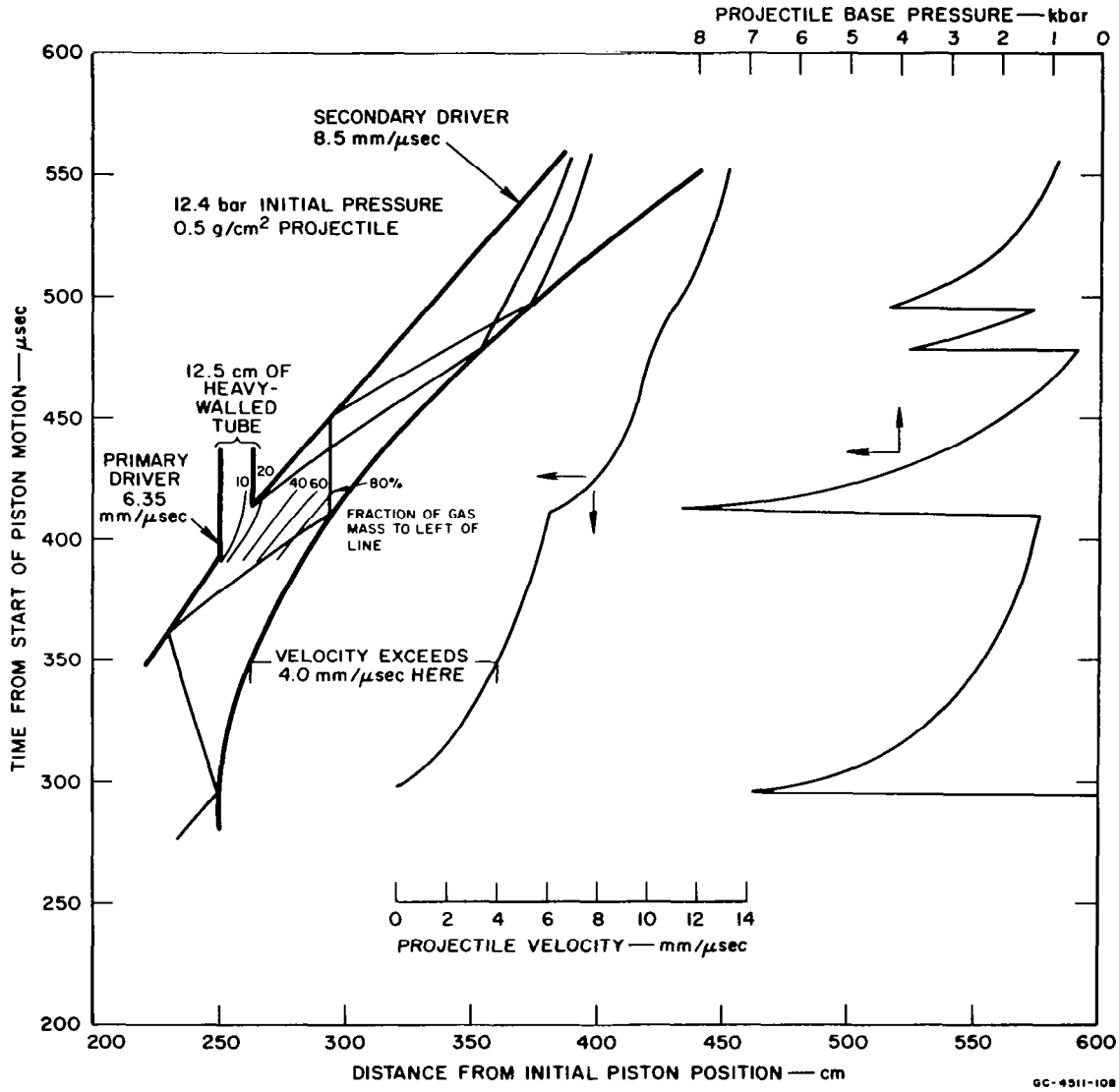

FIG. 3.4 CALCULATED OPERATION OF A STOP-START GUN

to projectile. The run shown in Fig. 3.4 was therefore made. In this run the restarted piston moved immediately at 8.5 mm/μsec; this is the detonation velocity of Octol and is close to the maximum detonation velocity available.

The calculated behavior of this design looks quite attractive. The second pressure peak is higher than is desirable; to offset this, additional gas mass should be included in a future run. Only 13% of the gas is lost when the piston is restarted; this loss might be reduced in a real gun if the glass jet has enough mass to push additional gas through the heavy-walled section. For higher performance a detonation speeded up by a conical collapsing driver should be added almost immediately after the transition section so that pressures will not fall off in the later stages.

SECTION 4

THEORETICAL CALCULATIONS

4.1 HELIUM GAS

To make accurate theoretical estimates of the magnitudes of the viscous boundary layer, the thermal boundary layer, and radiation energy transfer, and the influence of ionization on flow calculations, it is first necessary to determine the temperature, density, pressure, internal energy, and degree of ionization in the shocked gas of the gas gun driver. In addition, if the real gas effects produce an appreciable deviation from the state predicted by perfect gas theory, a reasonably accurate method of calculating the state of the driver gas at high internal energies must be included as a subroutine in the computer code for dynamic gas gun calculations.

For these reasons a relatively simple computer code was developed which calculates the thermodynamic state of helium gas behind a plane, steady shock front driven by a constant velocity piston. The thermodynamic state reached when this shock reflects from a rigid wall is also calculated. The simplified hydrodynamic situation allows most of the computational effort to be directed toward the calculation of thermodynamic quantities, yet is closely related to the actual situation in the gas gun.

The thermodynamic states so obtained may be considered upper bounds of internal energy, temperature, pressure, and density, since the action of a finite mass piston and a finite mass projectile will be to propagate relief waves into the shocked gas. As a consequence, the boundary layer, radiation, and ionization effects calculated on the basis of this idealized situation will be conservative upper bounds on the behavior in the actual gas gun.

The idealized gas gun also allows us to separate the difficulties associated with integrating the complete hydrodynamic equations from the problems of computing the thermodynamic state, and enables us to

concentrate on developing an effective subroutine for calculating the latter. This subroutine may then be easily included in the hydrodynamic calculations of the complete gas gun code.

Helium is a noble gas, and its two electrons are very tightly bound to the nucleus. As a consequence it is the most difficult of all gases to ionize. The first and second ionization potentials of helium are 24.46 and 54.14 volts, respectively. If we consider the maximum expected shock velocity in the helium to be 15 km/sec, the corresponding kinetic energy per atom of helium would be no more than 4.22 electron volts. At this energy level we expect a significant fraction of the helium atoms to become singly ionized, but any second ionization ought to be negligible.

The thermodynamics of the situation will determine how much of this kinetic energy will be converted by the shock into thermal energy, into interaction energy, into energy of ionization, and into residual kinetic energy.

The effects of interatomic forces on the thermodynamic properties of helium (real-gas effects) are fairly small at high temperatures. From the calculations of Harrison[6] we may conclude that for temperatures above 10,000°K and pressures lower than 3 kbar the interaction energy is less than 1% of the ideal gas internal energy. When ionization occurs, the forces of interaction are electromagnetic in nature and are strong compared with the interactions between neutral helium atoms. However, if the degree of ionization is small we should not expect a significant contribution of the interaction energy to the energy of the gas.

There is considerable theoretical difficulty involved in obtaining an accurate equation of state when the electron-ion interactions are included. A rather large number of approximate schemes for estimating these ionization correction terms in the equation of state has appeared in the recent literature.[7,8] For the present we shall neglect interaction corrections and consider each species to be a perfect gas, an approximation for which there is a well-developed statistical theory.

We assume the shocked helium to be a mixture of the three species He, He^+, and e^-, each of which is a perfect gas. Within the mixture we allow the chemical reaction

$$He \rightleftharpoons He^+ + e^- \qquad (4.1)$$

and define an ionization fraction by the ratio of the number of helium ions to the original number of helium atoms:

$$\alpha = \frac{n(He^+)}{n_0} \tag{4.2}$$

The fact that in general the equilibrium ionization ratio depends upon temperature and pressure indicates that the mixture of perfect gases is no longer a perfect gas. The equation of state of the ionizing gas may not be simply expressed, although the equation of state of each component is readily calculated.

For statistical calculations, the most convenient independent state variables are the temperature and molar volume; the thermodynamic function associated with these variables is the Helmholtz free energy function, F, defined by the relation

$$F = E - TS \tag{4.3}$$

where E is the internal energy, T the temperature, and S the entropy of the gas. For convenience in discussing the thermodynamics we shall consider all extensive variables, such as volume, internal energy, Helmholtz free energy, etc., to be taken with respect to one mole of the substance in question. The molar Helmholtz function is related to the statistically derived partition function Z, through the equation

$$F = -\mathrm{R}T\ell nZ(V,T) \tag{4.4}$$

where R is the universal gas constant.

The partition functions may be derived from statistical quantum mechanics or spectroscopic data on atomic energy levels, or both. A common approximation to the exact partition function for a single atom is to use spectroscopic data for the electronic energy levels within the atom, and to use the results of a quantum mechanical calculation for the translational energy levels within a volume V.

A certain amount of judgment must be exercised in calculating the partition functions associated with the electronic energy levels, for the exclusion of interaction effects generally causes the sum over an

infinite number of energy levels to diverge. A variety of schemes has been proposed* to avoid this divergence by summing only over a reasonable number of energy levels. For our purposes we shall include only the first few energy levels, a practice which is supported by a number of similar calculations[9,10] of the equation of state of helium gas. The partition functions for each species, which we consider good approximations for temperatures less than 50,000°K, are given by the expressions:

$$Z(\mathrm{He}) = V\left(\frac{2\pi M}{h^2}kT\right)^{3/2}(1 + 3e^{-230,000/T} + 13e^{243,000/T}) \qquad (4.5)$$

$$Z(\mathrm{He}^+) = V\left(\frac{2\pi M}{h^2}kT\right)^{3/2}(2 + 8e^{-473,000/T}) \qquad (4.6)$$

$$Z(\mathrm{e}^-) = V\left(\frac{2\pi m}{h^2}kT\right)^{3/2}(2) \qquad (4.7)$$

In these equations V is the molar volume of the species, M is the mass of the helium atom, m is the mass of the electron, h is Planck's constant, and k is Boltzmann's constant. These partition functions contain all the detailed information we shall need concerning the thermodynamic behavior of each species.

The molar Helmholtz free energy of each component of the ionized helium gas is determined from the partition function through the application of Eq. 4.3. This free energy is calculated from a zero point based on the ground state of the system. In order to account for the difference in ground state energy between the helium atom and the helium ion, we must include in the free energy of the latter a dissociation energy, D, of 24.46 electron volts.

Since we have neglected interaction energies, the free energy of the mixture of ions, electrons, and neutral atoms is given simply by adding the free energies of each species. If we start with one mole of neutral helium, then upon ionization we have $(1 - \alpha)$ moles of the neutral gas, α moles of the ion, and α moles of electrons. The common volume

* For a bibliography of these efforts, see Refs. 7 and 8.

we take to be V, so that the molar volumes are inversely proportional to the number of moles. The free energy of the ionized helium may thus be written in the form

$$F(\alpha, V, T) = (1 - \alpha)F_{He}\left(\frac{V}{1-\alpha}, T\right) + \alpha F_{He^+}\left(\frac{V}{\alpha}, T\right) + \alpha F_{e^-}\left(\frac{V}{\alpha}, T\right) + \alpha D \tag{4.8}$$

The Helmholtz free energy function is a complete equation of state in that all thermodynamic functions may be derived from it. For example, we have

$$P = -\left(\frac{\partial F}{\partial V}\right)_{T,\alpha} \tag{4.9}$$

$$S = -\left(\frac{\partial F}{\partial T}\right)_{V,\alpha} \tag{4.10}$$

$$E = F + TS \tag{4.11}$$

$$H = F + TS + PV \tag{4.12}$$

$$G = F + PV \tag{4.13}$$

The equilibrium value of the ionization fraction is given by the condition that at equilibrium the Helmholtz free energy must be a minimum with respect to variations in α; hence we have

$$\left(\frac{\partial F}{\partial \alpha}\right)_{T,V} = 0 \tag{4.14}$$

For later reference we shall indicate here the results of calculations concerning the pressure, enthalpy, and equilibrium ionization fraction. Rather than expressing the result in molar quantities, we shall choose as the basic quantal unit a unit mass of neutral helium gas. We introduce the gas constant per unit mass of helium:

$$R = \frac{\mathcal{R}}{M} = \frac{8.3144 \times 10^7}{4.003} = 2.077 \times 10^7 \text{ ergs/°K - gm} \tag{4.15}$$

It is convenient to express the thermodynamic functions in terms of a unit mass of gas, and to denote them by lower case letters. Expressing the numerical quantities in cgs units and the Kelvin scale of temperature, we obtain

$$pv = (1 + \alpha)RT \tag{4.16}$$

$$e = (1+\alpha)\frac{3}{2}RT + (1-\alpha)R\left\{\frac{3\times 2.3\times 10^5 e^{-2.3\times 10^5/T} + 13\times 2.43\times 10^5 e^{-2.43\times 10^5/T}}{1 + 3e^{-2.3\times 10^5/T} + 13e^{-2.43\times 10^5/T}}\right\}$$

$$+ \alpha R\left\{\frac{8 \times 4.73 \times 10^5 e^{-4.73\times 10^5/T}}{2 + 8e^{-4.73\times 10^5/T}}\right\} + \alpha R(2.85 \times 10^5) \tag{4.17}$$

$$\alpha = \sqrt{\frac{k(T)}{p + k(T)}} \tag{4.18}$$

where

$$k(T) = (0.333)T^{5/2}\left\{\frac{(2 + 8e^{-4.73\times 10^5/T})(2)e^{-2.85\times 10^5/T}}{(1 + 3e^{-2.3\times 10^5/T} + 13e^{-2.43\times 10^5/T}}\right\} . \tag{4.19}$$

This is the basic set of thermodynamic equations which must be solved simultaneously to obtain an equation of state for ionizing helium gas. An iterative scheme for this purpose has been developed which successfully calculates pressure, temperature, degree of ionization, and speed of sound as functions of the density and internal energy of the gas. The program is written in such a way that it can be included as a subroutine either in the Hugoniot calculations or in the complete flow calculations.

The iteration proceeds by a Newton-Raphson technique using temperature as the variable. The difference between calculated and given values of the internal energy is tested, and when the relative deviation is less than some predetermined accuracy (usually 10^{-5}) the iteration stops. The number of iterations required depends upon an initial guess for the temperature. If the guess is reasonably good (as it is in a

flow computation if the previous temperature of a cell is taken as the guess), the iterative procedure converges in one or two iterations.

4.2 HUGONIOT CALCULATIONS

Using a standard notation, the Hugoniot jump conditions in a hydrodynamic material are:

$$\rho_0(u_s - u_0) = \rho_1(u_s - u_1) \tag{4.20}$$

$$p_1 - p_0 = \rho_0(u_s - u_0)(u_1 - u_0) \tag{4.21}$$

$$e_1 - e_0 = \frac{1}{2}(p_1 + p_0)\left(\frac{1}{\rho_0} - \frac{1}{\rho_1}\right) = \frac{1}{2}(p_1 + p_0)(v_0 - v_1) \tag{4.22}$$

Assuming we know all quantities associated with the initial state, we have five unknowns: u_s, u_1, ρ_1, e_1, p_1. The three equations shown above and a thermodynamic relation connection p, ρ, and e reduce the number of independent unknowns to one. The shocked state is therefore completely specified by any one of the unknowns. For the implosive gas gun driver the most useful variable was found to be the particle velocity, u_1.

The basic problem is, given a thermodynamic specification of the material in the form $p = p(\rho, e)$, to find a method for determining the flow variables in the shocked state. One technique in common use is the graphical technique, in which a portion of the Hugoniot curve defined by Eq. 4.22 is sketched in the p-v plane and graphical constructions are used to obtain the shocked state. Several difficulties prevent this method from being useful in studies of the implosive driver. In the first place it is not possible to solve directly for the Hugoniot line, so an iterative technique must be used for each calculated point. Second, even were such a Hugoniot constructed, it would be valid only for a particular initial state. The construction would be useless in comparative studies based on a varying initial pressure, and it would be useless in obtaining the state of reflected shocks. Thus the large number of calculations that would go into the construction of a single Hugoniot curve would be to a large degree unnecessary.

A different approach was tried during this project. A procedure was developed which obtained directly the shocked state, given the particle velocity, with a minimum of numerical calculations. We first eliminate the shock velocity from the mass conservation equation (Eq. 4.20):

$$\mu(u_s - u_0) = (u_1 - u_0) \tag{4.23}$$

where we define

$$\mu = 1 - \frac{\rho_0}{\rho_1} \tag{4.24}$$

If we now eliminate the shock velocity from Eq. 4.21, we obtain

$$p_1 = p_0 + \frac{\rho_0}{\mu}(u_1 - u_0)^2 \tag{4.25}$$

Eliminating the pressure from Eq. 4.22 we obtain

$$e_1 = e_0 + \mu\frac{p_0}{\rho_0} + \frac{1}{2}(u_1 - u_0)^2 \tag{4.26}$$

We now have the situation in which, given a value for μ, we may obtain values for p_1, ρ_1, and e_1. For a compressive shock, we have

$$0 < \mu < 1$$

and hence

$$e_0 + \frac{1}{2}(u_1 - u_0)^2 < e_1 < e_0 + \frac{p_0}{\rho_0} + \frac{1}{2}(u_1 - u_0)^2$$

$$p_0 + \rho_0(u_1 - u_0)^2 < p_1 < \infty$$

For every value of ρ_1, e_1 we may calculate a value of p from the thermodynamic relation $p = p(\rho_1, e_1)$. As a consequence, for every value of μ we may calculate the percentage difference between these two pressures:

$$F(\mu) = \frac{p - p_1}{p}$$

If $p(\rho, e)$ is bounded for finite values of ρ, e and approaches ∞ as ρ approaches ∞, then $F(\mu)$ goes continuously from $-\infty$ to +1.

From the knowledge that $F(\mu) > 0$ as $\mu \to 1$ and $F(\mu) < 0$ as $\mu \to 0$ we may bracket the root $F(\mu) = 0$. This corresponds to matching the thermodynamic description of the material with the shock jump conditions, and will obtain the desired state of the shocked material. It should be noted that the root is already necessarily bracketed between $\mu = 0$ and $\mu = 1$ regardless of the thermodynamic description of the material, so that a numerical search procedure need not be very sophisticated to find the root to any desired degree of accuracy.

The procedure chosen for the gas gun calculations is the "*regula falsi*" method dating back to Newton. A root of $F(\mu)$ is first bracketed within a small interval $\Delta\mu$ by the following method: if $F(\mu) > 0$ then change μ by $-\Delta\mu$; if $F(\mu) < 0$ then change μ by $+\Delta\mu$. We know that $F(\mu) = 0$ somewhere between the points μ_0 and μ_1 at which $F(\mu)$ changes sign, and proceed to an iteration defined by

$$\mu_{k+1} = \mu_k - \frac{F(\mu_k)}{G}$$

where G is the slope of the line connecting P_0 and P_1:

$$G = \frac{F(\mu_1) - F(\mu_0)}{\Delta\mu}$$

A program incorporating this iterative procedure was combined with the equation of state subroutine for ionizing helium, and several cases were calculated. In addition to the "real gas" computations for helium, calculations were performed for a perfect gas. The only change necessary in the program was to insert the equation of state for a perfect gas:

$$p = (\gamma - 1)\rho e$$

The calculations were carried out to an accuracy of five figures and rounded to four. Cases were run for initial helium pressures between 0.1 and 40 atmospheres, with piston velocities ranging from 5 to 15 km/sec. A representative sample of these calculations is shown in Figs. 4.1 through 4.6, including both the real gas and the perfect gas results.

The sharpest and earliest deviation from perfect gas predictions is found in the reflected shock velocity, Fig. 4.4. At a piston velocity of 10 km/sec, the reflected shock velocity in a perfect gas is about 26% higher than in the real gas. Since this reflected shock velocity will affect the timing of important events in the gas gun, it is necessary to include the nonperfect gas thermodynamics in the final gas gun code for initial shock velocities of 10 km/sec or higher.

It is interesting to note that, at piston velocities at which the change in the reflected shock velocity becomes apparent, the ionization fraction due to the first shock is less than 1/10th of 1 percent and rises to approximately 1 percent behind the reflected shock. This apparent anomalous influence of small amounts of ionization is partially due to the fact that a small percentage change in the ratio of velocities on either side of the shock in material coordinates becomes greatly magnified on transforming to laboratory coordinates. In addition, the deviation from perfect gas thermodynamics is compounded, since the calculated state behind the incident shock is the initial state for the reflected shock.

4.3 BOUNDARY LAYER CALCULATIONS

The initial shock propagating into undisturbed helium gas simultaneously accelerates the gas to a certain particle velocity and greatly increases its temperature. Consequently, just behind the shock front there is a discontinuous jump between the velocity and temperature of the gas and the velocity and temperature of the wall. Viscosity and thermal conduction tend immediately to diffuse these discontinuities into the gas, thereby producing zones of disturbance called the viscous and thermal boundary layers.

If either or both of these boundary layers penetrate deeply into the driver gas, the performance of the gas gun may be detrimentally affected. It is therefore necessary to estimate the thickness of both boundary layers for typical experimental situations. As a basis for

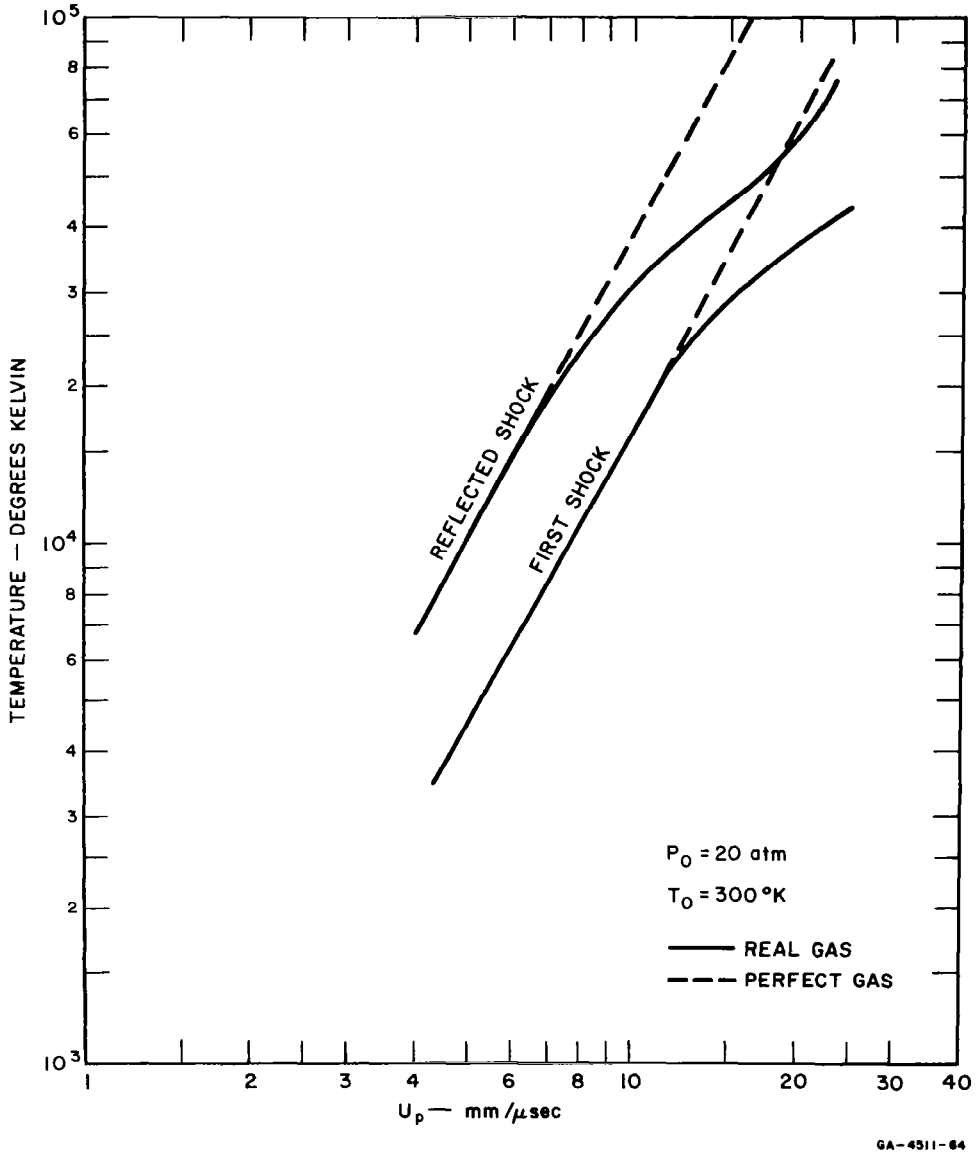

FIG. 4.1 HELIUM GAS GUN EQUILIBRIUM TEMPERATURES vs. PISTON VELOCITY

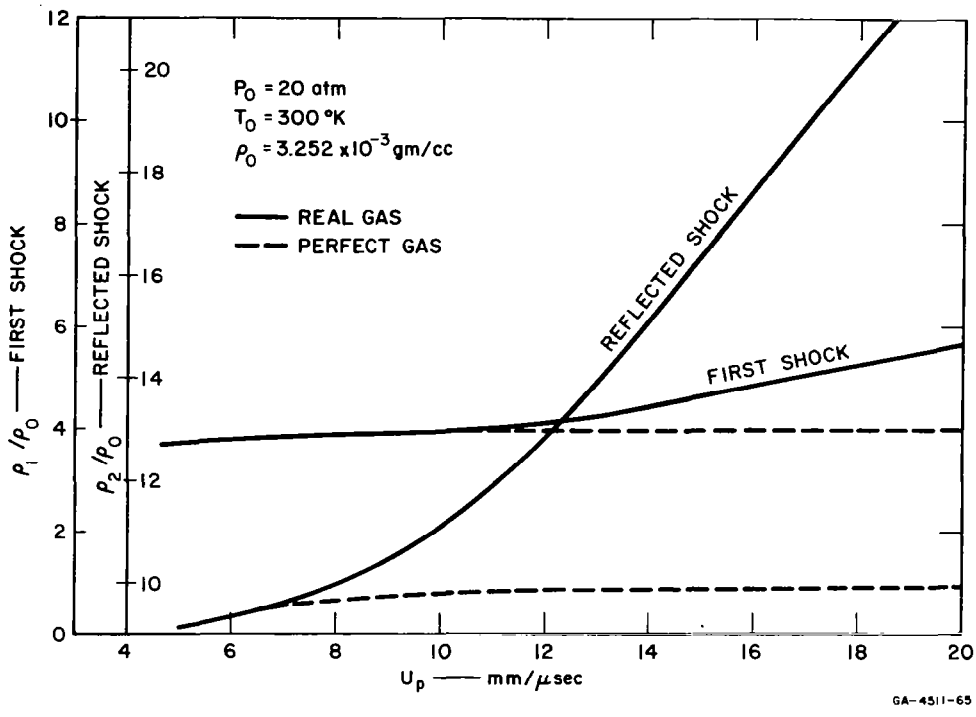

FIG. 4.2 HELIUM GAS GUN EQUILIBRIUM DENSITY RATIOS vs. PISTON VELOCITY

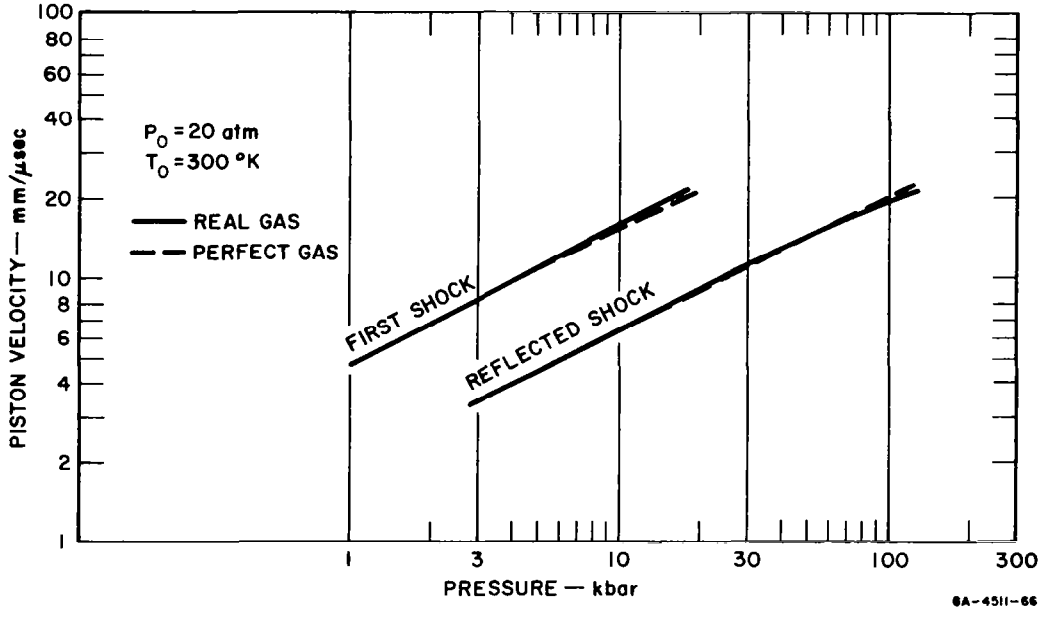

FIG. 4.3 HELIUM GAS GUN PRESSURE vs. PISTON VELOCITY

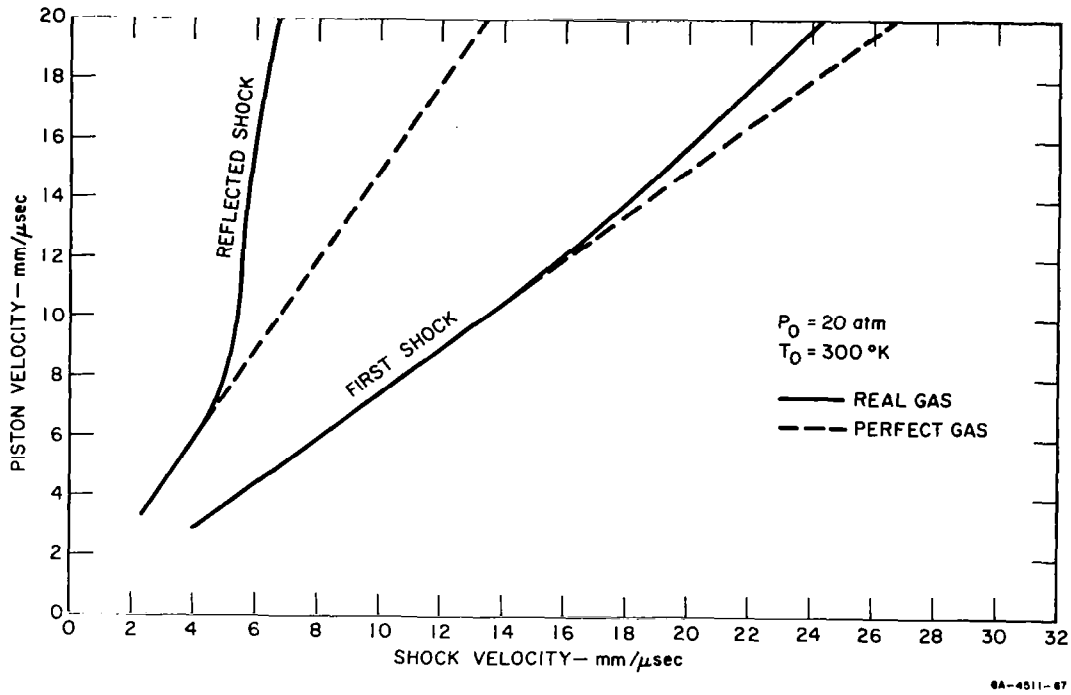

FIG. 4.4 HELIUM GAS GUN SHOCK VELOCITY vs. PISTON VELOCITY

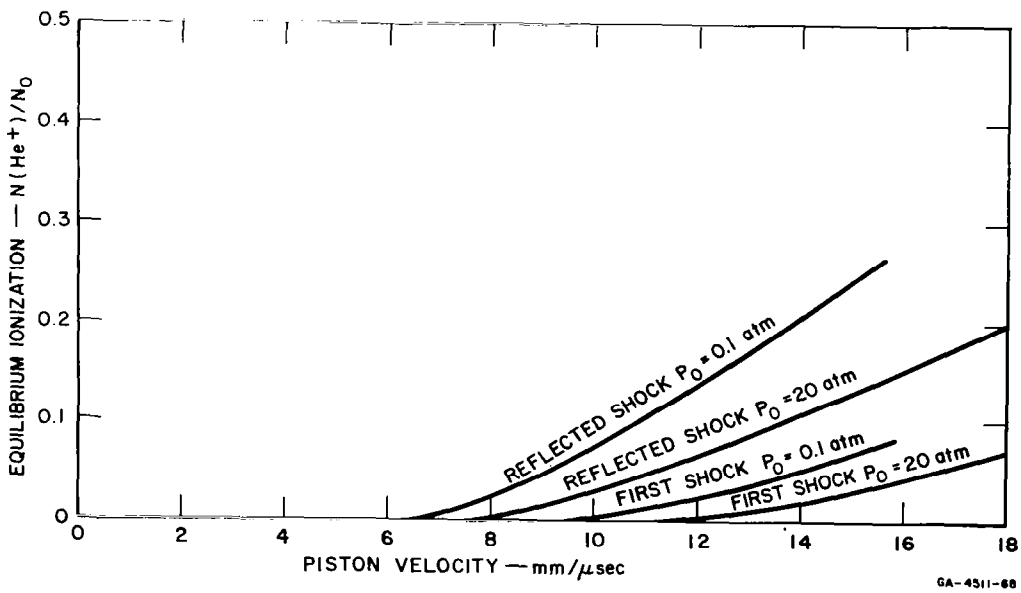

FIG. 4.5 EQUILIBRIUM IONIZATION IN HELIUM vs. PISTON VELOCITY

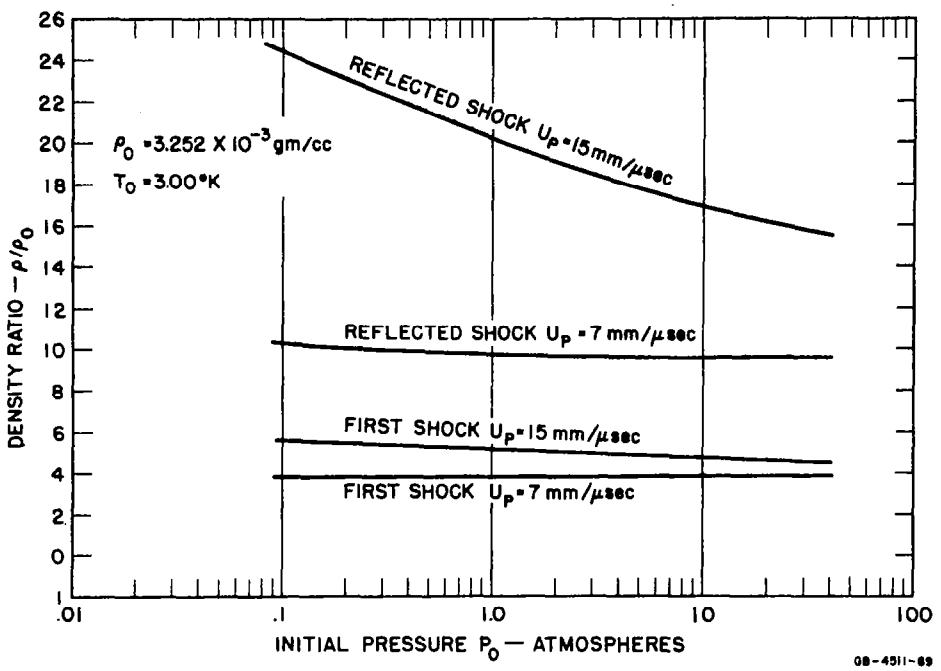

FIG. 4.6 HELIUM GAS GUN EQUILIBRIUM DENSITY RATIO vs. AMBIENT PRESSURE

these calculations we will use the velocities and thermodynamic states calculated for the idealized gas gun mentioned previously.

A steady, plane shock wave may most readily be considered in material coordinates, in which the shock front is stationary (see Fig. 4.7). In these coordinates the gas streams in from the left at a velocity $u_0 (= u_s)$ and streams out at the right at a velocity $u_1 (= u_s - u_p)$. The wall is moving to the right at a constant velocity $u_w (= u_s)$.

Characteristically, discontinuities in temperature and velocity diffuse into an undisturbed medium. As in all diffusion problems, the disturbance is contained approximately in a region bounded by a surface where $y/\sqrt{Dt}$ is a constant (D is the diffusivity of the medium), and the magnitude of the disturbance within this region is proportional to the magnitude of the discontinuity. In the boundary layer the disturbance is swept along with the stream at the velocity u_1; hence we have, approximately, the relation $x/u_1 = t$. As a consequence of the simultaneous influence of this convection and diffusion, the boundary layer is contained within a region bounded (see Fig. 4.7) roughly by

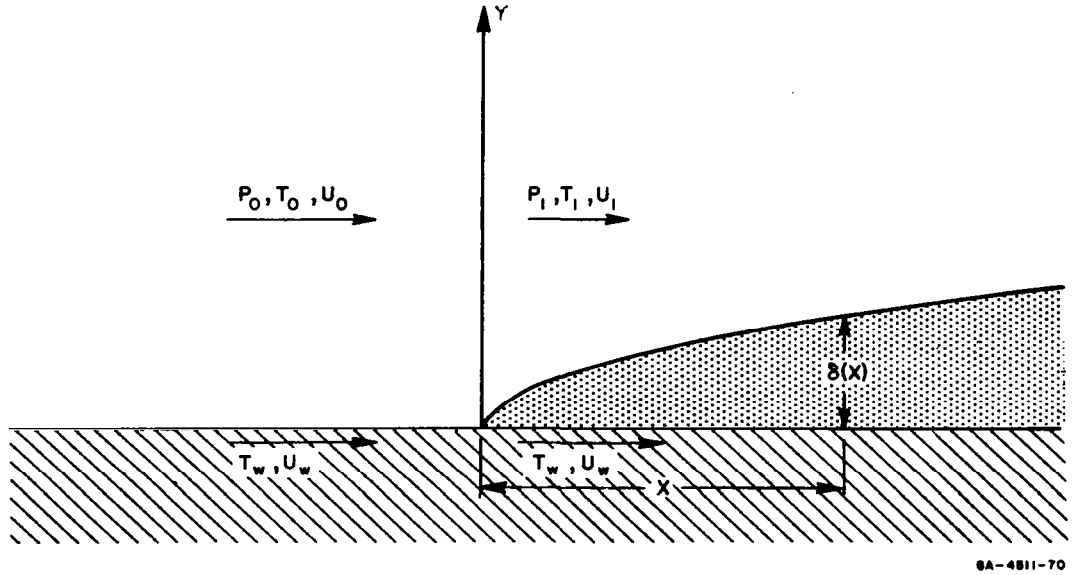

FIG. 4.7 BOUNDARY LAYER GROWTH BEHIND A SHOCK FRONT IN MATERIAL COORDINATES

$$\delta(x) = c\sqrt{\frac{Dx}{u_1}} \tag{4.27}$$

Here $\delta(x)$ is the thickness of the boundary layer, and c is a dimensionless parameter of order unity, whose exact value depends upon the definition of the edge of the boundary layer.

The diffusivities connected with thermal and viscous diffusion in a gas are given by

$$D_T = \frac{k}{\rho c_p} \tag{4.28}$$

$$D_\nu = \frac{\mu}{\rho} \tag{4.29}$$

and the boundary layer thicknesses are determined accordingly. (Here k is the thermal conductivity, μ is the viscosity, and c_p is the specific heat at constant pressure of the gas.)

These considerations may be justified in detail by reference to the complete Navier-Stokes equations for a viscous, heat-conducting gas, or by reference to a standard textbook on gas dynamics.[11] The order of magnitude of the boundary layer thicknesses calculated in this fashion is correct, even if the flow is complicated by turbulence.

Physically the situation remains much the same when ionization occurs within the gas. We must then consider an additional diffusion mechanism, that of the diffusion of chemical species (*i.e.*, ions, electrons, and neutral atoms) with the associated boundary layer. We do not expect the effects of this boundary layer on the performance of the gas gun to be appreciable, and it will be neglected.

The usual definition of boundary layer thickness is in terms independent of the magnitude of the discontinuity causing the disturbance. For example, we might define the edge of the thermal boundary layer by requiring that the temperature in the boundary layer achieve 90% of the difference between the wall temperature and the free-stream temperature. Such a definition is independent of the magnitude of the difference. However, this type of definition is rather poor for comparing the effects of two different discontinuities on the flow pattern.

A better definition for comparative purposes would be to define the edge of the boundary layer as a definite absolute disturbance, so that the boundary layer thickness vanishes when the discontinuity vanishes. As a consequence of this definition, the parameter c in Eq. 4.27 is a function of the strength of the discontinuity. It should be a monotonic function of the discontinuity, vanishing when the discontinuity vanishes. To obtain the correct functional form the exact boundary layer equations should be solved, but because of the difficulty of finding such a solution, the function was arbitrarily chosen to be the square root of the strength of the discontinuity. Further study may improve this estimate, but the order of magnitude of the calculated boundary layer thickness should be correct. We therefore assume the thicknesses δv and δT of the viscous and thermal boundary layers to be given by

$$\delta v = \sqrt{\left|\frac{u_1 - u_w}{u_1}\right|}\ \sqrt{\frac{\mu_1 x}{\rho_1 \mu_1}} \tag{4.30}$$

$$\delta T = \sqrt{\left|\frac{T_1 - T_w}{T_1}\right|}\ \sqrt{\frac{k_1 x}{\rho_1 c_p u_1}} \tag{4.31}$$

Using the values of shock temperatures and velocities computed for the simplified gas gun, we may calculate typical values of the boundary layer thickness. The results of these calculations appear in Table 4.1. The ratio of boundary layer thickness to driver tube radius is calculated for a standard experimental situation; the results are presented in Table 4.2. The standard configuration is taken to be a driver tube of 0.3-cm radius, with 30 cm of shock-compressed gas behind the shock (a highly conservative estimate).

Table 4.1

BOUNDARY LAYER THICKNESS
(CGS UNITS)

PISTON VELOCITY, u_p	INITIAL SHOCK		REFLECTED SHOCK	
	$\delta v/\sqrt{x}$	$\delta T/\sqrt{x}$	$\delta v/\sqrt{x}$	$\delta T/\sqrt{x}$
5×10^5	1.25×10^{-3}	1.14×10^{-3}	0	5.69×10^{-4}
9×10^5	1.41×10^{-3}	1.30×10^{-3}	0	6.41×10^{-4}
13×10^5	1.55×10^{-3}	1.42×10^{-3}	0	6.14×10^{-4}
17×10^5	1.69×10^{-3}	1.56×10^{-3}	0	6.46×10^{-4}

Table 4.2

MAXIMUM RATIO OF BOUNDARY LAYER THICKNESS TO DRIVER TUBE RADIUS FOR A STANDARD EXPERIMENTAL CONFIGURATION*

PISTON VELOCITY, u_p (mm/μsec)	INITIAL SHOCK		REFLECTED SHOCK	
	$\delta v/R$	$\delta T/R$	$\delta v/R$	$\delta T/R$
5	0.0228	0.0208	0	0.0104
9	0.0258	0.0238	0	0.0117
13	0.0284	0.0260	0	0.0112
17	0.0309	0.0285	0	0.0118

* 30-cm length of compressed gas behind the shock in a 0.3-cm-radius tube.

We may also obtain a rough estimate of the laminar heat transfer rate per unit area, q_T, from the driver gas to the walls of the driver tube:

$$q_T = k \left| \frac{T_1 - T_w}{\delta T} \right| \tag{4.32}$$

The turbulent heat transfer rate may be appreciably higher than the laminar heat transfer, and ionization effects would further increase the effect. However, the inclusion of these complications is extremely difficult and it would be necessary to rely heavily on experimental data which are at present unavailable. Calculation of the laminar heat transfer rate should give a reasonable order of magnitude estimate of the effect, but the results must be treated with caution.

Using the values for the thermodynamic state calculated for the simplified gas gun, the laminar heat transfer rate was calculated and is presented in Table 4.3. The initial rate of heat transfer is fairly high, but it falls off inversely as the square root of the distance from the shock front.

Table 4.3

LAMINAR HEAT TRANSFER RATE
(CGS UNITS)

PISTON VELOCITY, u_p	INITIAL SHOCK, $q\sqrt{x}$	REFLECTED SHOCK, $q\sqrt{x}$
5×10^5	6.95×10^{10}	5.65×10^{11}
9×10^5	3.98×10^{11}	2.76×10^{12}
13×10^5	1.02×10^{12}	5.40×10^{12}
17×10^5	1.48×10^{12}	8.26×10^{12}

In order to estimate the seriousness of the thermal power loss through the walls of the driver tube, the total power loss, Q_T, was computed for the standard configuration mentioned above and compared to the rate of work, $P_1 u_p$, performed by the piston on the driver gas. The results are given in Table 4.4. We may conclude from these computations that the energy loss due to thermal conduction may safely be neglected.

4.4 RADIATION EFFECTS

Referring to Fig. 4.1 we see that temperatures to be expected in the incident and reflected shocks in a helium gas gun with piston velocities of 5 to 15 km/sec range from 5000 to 45,000°K. In order to estimate the importance of radiative heat transfer at these temperatures

let us compute the blackbody heat transfer rate per unit area, q_R, defined in terms of the absolute temperature, T, and the Stefan-Boltzmann constant, σ:

$$q_R = \sigma T^4 \quad . \tag{4.33}$$

The results of this calculation, based on the temperatures calculated for the simplified gas gun, are shown in Table 4.5.

Table 4.4

MAXIMUM RATIO OF POWER LOST BY THERMAL CONDUCTION TO POWER SUPPLIED BY PISTON FOR A STANDARD EXPERIMENTAL CONFIGURATION*

PISTON VELOCITY, u_p (mm/μsec)	INITIAL SHOCK, $Q_T/P_1 u_p$	REFLECTED SHOCK, $Q_T/P_2 u_p$
5	0.0090	0.0131
9	0.0238	0.0183
13	0.0206	0.0192
17	0.0185	0.0158

* *30-cm length of compressed gas behind the shock in a 0.3-cm-radius tube.*

Table 4.5

BLACKBODY RADIATIVE HEAT TRANSFER RATE (CGS UNITS)

PISTON VELOCITY, u_p	INITIAL SHOCK, q_R	REFLECTED SHOCK, q_R
5×10^5	2.27×10^{10}	6.2×10^{11}
9×10^5	1.85×10^{12}	3.41×10^{13}
13×10^5	2.1×10^{13}	1.76×10^{14}
17×10^5	6.3×10^{13}	5.78×10^{14}

Let us assume as a first estimate that the emissivity of the helium is 1, so that the gas radiates like a blackbody. We may then compute the total rate of radiant heat loss, Q_R, for the standard configuration and compare it with the rate at which the piston does work against the driver gas, $P_1 u_p$. The results of this computation are shown in Table 4.6. Evidently a significant fraction of the driver energy may be lost through the tube walls for a piston velocity of 9-km/sec or more; in this case,

therefore, a more rigorous and accurate treatment of radiation losses should be included in performance calculations for the actual gas gun.

Table 4.6

MAXIMUM RATIO OF POWER LOST BY THERMAL RADIATION TO POWER SUPPLIED BY PISTON FOR A STANDARD EXPERIMENTAL CONFIGURATION*

PISTON VELOCITY, u_p (mm/μsec)	INITIAL SHOCK, $Q_R/P_1 u_p$	REFLECTED SHOCK, $Q_R/P_2 u_p$
5	0.00806	0.0394
9	0.116	0.379
13	0.461	0.660
17	0.631	0.889

* 30-cm length of compressed gas behind the shock in a 0.3-cm-radius tube; helium emissivity assumed to be unity.

4.5 FLOW COMPUTATIONS

A new computer technique was developed during this project for the purpose of integrating the equations of unsteady hydrodynamic flow. Several techniques are already available for these computations (*e.g.*, the von Neumann-Richtmyer method,[12] the Lax stagger scheme,[13] the Lax-Wendroff technique[14]), but several problems are encountered in applying them directly to the explosive driver computations.

The principal difficulty is the problem of introducing the proper thermodynamic description of the gas into the flow calculations. The von Neumann-Richtmyer scheme[12] requires an iteration between the thermodynamic specification of the material and the equations of motion, leading to an indeterminate number of calculations at each cell. Since it was expected that the time spent in thermodynamic computations would be appreciable, other techniques were investigated.

The Lax-Wendroff method[14] appeared to be the most appropriate for these calculations; not only is it completely explicit in its method of computation, but it also is several times faster than the von Neumann method. There is, however, a serious practical difficulty in that the Lax-Wendroff method requires the knowledge not only of the equation of state but also of the associated partial derivatives. As these are

generally difficult to obtain numerically, some thought was given to an extension or modification of the scheme.

The result of these investigations proved to be surprisingly simple conceptually. Rather than going into the development of the ideas which led up to the present state of the method, we shall describe as concisely as possible the technique as it is now used.

The first step is to write the equations of motion in a vector form:

$$\frac{\partial \vec{U}}{\partial t} = \overleftrightarrow{T} \frac{\partial \vec{F}}{\partial r} + \vec{G}$$

where the matrix $\overleftrightarrow{T}$ and the vectors $\vec{F}$ and $\vec{G}$ are nonlinear functions of $\vec{U}$, r, and t (if irreversible effects are included $\vec{F}$ is also a function of $\partial \vec{U}/\partial r$).

As an example of the equations of motion written in this form we may consider the equations actually used in the project:

$$\frac{\partial x}{\partial t} = u$$

$$\frac{\partial u}{\partial t} = -\frac{A(x)}{m(r)} \frac{\partial (p + q)}{\partial r}$$

$$\frac{\partial v}{\partial t} = \frac{1}{m(r)} \frac{\partial (Au)}{\partial r}$$

$$\frac{\partial e}{\partial t} = -\frac{(p + q)}{m(r)} \frac{\partial (Au)}{\partial r} - \frac{kT^4}{\rho \sqrt{A(x)}}$$

The vector $\vec{U}$ is given by (x, u, v, e); the functions $\overleftrightarrow{T}$, $\vec{F}$, and $\vec{G}$ are obtained by inspection of the equations of motion. The cross-sectional area $A(x)$ is presumed known, as is the equation of state $p(\rho, e)$.* The Lagrangian mass density $m(r)$ is computed from the initial state:

$$m(r) = \rho A \left. \frac{\partial x}{\partial r} \right|_{t=0}$$

*$\rho = 1/v$.

An artificial viscosity introduced by von Neumann[12] has been included to smooth shock discontinuities; it is defined by

$$q = \mu\rho\left(\frac{\partial u}{\partial r}\right)^2 \operatorname{sgn}\left(\frac{\partial u}{\partial r}\right)$$

where μ, a dimensionless variable, is chosen for the best results ($\mu = 2$ has proved satisfactory).

Having defined the independent variables $\vec{U}$ and the corresponding functions $\overleftrightarrow{T}$, $\vec{F}$, and $\vec{G}$, we may now proceed to the method of calculation. Suppose $\vec{U}$ is known at some time $t = n\Delta t$ at the points $r = j\Delta r$. We may then calculate the corresponding values of $\overleftrightarrow{T}$, $\vec{F}$, and $\vec{G}$:

$$\overleftrightarrow{T}_j^{\,n} \equiv \overleftrightarrow{T}\left(\vec{U}_j^{\,n},\ j\Delta r,\ n\Delta t\right)$$

$$\vec{F}_j^{\,n} \equiv \vec{F}\left[\vec{U}_j^{\,n},\ \left(\frac{\partial \vec{U}}{\partial r}\right)_j^{n},\ j\Delta r,\ n\Delta t\right]$$

where

$$\left(\frac{\partial \vec{U}}{\partial r}\right)_j^{n} \equiv \frac{\vec{U}_{j+1}^{\,n} - \vec{U}_{j-1}^{\,n}}{2\Delta r}$$

and so forth.

Having calculated these quantities we are now able to step forward in time. It is here that questions of stability arise, for not all methods of forward time-stepping are successful. Two basic principles may be invoked here to eliminate fruitless methods. The first principle is that a computed point must lie within the characteristic domain of dependence of the points on which the computation depends. The second basic principle is that a first order differential should be replaced where possible by a first order difference. The stagger scheme proposed by Lax[13] in 1954 for a special choice of the equations of motion satisfies both of these fundamental considerations, and we shall use it to step forward in time.

Let us first, however, consider an old and well-known method of integration familiar from ordinary differential equations. We put:

$$\frac{dy}{dt} = F(y,t) \quad .$$

The simplest method for stepping forward in time would be to put:

$$y^{n+1} = y^n + \Delta t F(y^n, t^n) = y^n + \Delta t F^n \quad ,$$

but this is accurate only to first order in Δt, as we can easily see by expanding $y(t)$ in a Taylor series. Hence only terms up to the first order in Δt agree. A second order accuracy is easily obtained by the following method:

$$y^{n+1} = y^n + \Delta t F\left(y^n + \frac{\Delta t}{2} F^n,\ t + \frac{\Delta t}{2}\right) = y^n + \Delta t F^{n+\frac{1}{2}} \quad .$$

This method is one of a general class of similar techniques known as Runge-Kutta techniques.[15] Exactly the same principle may be used with the stagger scheme to achieve second order accuracy in the continuum calculations.

We set:

$$\vec{U}_{j+\frac{1}{2}}^{n+\frac{1}{2}} = \left(\frac{\vec{U}_{j+1}^{n} + \vec{U}_j^n}{2}\right) + \frac{\Delta t}{2}\left[\left(\frac{\overleftrightarrow{T}_{j+1}^{n} + T_j^n}{2}\right)\left(\frac{\vec{F}_{j+1}^{n} - \vec{F}_j^n}{\Delta r}\right) + \left(\frac{\vec{G}_{j+1}^{n} + \vec{G}_j^n}{2}\right)\right].$$

Having obtained these "halfway" values $\vec{U}_{j+\frac{1}{2}}^{n+\frac{1}{2}}$, we may calculate the corresponding functions $\vec{T}$, $\vec{F}$, and $\vec{G}$. These values, now properly centered in r and t, are used to step $\vec{U}$ forward a full time step:

$$\vec{U}_j^{n+1} = \vec{U}_j^n + \Delta t\left[\left(\frac{\overleftrightarrow{T}_{j+\frac{1}{2}}^{n+\frac{1}{2}} + \overleftrightarrow{T}_{j-\frac{1}{2}}^{n+\frac{1}{2}}}{2}\right)\left(\frac{\vec{F}_{j+\frac{1}{2}}^{n+\frac{1}{2}} - \vec{F}_{j-\frac{1}{2}}^{n+\frac{1}{2}}}{\Delta r}\right) + \left(\frac{\vec{G}_{j+\frac{1}{2}}^{n+\frac{1}{2}} + \vec{G}_{j+\frac{1}{2}}^{n+\frac{1}{2}}}{2}\right)\right].$$

A simple Taylor series expansion indicates that the accuracy is of the second order in both Δr and Δt.

The principal advantage of this scheme is that stability and accuracy are obtained without ever requiring more than the explicit calculation of the functions $\overleftrightarrow{T}$, $\vec{F}$, and $\vec{G}$ in terms of known values of $\vec{U}$. Hence no iterations are necessary nor are thermodynamic derivatives ever required.

In addition, the method is superior to a similar method mentioned by Richtmyer[16] in that the choice of the vector variable $\vec{U}$ is arbitrary and need not be confined to the Lax conservation variables. This advantage is particularly important from a practical standpoint. The Lax conservation variables, although they lead to a convergent scheme and are fairly useful in some applications, are an extremely bad choice when the quasi-linear equations in a tube of varying cross sections are to be solved. Use of the Lax conservation variables leads to an anomalous situation in which gas at rest is accelerated in a region of varying cross section. This anomalous acceleration decreases as the square of the cell size, but useful results are not obtained without an excessive number of cells and an enormous increase in computation time.

The variables chosen for the calculations in this project are the position, velocity, density, and internal energy of a gas cell—the variables used in the popular von Neumann-Richtmyer technique. In fact, the method described above has many of the characteristics of the von Neumann-Richtmyer scheme. It would be interesting, to make a detailed comparison of the two methods.

The program that was written using the method described above has been used extensively to define useful operating regimes for the explosive gas gun and to test various concepts concerning the optimal characteristics of the explosive driver. Some of the results of these calculations are presented as "numerical experiments" in the experimental section of this report.

The convergence and stability of the method have been tested numerically, and accord very closely with theoretical predictions. In addition, numerical tests have been run in several cases in which the exact solutions are known, and no unusual behavior has been noted.

4.6 JET CALCULATIONS

The helium shock velocities observed in much of the work during the first year of this study were significantly higher than one would expect on the basis of a piston moving at detonation velocity. Typically, a nitromethane driver produces a shock of 9.5 to 10 mm/μsec velocity, which should require a piston moving at least 7.1 mm/μsec, well above the 6.3 mm/μsec detonation velocity of nitromethane. This high velocity suggests that, although a compact jet has never been observed in the coaxial glass design, some sort of a diffuse cloud of material may be pushed out ahead of the detonation front so as to give performance better than that expected. During the current year some theoretical effort was expended to see if the characteristics of this diffuse jet could be predicted so that a design which would maximize its mass could be determined.

4.6.1 Implosion Velocity Prediction

R. W. Gurney[17] has predicted with surprising accuracy the velocity of fragments produced by the detonation of a charge of explosive surrounded by a shell of metal. His method consists essentially of assuming a flow field for the detonation gases and applying the conservation laws. T. E. Sterne[18] extended the technique to a number of related cases and compared the results with a more accurate computation based on perfect gas dynamics. The results of the comparison indicate that the simple Gurney approach remains within a few percent of the more accurate approach over a fairly wide range of variables.

To calculate the velocity imparted to the inner wall of a cylinder by a concentric cylinder of high explosive we can use essentially the same technique. Assuming constant density in the explosive, a velocity varying linearly with the radius, negligible confinement on the outside of the explosive, and a liner thickness small compared with its radius, we arrive at an expression of the same form as the Gurney formula for flat plate acceleration:

$$V = \sqrt{2E}\ \sqrt{\frac{\frac{c}{m}}{R\frac{c}{m} + S + T\frac{m}{c}}}$$

where E is specific energy of the explosive, c is the mass per unit length of the charge, and m is the mass per unit length of the liner.

The values of R, S, and T depend only on the ratio of outside to inside diameter and have been calculated for values of this ratio from 1 to 50. These values are shown in Fig. 4.8.

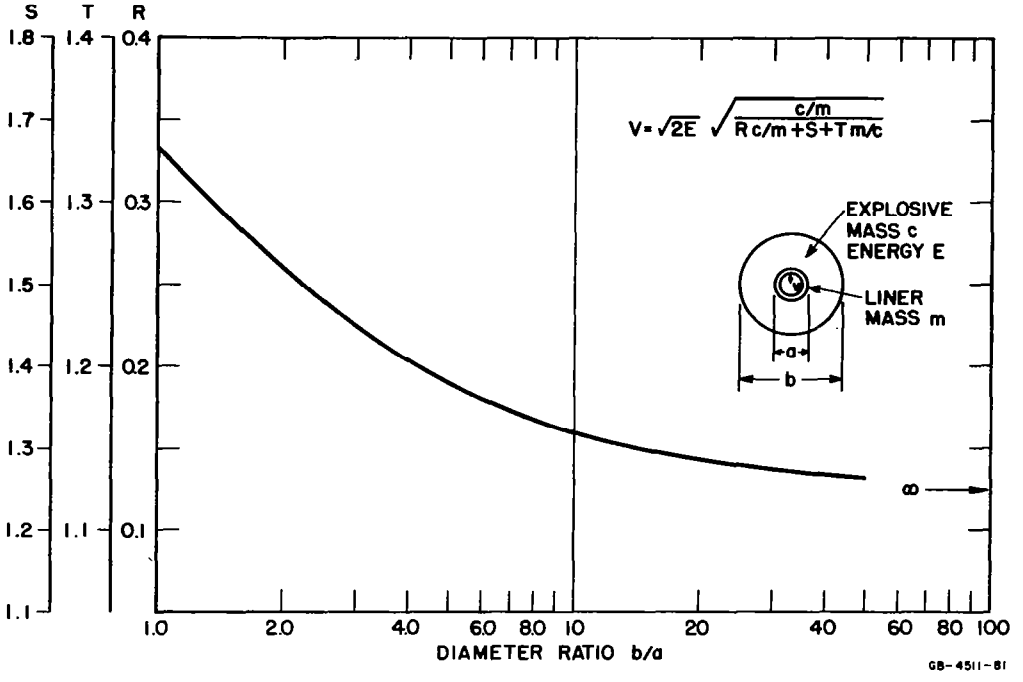

FIG. 4.8 COEFFICIENTS FOR THE GURNEY EQUATION FOR IMPLODING COAXIAL CYLINDERS

4.6.2 JETTING

If we follow Birkhoff's analysis[19] assuming hydrodynamic flow during the collapse process and negligible density change, it can be shown that the situation in Fig. 4.9 obtains when the process is viewed in a coordinate system moving with the detonation front. The mass in the jet under these circumstances is determined by the requirement of conservation of momentum. After the wall is turned and accelerated inward by the detonation front, there is an increase in the rightward-going axial momentum given by

$$p = mv^2/2D$$

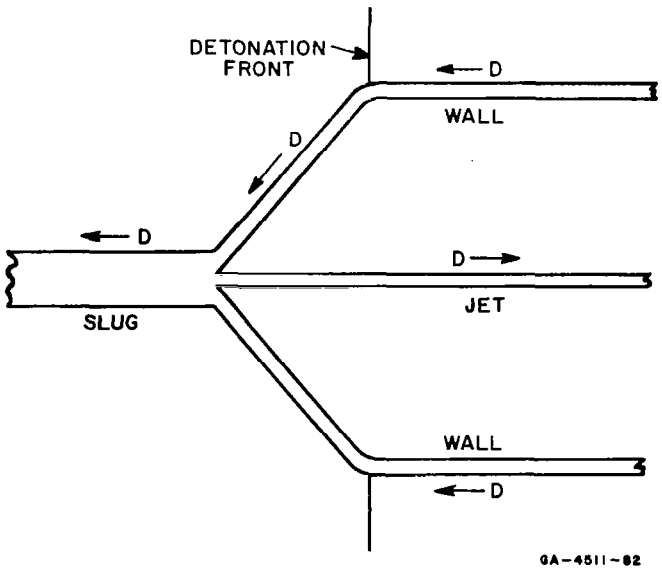

FIG. 4.9 JETTING PROCESS IN COORDINATES MOVING WITH DETONATION FRONT

where m is the wall mass per unit length and v is the inward-going radial component of the wall velocity. We now transfer to laboratory coordinates, in which the jet velocity is $2D$. After collapse this axial momentum manifests itself in the jet mass, m_j moving to the right. Thus:

$$2Dm_j = mv^2/2D$$

$$\frac{m_j}{m} = \frac{v^2}{4D^2}$$

Substituting the Gurney expression for the wall velocity we obtain:

$$\frac{m_j}{m} = \frac{E}{2D^2}\left(\frac{\frac{c}{m}}{R\frac{c}{m} + S + T\frac{m}{c}}\right)$$

A typical Comp B shot fired during this project has a c/m of 10 and a diameter ratio of 3. Taking a value of 2.7 mm/μsec for $\sqrt{2E}$ for Comp B, we would expect an implosion velocity of 4.34 mm/μsec and a m_j/m of 0.075. The implosion velocities actually observed by the X-ray unit for such shots range from 2.8 to 3.4 mm/μsec. This is the closest agreement between theory and experiment that has been observed on this project. Nitromethane shots, in particular, show a much lower implosion velocity than that predicted by theory, for reasons which are not now known. The m_j/m predicted for the theoretical collapse velocity of 4.34 mm/μsec is 0.075, and since the liner mass per unit length is about 1.0 g/cm, the jet mass per unit length should be 0.075 g/cm.

If the jet is spread out over the whole 11-mm tube diameter, the glass density will be 0.079 g/cm.[3] Since this is only about six times the shocked helium density, and the jet in the real case will probably give an even lower density, it does not seem likely that the glass cloud can be described as a rigid piston. It may give a temporarily higher shock velocity during the early stages of an experiment, but after that the only effect will probably be to change the details of later shock reflections from the piston. It seems reasonable to treat the tube collapse at the detonation front as the piston and to ignore the glass jet except for such second order effects. For this reason no further effort to optimize this aspect of the design was carried out.

SECTION 5

SUMMARY AND RECOMMENDATIONS

5.1 SUMMARY

The work reported here has experimentally demonstrated the operation of all the important parts of a high-performance, explosively driven launcher, including:

1. Acceleration of projectiles by shock pressures in the 5 to 10 kbar range through steel launch tubes (Section 2.2.2).
2. Transition, if necessary, to glass launch tubes and continued acceleration through them (Section 2.2.4).
3. Achievement of detonation phase velocities at least twice the normal detonation velocity (Section 2.5.2).
4. Computer design of a gun incorporating these parts which is theoretically capable of projectile velocities of 12 mm/μsec after 150 cm of acceleration (Section 3.5).

The theoretical understanding of the high performance explosively driven launcher has advanced significantly. The theoretical studies have been concerned with all phases of launcher operation, and include:

1. A study of the effect of nonideal gas behavior on the operation of the launcher and the inclusion of these effects in flow computations (Sections 4.1 and 4.2).
2. A study of the boundary layer effects on the operation of the launcher (Section 4.3).
3. A study of radiation loss from the shock-heated driver gas and the effects of this loss on launcher operation (Section 4.4).
4. A new method for numerically integrating the equations of motion of a compressible gas which can include radiative losses, an arbitrary thermodynamic equation of state, and an area change in the launch tube (Section 4.5).

5. A theoretical study of the implosion process, including the prediction of implosion velocities and jet mass (Section 4.6).

Fair agreement between theoretical and experimental performance has been shown. This agreement makes it reasonable to perform experiments with the computer, and the availability of the fast computer code has made this an economically attractive way to operate (the run resulting in Fig. 3.4, for example, cost less than $15.00).

In addition to the demonstration of the essentials of a gun, much theoretical and experimental work has been done on the refinements which will be required for a design approaching optimum. These include:

1. Low-velocity explosive development, which has progressed through preliminary stages. At present, velocities below the 6.3 mm/μsec of nitromethane are not readily available, but a small amount of additional work should provide velocities at least as low as 4 mm/μsec.

2. Multiple shock systems to provide more uniform acceleration have been studied by computer and have been shown to be feasible. Inclusion in a realistic gun design will require additional computer runs.

3. Methods for programming the piston motion, to make possible the required reductions in gas mass, have been investigated and a promising system has been found.

4. A constant acceleration piston design has been developed which appears reasonably easy to construct.

5.2 RECOMMENDATIONS FOR FUTURE WORK

With much of the basic work accomplished, the next objective should be to achieve the really high velocities predicted by computer runs such as that shown in Fig. 3.4. This design can be constructed in various ways. The primary driver can be glass or thin-walled steel; the heavy-walled tube can be thick-walled steel tubing, reinforced thin-wall steel tubing, or reinforced precision-bore glass tubing; and the secondary driver can be either thin-walled steel or precision-bore glass. The combination glass - thick-walled steel - glass design is the one which has been most studied here and gives the greatest freedom for explosive loading since significant jets are not formed. If the joint in the launch tube is objectionable, the glass could extend the full length of the launcher

and be surrounded by massive confinement for the first portion. To give the glass even more resistance to internal pressures in this region, it might be possible to cause the confinement to prestress the glass.

Only when a gun has been made to operate at velocities above 10 mm/μsec should additional work on optimization be attempted. Such work would include low-velocity explosive development, calculations on multiple shock designs and designs to reduce the required gas mass, and construction of a constant acceleration piston.

APPENDIX A

CALCULATIONS PERFORMED FOR THE NASA-AMES 4"-1" DEFORMABLE-PISTON LIGHT GAS GUN

APPENDIX A

CALCULATIONS PERFORMED FOR THE NASA-AMES 4"-1" DEFORMABLE-PISTON LIGHT GAS GUN

During the course of this project it was noted that the computer code developed for predicting the performance of the explosively driven gas gun was equally capable of predicting the performance of the various light gas guns at the Hypervelocity Free Flight Facility at NASA-Ames. At the request of the project monitor the program was modified sufficiently to make these performance calculations in a number of test cases.

A simplified sketch of the Ames 4"-1" light gas gun is shown in Fig. A.1. Gunpowder is loaded in the pressure chamber and ignited, thus building up sufficient pressure to propel a polyethylene piston down the first stage of the gun. The piston compresses the hydrogen-driven gas in a nearly adiabatic fashion, building up to a pressure of approximately 138 bars (20,000 psi) by the time the piston reaches the convergent section of the tube. At this point the diaphragm ruptures and the projectile begins to accelerate.

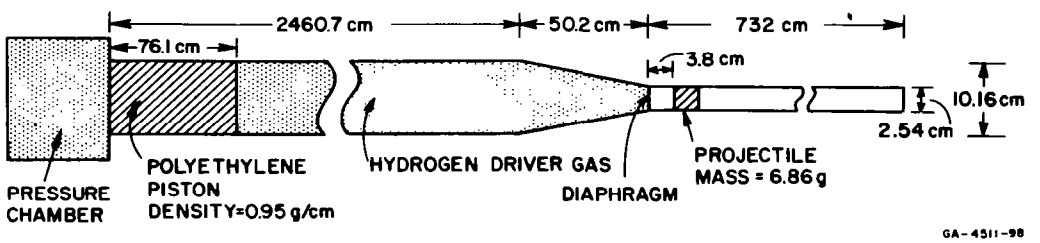

FIG. A.1 SCHEMATIC DIAGRAM AND PERTINENT DIMENSIONS OF THE NASA-AMES 4" - 1" DEFORMABLE-PISTON LIGHT GAS GUN

As the gas pressure begins to drop behind the accelerating projectile, the piston enters the constriction and begins to deform plastically. As a consequence the front surface of the piston accelerates and a compression wave is propagated into the driver gas. This

compression wave tends to counteract the decrease in pressure behind the accelerating projectile, and thus tends to extend the time during which the maximum sustainable acceleration is applied to the projectile. The timing and physical configuration of the device must be carefully chosen to provide this augmentation of base pressure over a significant time and yet to avoid a destructive overpressure.

The principal modifications necessary to adapt the computer code developed during this project to perform calculations of the Ames gun were: (1) to include the equations of motion of a plastically deforming piston; (2) to include a diaphragm. The latter inclusion is trivial, but the first took considerable study and experimentation before it was perfected. In addition, it was found while running the Ames gas gun cases that the equations of motion originally chosen led to a particularly inefficient calculation when area changes were great, as in the Ames gun. The equations of motion were rewritten using a different set of variables and this problem was removed.

The description of the motion of the deformable piston as it flows into the convergent section of the gas gun closely resembles the classical theory of wire drawing and wire extrusion.* We assume that: (1) the axial, radial, and hoop stresses are the principal stresses; (2) the radial stress is equal to the hoop stress; and (3) these stresses are functions of x only. We assume further that: (4) the piston is a perfectly plastic body with a yield stress in pure shear of k_p; (5) the wall friction stress on the piston is shear stress limited to this same value k_p; (6) the piston is in a state of plastic yield as it flows through the constriction; and (7) the piston is incompressible.

All these assumptions are typical of the theory of extruding wires. Probably the worst assumption in the case of a polyethylene piston converging into the constriction in the gun is that the piston behaves like a classical plastic body; one would in fact expect that rate-dependent stresses might be significant in polyethylene and in addition that the plastic yield strength k_p might depend upon the state of the material.

* For example, see A. Phillips, *Introduction to Plasticity*, The Ronald Press Company, New York, 1956, pp. 149-152.

From the assumptions on the distribution of stress it follows that τ_0, the octahedral shearing stress, becomes

$$\tau_0 = \frac{\sqrt{2}}{3}(\sigma_x - p) \tag{A.1}$$

But since the material is in a state of collapse we have $\tau_0 = \pm k_p$, where the sign opposes that of $\partial u/\partial x$, and we have

$$\sigma_x = -\left[p + \frac{3k_p}{\sqrt{2}} \operatorname{sgn}\left(\frac{\partial u}{\partial x}\right)\right] \tag{A.2}$$

The equations of motion for a differential section of the piston (see Fig. A.2) are readily written in Lagrangian coordinates. The normal force at the tube wall acting on the piston is the pressure p; the tangential force is given by the shear stress limited friction k_p.

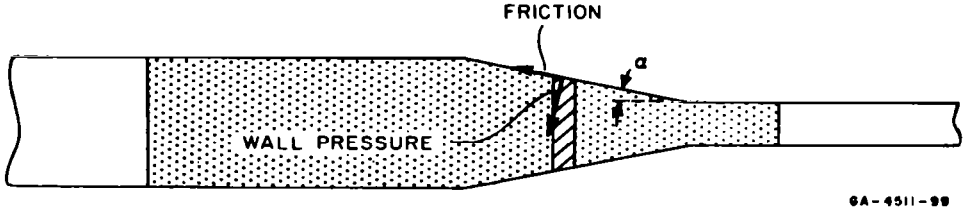

FIG. A.2 PISTON DEFORMATION PROCESS

The resulting momentum equation for a differential slab of material is:

$$m(r)\frac{\partial u}{\partial t} = \frac{\partial}{\partial r}(\sigma_x A) + p\frac{\partial A}{\partial r} - \frac{k_p}{\tan\alpha}\frac{\partial A}{\partial r} \tag{A.3}$$

where

$$m(r) = \rho A \frac{\partial x}{\partial r}\bigg|_{t=0} \tag{A.4}$$

is the density of the piston in Lagrangian coordinates. Assuming that sgn $(\partial u/\partial x) = +1$ in all cases of interest, Eq. A.3 can be simplified to read:

$$m(r)\frac{\partial u}{\partial t} = -A\frac{\partial}{\partial r}\left(p + \frac{3k_p}{\sqrt{2}}\right) - \left(\frac{3k_p}{\sqrt{2}} + \frac{k_p}{\tan\alpha}\right)\frac{\partial A}{\partial r} \qquad (A.5)$$

The equations of motion of the deforming piston may be exactly calculated by a recently developed technique.* Since the piston is incompressible the mass flow must depend on time alone, so that we have

$$\rho_0 uA = f(t) \qquad (A.6)$$

Differentiating this expression we obtain

$$\frac{df}{dt} = \rho_0 A\frac{\partial u}{\partial t} + \rho_0 u\frac{\partial A}{\partial t} \qquad (A.7)$$

But it can easily be shown that

$$\frac{\partial A(x)}{\partial t} = \frac{f(t)}{m(r)}\frac{\partial A}{\partial r} \qquad (A.8)$$

so that

$$\frac{df}{dt} = \rho_0 A\frac{\partial u}{\partial t} + \frac{f^2(t)}{Am(r)}\frac{\partial A}{\partial r} \qquad (A.9)$$

Rearranging terms, we obtain

$$m(r)\frac{\partial u}{\partial t} = \frac{1}{\rho_0 A}m(r)\frac{df}{dt} - \frac{f^2}{A}\frac{\partial A}{\partial r} \qquad (A.10)$$

---

* M. Cloutier and D. P. Flemming, Canadian Armament Research and Development Establishment, private communication, 14 May 1965.

Substituting this expression into the momentum equation (Eq. A.5) and simplifying, we obtain:

$$\frac{\partial}{\partial r}\left(p + \frac{3k_p}{\sqrt{2}}\right) = -\left(\frac{3k_p}{\sqrt{2}} + \frac{k_p}{\tan\alpha}\right)\frac{\dfrac{\partial A}{\partial r}}{A} - \frac{df}{dt}\frac{m}{\rho_0 A^2} + f^2\frac{\dfrac{\partial A}{\partial r}}{\rho_0 A^3} \tag{A.11}$$

Integrating from one end of the piston to the other, and noting that the axial stress is prescribed at both ends to be the pressure acting on the piston, we obtain:

$$p_2 - p_1 = -\left(\frac{3k_p}{2} + \frac{k_p}{\tan\alpha}\right)ln\left(\frac{A_2}{A_1}\right) - \frac{df}{dt}\int_{x_1}^{x_2}\frac{dx}{A} - \frac{f^2}{2\rho_0}(A_2^{-2} - A_1^{-2}) \tag{A.12}$$

Here we indicate the forward surface of the piston by the subscript 2, and the rear surface by the subscript 1. We have used Eq. A.4 to rearrange the integrals into the form shown.

From Eq. A.12 we obtain a differential equation for the mass flow, $f(t)$. It should be noted that this relation is an exact integral of the equations of motion at an instant of time and obtains for us the detailed motion of the piston in terms of the boundary conditions alone. We have

$$I\frac{df}{dt} = p_1 - p_2 - \left(\frac{3k_p}{\sqrt{2}} + \frac{k_p}{\tan\alpha}\right)ln\left(\frac{A_2}{A_1}\right) - \frac{f^2(t)}{2\rho_0}(A_2^{-2} - A_1^{-2}) \tag{A.13}$$

where

$$I(x) = \int_{x_1}^{x_2}\frac{dx}{A(x)} \tag{A.14}$$

After numerically obtaining a solution for the mass flux $f(t)$, we can then obtain detailed knowledge of the state of the piston. For instance, the velocity at any section is given by

$$u(x,\ t) = \frac{f(t)}{\rho_0 A(x)} \tag{A.15}$$

A short subroutine which calculates the motion of the deforming piston has been written and used successfully to perform calculations for the Ames gas gun. The first set of calculations was performed with $k_p = 0$, that is, the piston was assumed to be a perfect fluid. The pressures obtained at the base of the projectile for this case were greatly excessive, much more than the estimated base pressures in the real gun. When a value of 0.94 kbar was chosen for k_p (an approximate handbook value for polyethylene), the base pressures were quite reasonable and the resulting projectile motion was in fair qualitative agreement with the real gun. The final velocity was, however, about 23% higher than the experimental value.

Several modifications to the program were attempted to find the cause of this velocity discrepancy, but they have not been successful. As a first step the value of k_p was changed approximately 25%. This had no appreciable effect on the final velocity. Next, a friction coefficient of 0.1 was included in the equations of motion of the projectile, but this again made little difference to the final velocity.

Additional work is necessary before the results of this numerical code can be compared with experiment. Some of the more important questions which should be looked into are: (1) the effect of heat losses from the gas into the tube walls; (2) the effect of rate-dependent plastic stresses; (3) a detailed comparison of the predicted piston and projectile motions with experimental data.

REFERENCES

1. Stephenson, W. B. and R. E. Knapp, "Performance of a Two-Stage Launcher Using Hydrogen," AEDC-TDR-62-32, Arnold Engineering Development Center, Arnold Air Force Station, Tennessee.

2. Curtis, John S., "An Accelerated Reservoir Light-Gas Gun," NASA TN-D1144, Ames Research Center, Moffett Field, California.

3. Fowles, G. R., W. M. Isbell, and F. H. Shipman, "Feasibility Study of an Explosive Gun," SRI Project GSU-4511, Final Report No. 1, Contract No. NAS 2-1361 for NASA-Ames Research Center, July 1964, p. 46.

4. Wheeler, W. C., "Cast Low Detonation Rate Explosive," Poulter Laboratories Internal Report 039-65, December 1956.

5. Kronmav, S. and A. Merendino, "Inhibited Jet Charge," Proc. Sixth Symposium on Hypervelocity Impact, Vol. I. 1963.

6. Harrison, E. F., "Intermolecular-Force Effects on the Thermodynamic Properties of Helium with Applications," AIAA Journal **2**, 1854 (1964).

7. Brush, S. G. and C. J. Wensrich, "Annotated Bibliography of Theories of the Equation of State of Ionized Gases and Strong Electrolyte Solutions," University of California Lawrence Radiation Laboratory, Livermore, Calif., Report No. UCRL-6473 (August 8, 1961).

8. Brush, S. G., "Annotated Bibliography of Theories of the Equation of State of High Temperature Gases," Supplement I to Ref. 7 (July 3, 1963).

9. "Helium Hypersonic Flow Properties," Boeing Airplane Co., Seattle, Washington, Document No. D2-11721 (Sept. 5, 1961).

10. "Thermodynamic Properties of High Temperature Helium," LTV Research Center, Report No. 0-71000/3R-11 (August, 1963).

11. Liepmann, H. W. and A. Rashko, *Elements of Gas Dynamics*, John Wiley and Sons, Inc., New York, 1957. See especially p. 316 ff.

12. von Neumann, J. and R. D. Richtmyer, "A Method for the Numerical Calculation of Hydrodynamic Shocks," J. Appl. Phys. **21**, 232-237 (1950).

13. Lax, P. D., "Weak Solutions of Nonlinear Hyperbolic Equations and Their Numerical Computation," Comm. on Pure and Appl. Math., Vol. VII, 159-193 (1954).

14. Lax, P. D. and B. Wendroff, "Systems of Conservation Laws," Comm. on Pure and Appl. Math., Vol. XIII, 217-237 (1960).

15. Hildebrand, F. B., *Introduction to Numerical Analysis*, McGraw-Hill Book Company, Inc., New York, 1956.

16. Richtmyer, R. D., "A Survey of Difference Methods for Nonsteady Fluid Dynamics," Nat. Cent. for Atmos. Res. Tech. Notes 63-2, Boulder, Colorado (August 27, 1962), p. 11.

17. Gurney, R. W., "The Initial Velocity of Fragments from Bombs, Shells, Grenades," BRL Report No. 405, September 1943.

18. Sterne, T. E., "A Note on the Initial Velocities of Fragments from Warheads," BRL Report No. 648, September 1947 (Confidential).

19. Birkhoff, G., D. P. MacDougall, E. M. Pugh, and G. Taylor, "Explosives with Lined Cavities," J. Appl. Phys. **19**, 563-582 (1948).

NASA-Langley, 1967 —— 11 CR-709